

Green Bond Valuation: A Numerical Mathematics Perspective

Assessing the Influence of Environmental
Factors

by

J.O.M. Rutten

to obtain the degree of Master of Science
at the Delft University of Technology,
to be defended publicly on Wednesday February 14, 2024 at 14:30 PM.

Student number: 4598180
Project duration: March 1, 2023 – February 14, 2024
Thesis committee: Prof. Dr. Ir. C. Vuik, TU Delft, Responsible Professor
Dr. Ir. Mr. V. Dwarka, TU Delft, Daily Supervisor
Prof. Dr. Ir. H.X. Lin, TU Delft, Thesis Committee

An electronic version of this thesis is available at <http://repository.tudelft.nl/>.

Acknowledgements

This thesis is written to obtain the degree Master of Science in Applied Mathematics - Financial Engineering at TU Delft. I would like to express my gratitude for the supervision and guidance of prof. Kees Vuik and assistant prof. Vandana Dwarka, who were always available, provided valuable feedback, and granted me the opportunity to conduct this research. I would also like to thank prof. Hai Xiang Lin for being part of my thesis committee.

I wish you a pleasant read,

J.O.M. Rutten
Delft, February 2024

Abstract

This thesis presents a novel approach to the pricing of green bonds, a growing segment in financial markets with an emphasis on environmental sustainability. Unlike traditional financial instruments, green bonds uniquely incorporate environmental considerations, particularly carbon price (c_t), along with traditional factors like the short rate (r_t), into their valuation. This integration is increasingly relevant in today's economy, reflecting a shift towards sustainable finance. The core of this research involves applying advanced numerical methods, including the Finite Difference Method, Crank-Nicolson discretization, GMRES and Bi-CGSTAB, in order to develop and analyze pricing models for both green and conventional bonds. The study aims to assess how environmental factors impact the efficiency of these numerical techniques and to compare the outcomes with conventional bond models.

The research reveals that green bonds, compared to conventional bonds, present unique numerical challenges, notably requiring more iterations for convergence in iterative methods GMRES and Bi-CGSTAB because of the high carbon price volatility (σ_c) and the 'Greenium' phenomenon. Moreover, the comparative analysis showed that while Bi-CGSTAB outperforms GMRES in the green bond model, the opposite is true for conventional bonds. This study not only contributes to the theoretical understanding of green bond pricing but also offers practical insights for financial analysts and investors navigating this evolving market.

Keywords: Green Bonds, Bond Pricing, Zero-Coupon Bond, Short Rate Modeling, Numerical Methods, Crank-Nicolson, GMRES, BiCGSTAB, Environmental Finance, Sustainable Investing, Comparative Analysis, Financial Modeling.

Contents

Acknowledgements	i
Abstract	ii
Acronyms	vii
1 Introduction	1
1.1 Bonds	1
1.2 Green Bonds	3
1.3 Related Literature	3
2 Pricing Financial Instruments	4
2.1 Preliminary Mathematical Concepts	4
2.2 Pricing Financial Derivatives	8
2.2.1 Risk-Neutral Valuation and the Market Price of Risk	8
2.2.2 Option Theory	9
2.2.3 Black Scholes	9
2.2.4 Short Rates	12
2.3 Conventional Bond	15
2.3.1 Derivation of Pricing Model	15
2.3.2 Parameter Analysis	17
2.4 Green Bond	21
2.4.1 Carbon Pricing	21
2.4.2 Pricing Model	21
2.4.3 Parameter Calibration	23
2.4.4 Parameter Analysis	25
3 Finite Difference Method	31
3.1 Theory	31
3.2 Conventional Bond	33
3.3 Green Bond	35
4 Numerical Results	38
4.1 Direct methods	38
4.2 Krylov subspace methods	38
4.3 The GMRES and Bi-CGSTAB methods	39
4.3.1 Preconditioning	40
4.3.2 Convergence of Iterative Methods	41
4.4 Conventional Bond Numerical Analysis	42
4.5 Green Bond GMRES analysis	49
4.6 Comparative Analysis of the Conventional and Green Bond models	58
5 Conclusion & Discussion	61
References	63
A Black-Scholes PDE Derivation	65

List of Figures

1.1	Cash flow for a zero-coupon bond, $B(t, T)$, with $FV = 1$ and maturity T	2
1.2	Cash flow for a coupon bond, $B(t, T)$, with $FV = 1$, coupon = c_j and maturity T	2
1.3	Yield curves	2
2.1	Itô multiplication table for a Wiener process	6
2.2	The payoff diagram of a call option (left) and a put option (right) with strike price $K = 10$	9
2.3	Stock price and call option value. Parameters: $S_0 = 100, K = 100, r = 0.05, \sigma = 0.05$	11
2.4	Stock price and call option value. Parameters: $S_0 = 100, K = 100, r = 0.05, \sigma = 0.2$	11
2.5	Stock price and call option value. Parameters: $S_0 = 100, K = 100, r = 0.1, \sigma = 0.2$	11
2.6	Stock price path and two barriers	12
2.7	Bond price for constant short rate r	12
2.8	Bond price for time-dependent short rate r	13
2.9	CIR (left) and Vašiček (right) short rate paths for different values of σ	14
2.10	CIR (left) and Vašiček (right) short rate paths for different values of α	14
2.11	CIR (left) and Vašiček (right) short rate paths for different values of β	15
2.12	Value of a Coupon Bond, CIR model (left) and Vašiček model (right), $\alpha = 1.0, \beta = 0.05, \sigma_r = 0.15, \lambda_r = 0.01, T = 4$	18
2.13	Value of a Coupon Bond, CIR model (left) and Vašiček model (right), $\alpha = 1.0, \beta = 0.05, \lambda_r = 0.01, T = 4$	18
2.14	Value of a Coupon Bond, CIR model (left) and Vašiček model (right), $\beta = 0.05, \sigma_r = 0.15, \lambda_r = 0.01, T = 4$	19
2.15	Value of a Coupon Bond, CIR model (left) and Vašiček model (right), $\alpha = 1.0, \sigma_r = 0.15, \lambda_r = 0.01, T = 4$	19
2.16	Bond Value over time, CIR model (left) and Vašiček model (right), $\alpha = 1.0, \beta = 0.05, \sigma_r = 0.15, T = 4$	20
2.17	Yield curve spot rate, 4-year maturity - Government bond, rating triple A - Euro area	24
2.18	EU ETS	25
2.19	Difference in short rate r_t	26
2.20	Valuation of coupon V_1 at different times t	26
2.21	Sensitivity coupon V_1 for different values of σ_c	27
2.22	Sensitivity coupon V_1 for different values of μ	27
2.23	Sensitivity coupon V_1 for different values of λ_c	28
2.24	Sensitivity coupon V_1 for different values of ρ	28
2.25	Difference in short rate r_t	28
2.26	Valuation of coupon V_2 at different times t	29
2.27	Sensitivity coupon V_2 for different values of σ_c	29
2.28	Sensitivity coupon V_2 for different values of μ	29
2.29	Sensitivity coupon V_2 for different values of λ_c	30
2.30	Sensitivity coupon V_2 for different values of ρ	30
3.1	Representation of how the explicit method (upper left), implicit method (upper right) and Crank-Nicolson method (low middle) work on the nodes of a grid.	32
4.1	Eigenvalue distribution for different values of σ_r and $N = 100$	43
4.2	Diagonals of the matrix for different values of σ_r and $N = 100$. (For a higher σ_r the upper and lower diagonals are further apart from each other)	44
4.3	GMRES vs Bi-CGSTAB, for different values of $\sigma_r, tol = 10^{-8}$	44
4.4	Eigenvalue distribution for different values of α and $N = 100$	45
4.5	Diagonals of the matrix for different values of α and $N = 100$	45

4.6	GMRES vs Bi-CGSTAB, for different values of α , $tol = 10^{-8}$	46
4.7	Eigenvalue distribution for different values of β and $N = 100$	47
4.8	Diagonals of the matrix for different values of β and $N = 100$	47
4.9	GMRES vs Bi-CGSTAB, for different values of β , $tol = 10^{-8}$	48
4.10	Eigenvalue distribution for different values of λ_r and $N = 100$	48
4.11	Diagonals of the matrix for different values of λ_r and $N = 100$	49
4.12	GMRES vs Bi-CGSTAB, for different values of λ_r , $tol = 10^{-8}$	49
4.13	Eigenvalue distribution for different values of σ_c and $N = 10$	51
4.14	GMRES vs Bi-CGSTAB for different values of σ_c	52
4.15	Eigenvalue distribution for different values of ρ and $N = 10$	52
4.16	GMRES vs Bi-CGSTAB for different values of ρ	53
4.17	Eigenvalue distribution for different values of μ and $N = 10$	54
4.18	GMRES vs Bi-CGSTAB for different values of μ	55
4.19	Eigenvalue distribution for different values of λ_c and $N = 10$	55
4.20	GMRES vs Bi-CGSTAB for different values of λ_c	56
4.21	GMRES vs Bi-CGSTAB for different values of λ_r	57

List of Tables

4.1	Matrix properties different values of σ_r , $M = 11$, $\alpha = 1.0$, $\beta = 0.05$, $\lambda_r = 0.01$	43
4.2	Performance of GMRES for various σ_r values	44
4.3	Performance of Bi-CGSTAB for various σ_r values	44
4.4	Matrix properties different values of α , $M = 11$, $\sigma_r = 0.2$, $\beta = 0.05$, $\lambda_r = 0.01$	45
4.5	Performance of GMRES for various α values	46
4.6	Performance of Bi-CGSTAB for various α values	46
4.7	Matrix properties different values of β , $M = 11$, $\sigma_r = 0.2$, $\alpha = 1.0$, $\lambda_r = 0.01$	46
4.8	Performance of GMRES for various β values	47
4.9	Performance of Bi-CGSTAB for various β values	47
4.10	Matrix properties for different values of λ_r , $M = 11$, $\sigma_r = 0.2$, $\alpha = 1.0$, $\beta = 0.05$	48
4.11	Performance of GMRES for various λ_r values	49
4.12	Performance of Bi-CGSTAB for various λ_r values	49
4.13	Matrix properties for different values of σ_c	51
4.14	Performance of GMRES for various σ_c values	51
4.15	Performance of Bi-CGSTAB for various σ_c values	51
4.16	Performance of GMRES for various σ_r values	52
4.17	Performance of Bi-CGSTAB for various σ_r values	52
4.18	Matrix properties for different values of ρ	53
4.19	Performance of GMRES for various ρ values	53
4.20	Performance of Bi-CGSTAB for various ρ values	53
4.21	Matrix properties for different values of μ	54
4.22	Performance of GMRES for various μ values	54
4.23	Performance of Bi-CGSTAB for various μ values	54
4.24	Matrix properties for different values of λ_c	55
4.25	Performance of GMRES for various λ_c values	56
4.26	Performance of Bi-CGSTAB for various λ_c values	56
4.27	Performance of GMRES for various λ_r values	56
4.28	Performance of Bi-CGSTAB for various λ_r values	56
4.29	Performance of GMRES and Bi-CGSTAB for different coupons	57
4.30	Performance of GMRES and Bi-CGSTAB for various σ_r values in the Green Bond model	58
4.31	Performance of GMRES and Bi-CGSTAB for various σ_c values in the Green Bond model	58
4.32	Performance of GMRES and Bi-CGSTAB for various σ_r values in the Conventional Bond model	58
4.33	Performance of GMRES and Bi-CGSTAB for lower σ_c values in the Green Bond model	59
4.34	Performance of GMRES and Bi-CGSTAB for various μ values in the Green Bond model	59
4.35	Performance of GMRES and Bi-CGSTAB for various λ_c values in the Green Bond model	59
4.36	Performance of GMRES and Bi-CGSTAB for various λ_r values in the Green Bond model	60
4.37	Performance of GMRES and Bi-CGSTAB for various λ_r values in the Conventional Bond model	60

Acronyms

ZCB	Zero-Coupon Bond
CB	Coupon Bond
FV	Face Value
CF	Cash Flow
EIB	European Investment Bank
GBM	Geometric Brownian Motion
SDE	Stochastic Differential Equation
PDE	Partial Differential Equation
OTM	Out-Of-The-Money
ITM	In-The-Money
CIR	Cox-Ingersoll-Ross
ETS	Emission Trading System
GMRES	Generalized Minimum Residual
Bi-CGSTAB	BiConjugate Gradient Stabilized
CG	Conjugat Gradient
ILU	Incomplete LU factorization

1

Introduction

This thesis explores the innovative field of green bond pricing, introducing a novel model that incorporates environmental factors, a feature that sets these bonds apart from traditional financial instruments. The research focuses on the application of advanced numerical methods, including the Finite Difference Method, Crank-Nicolson discretization, Generalized Minimum Residual method and Biconjugate Gradient Stabilized method, to solve the pricing models for both green and conventional bonds. The aim is to evaluate the impact of environmental factors on the efficiency of these numerical methods and compare the results with those obtained from conventional bond models.

1.1. Bonds

Bonds are a fundamental financial instrument, representing a loan made by an investor to a borrower, which typically includes entities like corporations or various levels of government. They are essential for entities to finance projects and operations, particularly when large sums are required that exceed the capacity of average banks. Bonds are debt instruments. In a bond agreement, the issuer (borrower) commits to pay back the face value of the bond on a specified maturity date, along with interest payments (coupons) at agreed intervals (e.g., semiannually, annually). This interest rate, known as the coupon rate, forms part of the return that bondholders earn for lending their funds. Bonds are a key asset class in the financial market, commonly referred to as fixed-income securities. They differ from stocks (equities) in that bondholders have a creditor stake in the entity, as opposed to an equity stake like stockholders. This distinction means that in the event of bankruptcy, bondholders are prioritized over stockholders for repayment, although they rank behind secured creditors. The liquidity of bonds varies, with many being negotiable and transferable in the secondary market, which affects their market price and can significantly diverge from the face value. The most common types of bonds include municipal, corporate, and government bonds, each serving different financial and strategic purposes for both issuers and investors. Therefore they play a crucial role in the financial system, allowing large organizations and governments to raise capital efficiently and offering investors a way for lending funds with a structured return.

Definition 1 *The most basic form of a bond is the zero-coupon bond (ZCB), $B(t, T)$, which pays the investor 1 currency unit (the face value, FV) at maturity time T , i.e. $B(T, T) = 1$ [24]. ZCB's do not yield any payments to the bondholder before maturity T .*



Figure 1.1: Cash flow for a zero-coupon bond, $B(t, T)$, with $FV = 1$ and maturity T

Definition 2 The coupon bond (CB), provides periodic payments c_j 's (coupons) in addition to the face value FV at maturity [24]. The coupons are paid to the holder of the bond at a finite set of dates $\{t_1, t_2, \dots, t_n\} \subseteq [0, T]$. The amount of the coupons depends on the coupon rate $\alpha \in [0, 1]$, which is a percentage of the face value. This rate can be fixed, but can also be dependent on future market rates.

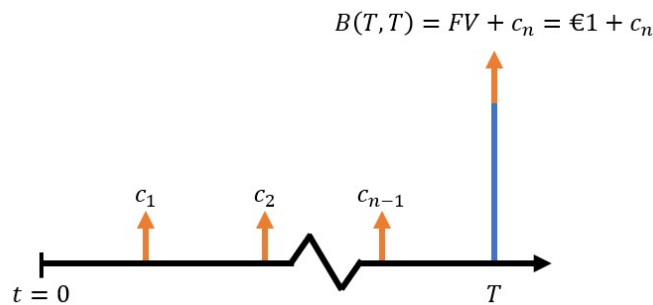


Figure 1.2: Cash flow for a coupon bond, $B(t, T)$, with $FV = 1$, coupon = c_j and maturity T

Continuing with the exploration of bonds, an important concept in understanding the bond market is the yield curve (figure 1.3). The yield curve is a graphical representation that plots the interest rates of bonds of different maturities for similar quality bonds. The yield curve is a key focus for economists and investors as it offers significant insights into the future trajectory of the economy. It serves as a predictive tool for shifts in economic growth, inflation, and interest rates. A 'normal' yield curve, characterized by significantly higher long-term rates compared to short-term rates, often suggests robust economic growth and increasing inflation. In such situations, the central bank might increase interest rates to temper the economy and keep inflation in check. When the yield curve is inverted, this typically suggests an upcoming recession. This scenario arises from investor expectations that the central bank will lower interest rates to boost economic activity.

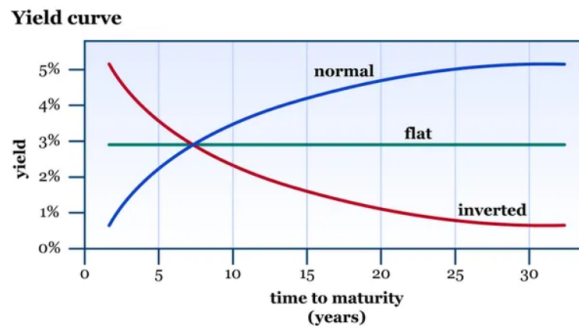


Figure 1.3: Yield curves

1.2. Green Bonds

Adding to the spectrum of bonds are Green Bonds. Green Bonds are specifically designed to support climate-related or environmental projects. They provide investors with an opportunity to finance projects that have a positive environmental impact, such as renewable energy, energy efficiency, sustainable waste management, and clean transportation initiatives. The green bond market [2] has grown rapidly since the first green bond issuance by the European Investment Bank (EIB) in 2007. Initially, the market was dominated by banks and public institutions, but in recent years, corporate issuers and governments have become increasingly active. The key feature that distinguishes green bonds from other types of bonds is the requirement that the funds will be invested in environmentally sustainable projects. Issuers of green bonds include governments, municipalities, and corporations, aligning their funding needs with environmental objectives. This creates a win-win situation, where investors receive the benefits of financial return—while also contributing to environmental sustainability. The growing demand among investors for sustainable investment opportunities is causing a trend where green bonds often trade at a premium compared to conventional bonds. Investors are increasingly willing to accept lower yields for the opportunity to contribute to environmentally beneficial projects. This phenomenon is called the 'Greenium' [25]. On the other hand, a significant concern with green bonds is the risk of 'greenwashing', where issuers might exaggerate or misrepresent their environmental impact. This issue arises when companies inaccurately label projects as environmentally friendly to meet green bond criteria, potentially compromising the integrity of green bonds. It is essential for investors and regulators to carefully verify the actual environmental benefits of these projects, ensuring that the funds raised are truly directed towards genuine green initiatives.

1.3. Related Literature

In this subsection I present some of the related literature that was most important during the research that formed this thesis. The study by Bhutta et al. (2022), cited as [2], provides a foundational understanding of green bonds, setting the stage for a deeper investigation into their unique characteristics and market dynamics. This is complemented by Hachenberg and Schiereck [16], who investigate the pricing differences between green and conventional bonds, laying the groundwork for a deeper exploration of these instruments. Moreover, the phenomenon of 'Greenium,' described in Pietsch and Salakhova's work ([25]), adds some important information to our understanding of the price of green bonds. In chapter 2 we will delve into the world of pricing of financial instruments. We start with a subsection providing preliminary mathematics. The stochastic calculus part comes from Oosterlee and Grzelak's "Mathematical Modeling and Computation in Finance" ([24]) and Bertsekas and Tsitsiklis's "Introduction to Probability" ([1]). The linear algebra part is obtained from Vuik and Lahaye's "Scientific Computing" ([32]). Option theory and other financial engineering concepts, such as risk-neutral pricing, are elaborated in works like Oosterlee and Grzelak's ([24]), Hull's "Options, Futures, and Other Derivatives" ([18]) and "Interest Rate Derivatives: Models of the Short Rate" ([17]), and Rásonyi's "Arbitrage pricing theory and risk-neutral measures" ([26]). Then we will explain start introducing the stochastic modeling of short rates, where we got the information from works of Cox, Ingersoll, and Ross ([11]) and Vasicek ([31]). These models are an essential element in the valuation of financial instruments like bonds. Hereafter we used [28] for developing the model of conventional bond and [35] and [34] for developing the model of the green bond coupon rate. From Dong et al [13] and Feng et al [14] we obtained important information about the volatility of the carbon price which we will extensively analyse in chapter 4. In chapter 3 we introduce the finite difference method and apply the finite difference method with knowledge obtained from Vuik and Lahaye's "Scientific Computing" [32] and the book from Domingo Tavella and Curt Randall [28]. In chapter 4 we will solve the obtained matrix equations that underlie the financial models with iterative solvers GMRES and Bi-CGSTAB, where Saad's "Iterative Methods for Sparse Linear Systems" ([27]) and again Vuik and Lahaye's "Scientific Computing" ([32]) have provided the necessary tools. Combining this diverse literature, this thesis presents a multidimensional understanding of the mathematics behind (green) bond valuation.

2

Pricing Financial Instruments

In financial engineering, we encounter an intersection of probability theory, stochastic processes and economic theory to price all kinds of financial instruments. We will start this chapter with a section where we introduce important mathematical definitions and theorems, both from stochastic calculus and linear algebra. In the subsequent sections and chapters will use them to develop financial models and analyse them.

2.1. Preliminary Mathematical Concepts

In this section we review some basics in stochastic calculus and numerical mathematics. We will define a Wiener process and outline several of its key properties. Hereafter, we develop the Itô integral, a crucial instrument for establishing Itô's formula. This formula enables us to compute derivatives of functions involving Wiener processes. Using this formula, we are able to derive the model of Black-Scholes and the models for a conventional and green bond. We also show some important matrix properties that influence the efficiency of numerical methods.

The following definitions and theorems all are cited from [24] or [32].

Definition 3 A stochastic process is a collection of random variables defined on a common probability space (Ω, \mathcal{F}, P) and indexed by a set T . Specifically, it is a family $\{X(t) : t \in T\}$ where:

- t typically represents time and can be discrete (e.g., $t = 0, 1, 2, \dots$) or continuous (e.g., $t \geq 0$).
- $X(t)$ is a random variable for each t , which represents the state of the process at time t .
- The common probability space (Ω, \mathcal{F}, P) captures the inherent randomness of the system.

The process is often denoted as $X(t, \omega)$, where $t \in T$ is the time index and $\omega \in \Omega$ is a specific outcome from the sample space.

Definition 4 (Wiener Process) A stochastic process $\{W(t) : t \geq 0\}$ is called a Wiener process (or Brownian motion) if the following conditions hold:

1. This process starts at 0, i.e. $W_0 = W(0) = 0$.
2. For all $t > 0$, W_t is normally distributed with mean equal to zero and variance equal to t , i.e., $W_t \sim N(0, t)$.
3. It has independent increments, i.e. for $0 \leq t_0 < t_1 < \dots < t_n$, the random variables $Y_i = W(t_i) - W(t_{i-1})$ are independent for all $i \in \{1, \dots, n\}$.
4. It is an almost surely continuous path.

Definition 5 (Stochastic Differential Equation) A stochastic differential equation (SDE) is a differential equation that incorporates a stochastic process. Its general form can be represented as:

$$dX_t = a(X_t, t)dt + b(X_t, t)dW_t \quad (2.1)$$

where:

- dX_t denotes the change in the process X_t .
- $a(X_t, t)$ is the deterministic drift term.
- $b(X_t, t)$ is the stochastic volatility term.
- W_t is a standard Wiener process or Brownian motion

The geometric Brownian Motion (GBM) model is widely recognized as the predominant process for modeling asset prices in finance. In this model, the asset price's logarithm follows an arithmetic Brownian motion, driven by a Wiener process denoted as $W(t)$.

Definition 6 (Geometric Brownian Motion) The asset price $S(t)$ is said to follow a GBM process, when it satisfies the following SDE:

$$dS(t) = \mu S(t) dt + \sigma S(t) dW(t), \quad \text{with } S(t_0) = S_0.$$

where $W(t)$ is a Brownian Motion, μ denotes the drift parameter, i.e. a constant deterministic growth rate of the stock, and σ is the (constant) percentage volatility parameter. This can also be written in integral formulation:

$$S(t) = S_0 + \int_{t_0}^t \mu S(z) dz + \int_{t_0}^t \sigma S(z) dW(z).$$

The amount by which an asset price differs from its expected value is determined by the volatility parameter σ . Volatility is thus a statistical measure of the tendency of an asset to rise or fall sharply within a period of time.

Itô's lemma plays a crucial role in the realm of stochastic processes, particularly to handle the Wiener increment $dW(t)$ as dt approaches zero. By this lemma we can derive solutions to SDE's and formulate PDE's used for pricing various financial instruments.

Let us consider the following SDE (Stochastic Differential Equation), corresponding to the Itô process $X(t)$,

$$dX(t) = \bar{\mu}(t, X(t)) dt + \bar{\sigma}(t, X(t)) dW(t), \quad \text{with } X(t_0) = X_0. \quad (2.2)$$

With stochastic process $X(t)$ determined by (2.5), another process $Y(t)$ can be defined as a function of t and $X(t)$, i.e., $Y(t) := g(t, X)$. $Y(t)$ is a stochastic process and its SDE (Stochastic Differential Equation) can also be determined.

To derive the dynamics $dY(t)$ for $Y(t) = g(t, X)$, we may take a look at the 2D Taylor series expansion around some point (t_0, X_0) , i.e.,

$$dg(t, X) = \frac{\partial g}{\partial t} dt + \frac{1}{2} \frac{\partial^2 g}{\partial t^2} (dt)^2 + \frac{\partial g}{\partial X} dX + \frac{1}{2} \frac{\partial^2 g}{\partial X^2} dX^2 + \frac{\partial^2 g}{\partial t \partial X} dX dt + \dots \quad (2.3)$$

The equality in 2.3 can be simplified, by neglecting the higher-order dt -terms, by writing,

$$dg(t, X) = \frac{\partial g}{\partial t} dt + \frac{\partial g}{\partial X} dX + \frac{1}{2} \frac{\partial^2 g}{\partial X^2} (dX)^2. \quad (2.8)$$

We need to make statements about the term $dXdX$, which, in the case of equation 2.2, reads:

$$(dX)^2 = \bar{\mu}^2(t, X) (dt)^2 + \bar{\sigma}^2(t, X) (dW)^2 + 2\bar{\mu}(t, X)\bar{\sigma}(t, X) dW dt.$$

For this we make use of Itô's table (proof can be found in [24]):

	dt	dW(t)
dt	0	0
dW(t)	0	dt

Figure 2.1: Itô multiplication table for a Wiener process

Theorem 1 (Itô's Lemma) Suppose a process $X(t)$ follows the Itô dynamics,

$$dX(t) = \bar{\mu}(t, X(t)) dt + \bar{\sigma}(t, X(t)) dW(t), \quad \text{with } X(t_0) = X_0,$$

where drift $\bar{\mu}(t, X(t))$ and diffusion $\bar{\sigma}(t, X(t))$ satisfy the standard Lipschitz conditions on the growth of these functions (see appendix).

Let $g(t, X)$ be a function of $X = X(t)$ and time t , with continuous partial derivatives, $\frac{\partial g}{\partial X}$, $\frac{\partial^2 g}{\partial X^2}$, $\frac{\partial g}{\partial t}$. A stochastic variable $Y(t) := g(t, X)$ then also follows an Itô process, governed by the same Wiener process $W(t)$, i.e.,

$$dY(t) = \left(\frac{\partial g}{\partial t} + \bar{\mu}(t, X) \frac{\partial g}{\partial X} + \frac{1}{2} \frac{\partial^2 g}{\partial X^2} \bar{\sigma}^2(t, X) \right) dt + \frac{\partial g}{\partial X} \bar{\sigma}(t, X) dW(t).$$

Definition 7 In probability theory [30], an event, A , is a member of a σ -algebra, Σ , of subsets of a sample space Ω . A probability measure, \mathbb{P} , is a normed measure over a measurable space (Ω, Σ) ; that is, \mathbb{P} is a real-valued function which assigns to every A in Σ , a probability, $\mathbb{P}(A)$, such that (a) $\mathbb{P}(A) \geq 0$ for all $A \in \Sigma$, (b) $\mathbb{P}(\Omega) = 1$; and (c) \mathbb{P} is countably additive, i.e., if $\{A_i\}$ is any collection of disjoint events, then

$$\mathbb{P} \left(\bigcup_i A_i \right) = \sum_i \mathbb{P}(A_i).$$

In probability theory, the following theorem is a key principle that describes the transformation of stochastic processes when there is a shift in the probability measure. This theorem holds significant value in the field of financial mathematics as it provides a framework for transitioning from the real-world probability measure to the risk-neutral measure which we will discuss in subsection 2.2.1.

Theorem 2 (Girsanov for Wiener Process, [15]) Let $\{f_t\}$ be a square integrable stochastic process adapted to \mathcal{F}_t such that $\mathbb{E}_{\mathbb{P}}[\mathcal{E}_t(f)] < \infty$ for all $t \in [0, T]$. Then

$$\tilde{W}_t = W_t - \int_0^t f_s ds$$

is a Brownian motion with respect to an equivalent probability measure \mathbb{Q} given by

$$d\mathbb{Q} = \mathcal{E}_T(f) d\mathbb{P} = \exp \left\{ \int_0^T f_s dW_s - \frac{1}{2} \int_0^T f_s^2 ds \right\} d\mathbb{P}.$$

Important to notice is that in this thesis W_t is a Wiener process under probability measure \mathbb{P} and that \tilde{W}_t is a Wiener process under probability measure \mathbb{Q}

Now we will introduce some important concepts in linear algebra and numerical mathematics that we will use to analyse the matrix equations we obtain in later chapters.

Definition 8 The matrix A is symmetric if and only if $A^T = A$.

Definition 9 The matrix A is called positive definite (positive semi-definite) if and only if

$$\forall \mathbf{u} \in \mathbb{R}^N \setminus \{0\} : \mathbf{u}^T \mathbf{A} \mathbf{u} > 0 \quad (\mathbf{u}^T \mathbf{A} \mathbf{u} \geq 0). \quad (2.4)$$

If the matrix is also symmetric, it is called a symmetric positive definite (SPD) matrix

Definition 10 The non-zero vector $\mathbf{v}^{[k]} \in \mathbb{C}^n \setminus \{0\}$ is an **eigenvector** corresponding to the **eigenvalue** $\lambda_k \in \mathbb{C}$ if and only if

$$A\mathbf{v}^{[k]} = \lambda_k \mathbf{v}^{[k]}.$$

The algebraic multiplicity of λ_k is defined as the multiplicity of the root of λ_k of the characteristic equation $\det(A - \lambda I) = 0$. The geometric multiplicity of λ_k is defined as the dimension of the space spanned by the corresponding eigenvectors. The set of all eigenvalues of A is called the **spectrum** of A and will be denoted as $\sigma(A)$.

In [32], we also learn that matrix norms are often involved when analyzing matrix algorithms: If the matrix used in solving equations is almost singular (meaning it almost does not have an inverse), the solver might not work well. To quantify how close a matrix is to being singular, we need a way to measure its "distance" from singularity. Using vector norms and norms induced by operators helps us define such a metric.

Definition 11 In the case of $p = 1$, $p = 2$ and $p = \infty$, the following expressions exist that allow to compute the matrix p -norm in practice:

$$\begin{aligned} \|A\|_1 &= \max_{1 \leq j \leq n} \sum_{i=1}^m |a_{ij}| \quad \text{maximum absolute column sum} \\ \|A\|_2 &= \sqrt{\max_{1 \leq i \leq n} \lambda_i(A^T A)} = \sqrt{\lambda_{\max}(A^T A)} \\ \|A\|_\infty &= \max_{1 \leq i \leq m} \sum_{j=1}^n |a_{ij}| \quad \text{maximum absolute row sum} \end{aligned}$$

The Frobenius norm of a matrix A is defined as

$$\|R\|_F = \sqrt{\sum_{i=1}^m \sum_{j=1}^n |r_{ij}|^2}$$

It can be viewed as the Euclidean norm of the vector obtained from all rows (or columns) of A .

From [32]: "Given the linear system $Au = f$, a small perturbation in the right-hand side vector $f \rightarrow f + \Delta f$ will cause a perturbation in the solution $u + \Delta u$. We will see later that the condition number of the matrix A , denoted as $\kappa_p(A)$, allows us to bound the magnitude of the perturbation Δu in terms of the magnitude of the perturbation Δf ."

Definition 12 The condition number measured in p -norm $\kappa_p(A)$ of an invertible $n \times n$ matrix A is defined as

$$\kappa_p(A) = \|A\|_p \|A^{-1}\|_p.$$

Observe that for any p , $\kappa_p(A) \in [1, \infty)$. By using the previous definition, we obtain that the condition number in 2-norm can be expressed as

$$\kappa_2(A) = \sqrt{\frac{\lambda_{\max}(A^T A)}{\lambda_{\min}(A^T A)}}.$$

Definition 13 The spectral radius $\rho(A)$ of a matrix $A \in \mathbb{R}^{n \times n}$ is defined as

$$\rho(A) = \max_{i=1, \dots, n} \{|\lambda_i| : \lambda_i \in \sigma(A)\}.$$

Note that in general $\rho(A) \notin \sigma(A)$. The computation of the spectral radius is not straightforward. The following theorem gives an upper bound on the spectral radius.

Theorem 3 Given $\|\cdot\|$ any multiplicative matrix norm, then

$$\rho(A) \leq \|A\|.$$

Proof. Assume (λ, \mathbf{u}) any eigenvalue-eigenvector pair of A . Then $A\mathbf{u} = \lambda\mathbf{u}$, and thus by virtue of the sub-multiplicative property

$$|\lambda|\|\mathbf{u}\| = \|\lambda\mathbf{u}\| = \|A\mathbf{u}\| \leq \|A\|\|\mathbf{u}\| \Rightarrow |\lambda| \leq \|A\|.$$

The result then follows from the fact that λ was chosen arbitrarily.

Definition 14 The matrix A is called row diagonal dominant if and only if

$$|a_{ii}| \geq \sum_{j=1, j \neq i}^n |a_{ij}| \quad \text{for } i = 1, \dots, n$$

with strict inequality for at least one i .

2.2. Pricing Financial Derivatives

Financial derivatives are instruments whose value is dependent on the performance of underlying assets such as stocks, bonds, commodities, or market indices. The pricing of these derivatives is a pivotal concept in financial mathematics and risk management, involving complex models and theoretical frameworks.

2.2.1. Risk-Neutral Valuation and the Market Price of Risk

Let us introduce a critical concept in derivative pricing, known as the risk-neutral valuation [18]. This principle suggests that in the valuation of derivatives we can assume investors are risk-neutral. In such a framework, investors do not demand higher expected returns for taking more risk. We name this hypothetical world where investors are risk-neutral a 'risk-neutral world'. In reality, our world is not risk-neutral; investors typically seek higher expected returns for taking higher risks. Using this risk-neutral assumption leads to accurate derivative pricing for both our actual world and a risk-neutral one. This approach conveniently deals with the challenge of determining the risk aversion levels participants in the financial market. Risk-neutral valuation may appear counter-intuitive. Given the inherent risks in options, should not individual risk preferences influence their pricing? Surprisingly, when pricing options relative to the underlying stock's price, the risk preferences of investors become irrelevant. As investors grow more risk-averse, stock prices may fall, but the relationship between stock prices and option prices remains constant. A risk-neutral world simplifies derivative pricing through two key characteristics [18]:

1. The expected return on any investment, such as stocks, aligns with the risk-free rate interest rate.
2. The discount rate used for calculating the present value of an expected payoff of a financial derivative is also the risk-free rate.

The term that connects the real world with the risk-neutral world is called the market price of risk. It represents the additional return that investors require to compensate for the extra risk above the risk-free rate. Mathematically, the market price of risk is used to transform the dynamics of asset prices from their real-world expectations to those under risk-neutral conditions. It adjusts the drift dynamics of asset prices in stochastic models, to equal the expected return with the risk-free rate. This transformation is essential in implementing risk-neutral valuation, as it enables the use of risk-neutral probabilities in pricing derivatives, ensuring that the prices are consistent with the no-arbitrage principle. Girsanov's Theorem (2.1) is fundamental in shifting from real-world probability measure \mathbb{P} to risk-neutral measure \mathbb{Q} in financial modeling, especially for risk-neutral valuation of derivatives. It modifies asset price dynamics, changing from a model incorporating a risk premium under \mathbb{P} to one reflecting growth at the risk-free rate under \mathbb{Q} . This transformation aligns asset returns with the risk-free rate, crucial for no-arbitrage derivative pricing. Girsanov's Theorem also aids in determining the market price of risk, showing how much extra return investors require for additional risk. Its application simplifies derivative pricing and deepens understanding of market dynamics and risk preferences, making it a key component in modern financial theory.

2.2.2. Option Theory

Financial derivatives are instruments that are based on the value of an underlying asset. Common types are options, which are differentiated between call and put options. A call option gives the owner the right to buy the underlying asset for a predetermined amount, K , whereas a put option gives the owner the right to sell the underlying asset for a predetermined amount. We can also distinct between European and American style options. European type options can only be exercised at the maturity time $t = T$, while, on the other hand American style options can be exercised at any time $t \leq T$. A European call option is exercised when the asset's price at maturity $S(T)$ exceeds the strike price K , leading to a profit of $S(T) - K$ as the asset can be immediately sold in the market. Conversely, if $S(T) \leq K$, the call option is not exercised and becomes valueless, as the asset could be bought for less than K in the market. For a put option this is exactly the other way around. So we can define the following payoff function, $V_c(T, S)$ for the call option on an underlying asset S , strike price K and maturity time T as

$$V_c(T, S(T)) = \max\{S(T) - K, 0\}$$

For a put option we have

$$V_p(T, S(T)) = \max\{K - S(T), 0\}$$

Figure 2.2 shows the diagram of the payoff of a call and a put option.

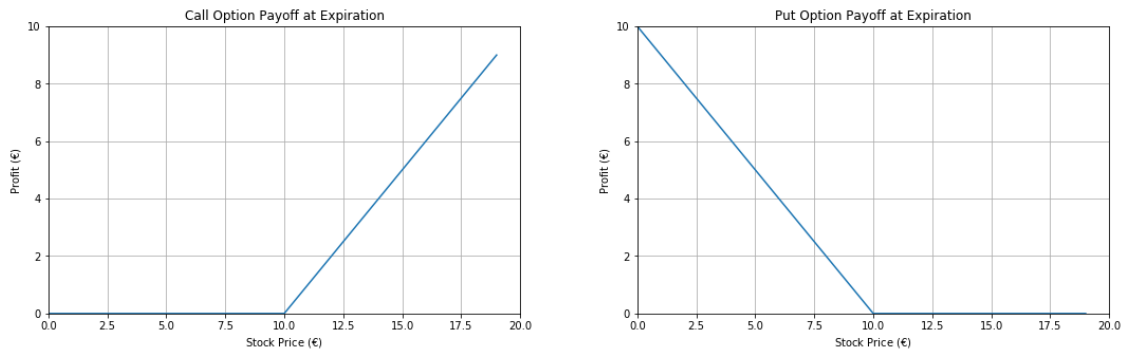


Figure 2.2: The payoff diagram of a call option (left) and a put option (right) with strike price $K = 10$

2.2.3. Black Scholes

One of the most fundamental models in derivative pricing is the Black-Scholes model [7]. Developed by Fischer Black, Myron Scholes, and Robert Merton in the early 1970s, this model provides a mathematical framework for estimating the price of European-style options. It revolutionized the field by offering a closed-form solution for options pricing, which was previously not available. The Black-Scholes model is predicated on several assumptions: the markets are efficient, the underlying asset's price follows a log-normal distribution [1], stock pays no dividends, there are no transaction costs, and the risk-free rate is constant. Moreover, the expected rate of return of the underlying asset is adjusted to be the risk-free rate, so the derivation of the Black-Scholes PDE involves changing the probability measure of the asset dynamics from the real-world measure \mathbb{P} to the risk-neutral measure \mathbb{Q} :

$$\text{Stock Price dynamics under } \mathbb{P}: dS_t = \mu S_t dt + \sigma S_t dW_t$$

$$\text{Stock Price dynamics under } \mathbb{Q}: dS_t = r S_t dt + \sigma S_t d\tilde{W}_t$$

Under risk-neutral measure \mathbb{Q} , the formula for an European call option is given by ([7]):

$$V_c(t, S(t)) = S(t)N(d_1) - Ke^{-r(T-t)}N(d_2)$$

$$d_1 = \frac{\ln\left(\frac{S(t)}{K}\right) + \left(r + \frac{\sigma^2}{2}\right)(T-t)}{\sigma\sqrt{T-t}}$$

$$d_2 = d_1 - \sigma\sqrt{T-t}$$

The formula takes into account the current price of the underlying asset S , the option's strike price K , the time to expiration $(T - t)$, the risk-free rate r , and the volatility σ of the underlying asset. $N(\cdot)$ denotes the cumulative distribution function of the standard normal distribution [1].

This model is especially noted for its role in the development of the options market, as it provides a standardized method to price options, enabling traders to estimate the fair value of options contracts. To better describe the dynamics of the option price over time, the Black-Scholes PDE was found:

$$\frac{\partial V}{\partial t} + rS \frac{\partial V}{\partial S} + \frac{1}{2} \sigma^2 S^2 \frac{\partial^2 V}{\partial S^2} - rV = 0.$$

The derivation of this formula can be found in appendix A. Let us break down each term from a mathematical perspective:

- $\frac{\partial V}{\partial t}$: The time derivative of the option price V , capturing how its value diminishes as expiration approaches, known as 'time decay'.
- $rS_t \frac{\partial V}{\partial S_t}$: The product of the risk-free rate r , stock price S_t , and the rate of change of V with respect to S_t , representing the option's delta (Δ) [18]. From a mathematical point of view this is a convection term (first-order derivative), which is related to the systematic or directional movement of the quantity being modeled.
- $\frac{1}{2} \sigma^2 S^2 \frac{\partial^2 V}{\partial S^2}$: This term is the most complex and significant part of the equation. It represents the option's gamma (Γ) [18], which is the rate of change of the option's delta with respect to the underlying asset's price. The term includes the variance of the underlying asset σ^2 , and S_t^2 , indicating the option's sensitivity to movements in S_t . From a mathematical perspective this is a diffusion term (second-order derivative), which is linked to random fluctuations, uncertainty, or risk, and it captures the dispersion of values over time.
- $-rV$: Represents the financing cost of holding the option.
- $= 0$: Aligns with the no-arbitrage principle, ensuring the option is priced to prevent risk-free profit opportunities.

Let us now look at figures (2.3), (2.4) and (2.5) below. On the left we have generated the same asset paths, S_t , for different values of the parameters r and σ and on the right we show the option value for different values of time t and asset S_t . Figures (2.3) and (2.4) capture the impact of the volatility parameter σ . We can see that with a higher volatility σ , the option value V increases. Especially for options that are 'out-of-the-money' (OTM), where $S_t - K < 0$, as they have a larger chance of becoming profitable. Furthermore, when σ increases, the diffusion term, $\frac{1}{2} \sigma^2 S^2 \frac{\partial^2 V}{\partial S^2}$ becomes more significant. This will contribute to a higher option price due to increased market uncertainty and risk premium. Generally, near expiration options depreciate in value over time, but a higher volatility can counteract this effect by maintaining or increasing their value. In figures (2.4) and (2.5) we can see the effect of the risk-free interest parameter r . An increase in r has a nuanced effect on option prices. For call options, as in our case, a higher r generally leads to increased prices due to a rise in the cost of carry, making the option to buy the underlying asset more attractive. For put options it will be the other way around. Additionally, the increased r enhances the present value of the option's payoff due to the discounting effect, which influences its overall price. But the impact of r also varies based on the strike price, and time to expiration. For example, deep in-the-money (ITM), $S_t > K$, call options might see a bigger price increase with bigger r compared to OTM call options. Also, options with a longer time to maturity are more sensitive to changes in r than short-term options because they have more time for compounding.

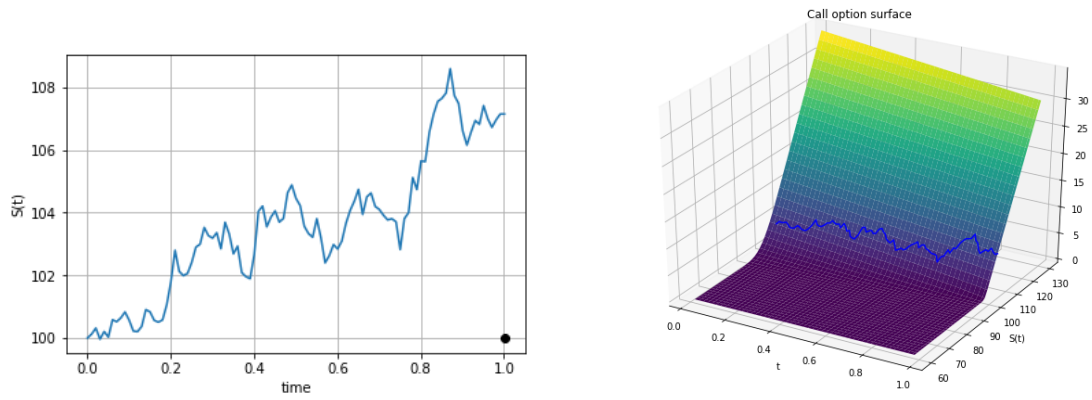


Figure 2.3: Stock price and call option value. Parameters: $S_0 = 100, K = 100, r = 0.05, \sigma = 0.05$

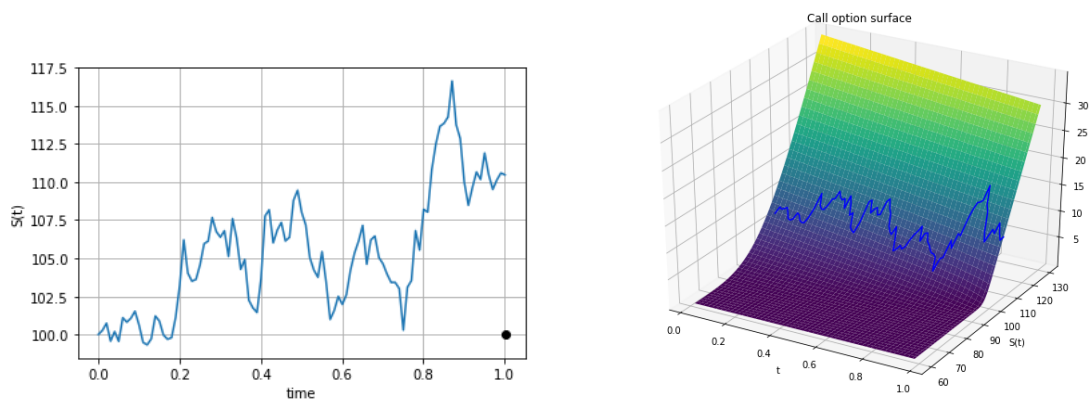


Figure 2.4: Stock price and call option value. Parameters: $S_0 = 100, K = 100, r = 0.05, \sigma = 0.2$

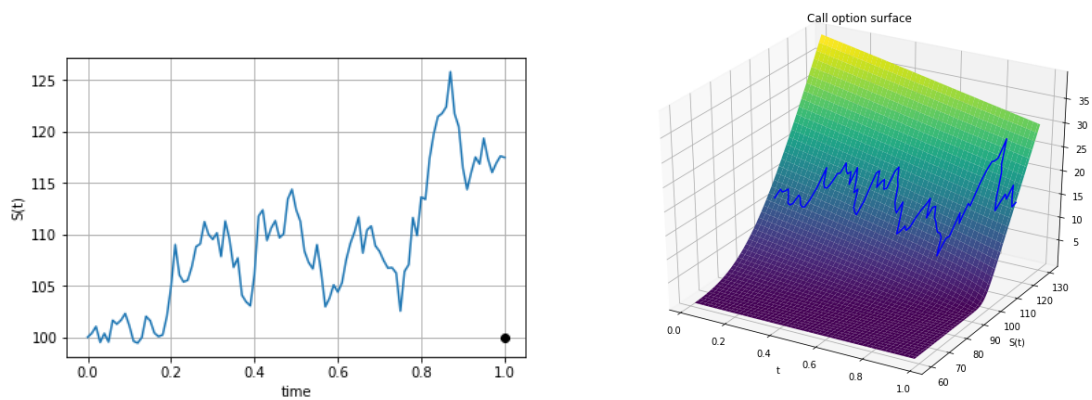


Figure 2.5: Stock price and call option value. Parameters: $S_0 = 100, K = 100, r = 0.1, \sigma = 0.2$

Another common type of option is the following, the barrier option.

Definition 15 *Barrier options are a type of exotic options [18] where the payoff depends on whether the underlying asset's price reaches a certain level (the barrier) during the life of the option.*

A barrier option can be categorized as either a knock-out or knock-in type, or a combination of these. In the case of a knock-out barrier option, the option becomes worthless if the underlying asset reaches

a specified price level, the barrier. This caps the potential gains for the holder and limits the losses for the issuer of the option. Alternatively, in a knock-in barrier option, the contract initially holds no value and only becomes valuable when the underlying asset reaches the specified price level. In this thesis we will use a double knock-out barrier option to describe the coupon value that green bond investors receive over time. In section 2.4 we will further describe how this mechanism can incentivize green bond issuers to perform well.

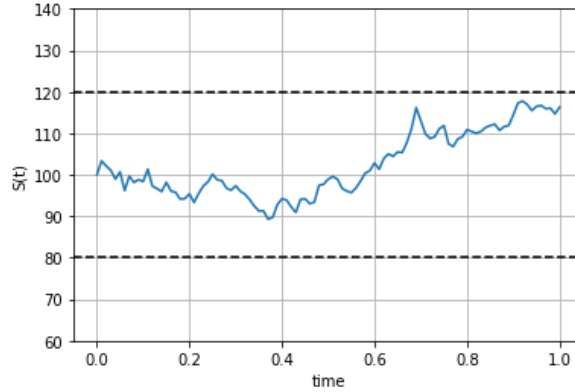


Figure 2.6: Stock price path and two barriers

2.2.4. Short Rates

Short rate models are fundamental in bond pricing, offering a comprehensive framework for understanding bond value fluctuations over time. They play a crucial role in modeling the interest rate, which is a fundamental in determining the present value of a bond’s future cash flows: the coupon payments and the face value repayment. Additionally, they exhibit an inverse relation with bond prices, as explained by [6]. When interest rates experience an increase, bond prices generally decline, and conversely, when interest rates decrease, bond prices tend to rise. For instance, assume we have a bond that has been issued with a fixed coupon rate. When market interest rates increase, new bonds are issued with higher coupon rates, which reduces the attractiveness of older bonds with lower coupons. To account for the lower coupon rate, the price of the older bond decreases. Conversely, in the scenario of falling market interest rates, the older bond’s higher coupon rate becomes more appealing, resulting in an increase in its price compared to newer bonds with lower coupon rates. This is a measure of a bond’s sensitivity to interest rate changes. A bond with a longer duration is more sensitive to interest rate shifts. Traditionally, interest rates are often modeled as deterministic functions of time:

1. Constant Deterministic Short Rate ($r > 0$):

In this scenario, where the short rate is a constant r , the bond price $B(t, T)$ must fulfill the equation $e^{r(T-t)} B(t, T) = B(T, T) = 1$. Consequently, this results in

$$B(t, T) = e^{-r(T-t)}, \quad 0 \leq t \leq T.$$

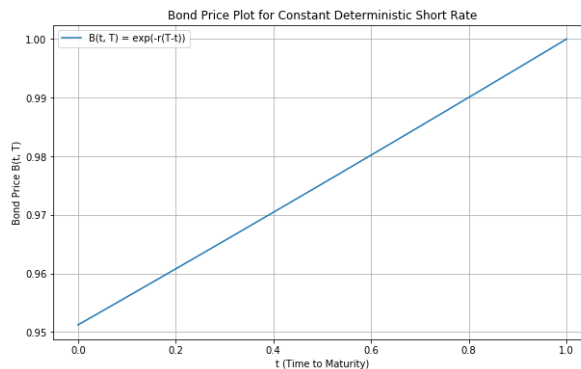


Figure 2.7: Bond price for constant short rate r

2. Time-dependent Deterministic Short Rate (r_t):

When the short rate r_t varies with time but is deterministic, the bond price $B(t, T)$ is shown to be

$$B(t, T) = e^{-\int_t^T r_s ds}, \quad 0 \leq t \leq T.$$

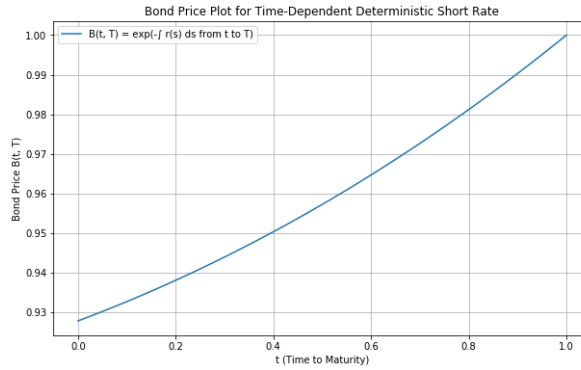


Figure 2.8: Bond price for time-dependent short rate r

but this approach is expanded in more sophisticated models where rates are represented by a stochastic instantaneous short-rate process r_t .

3. Stochastic Short Rate model r_t :

These models are represented by the following stochastic differential equation:

$$dr_t = m(t, r_t)dt + n(t, r_t)dW_t,$$

where $m(t, r_t)$ and $n(t, r_t)$ are the drift and the diffusion term of the short rate process, respectively, and W a Brownian Motion. In 1997, Vašiček [31] proposed that the real-world instantaneous spot rate follows an Ornstein-Uhlenbeck process with constant coefficients, described as

$$dr_t = \alpha(\beta - r_t)dt + \sigma dW_t,$$

where β represents the long-term mean of the short rate, α is the reversion rate parameter and σ the overall level of the volatility. In this model, a notable characteristic is its tendency for mean reversion. This means that when the short rate becomes larger than the long-term average ($r_t > \beta$), the drift becomes negative and will drive the short rate back to the long-term mean with rate α . On the other hand, when the short rate falls below the long-term mean ($r_t < \beta$), the drift term becomes positive, and elevates the short rate back to β again. The value of α indicates the speeds of this adjustment towards the long-term mean.

Another important model to describe the short rate is the Cox-Ingersoll-Ross (CIR) [11] model

$$dr_t = \alpha(\beta - r_t)dt + \sigma\sqrt{r_t}dW_t$$

We can see it has the same drift factor, $\alpha(\beta - r_t)$ as in the Vašiček model, signifying mean reversion towards the long-term mean β . However, in this model the diffusion term σ is multiplied with $\sqrt{r_t}$, which precludes negative values for r_t : As the interest rate nears zero, the volatility term $\sigma\sqrt{r_t}$ also approaches zero, negating randomness and keeping the rate non-negative. High short rates correspond to increased volatility, which is a desired property. When $2\alpha\beta \geq \sigma^2$, Feller proved that this guarantees a strictly positive short rate ($r_t > 0$) [11]. When we change to risk-neutral measure, \mathbb{Q} , following Girsanov's Theorem we obtain the following SDE for Vašiček

$$dr_t = (\alpha(\beta - r_t) - \lambda_r\sigma)dt + \sigma d\tilde{W}_t,$$

and for CIR

$$dr_t = (\alpha(\beta - r_t) - \lambda_r\sigma\sqrt{r_t})dt + \sigma\sqrt{r_t}d\tilde{W}_t,$$

where in both models the constant λ_r represents the market price of risk. Let us now look at the parameters α , β , σ and λ_r and the effect they have on the two short rate models. In figures (2.9)-(2.15), we plotted both models with the same parameters setting and the same randomness W_t . We observe that the short rate under the Vašiček model can become negative and that the damping factor $\sqrt{r_t}$ has significant effect on the volatility factor in the CIR model. In figure 2.14, we can see that when α is increased, the variation of the short rate decreases.

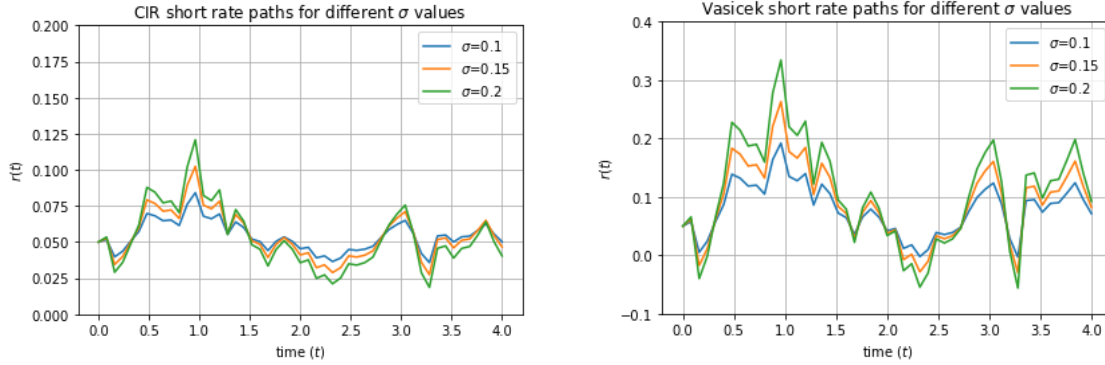


Figure 2.9: CIR (left) and Vašiček (right) short rate paths for different values of σ

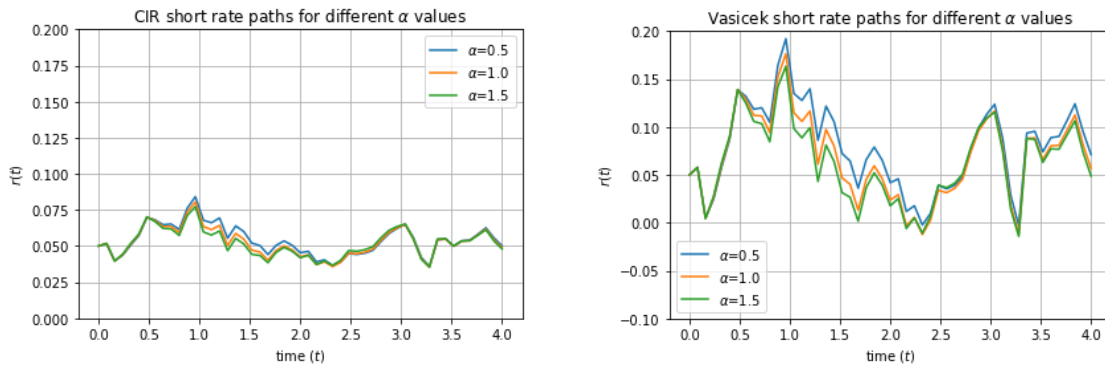


Figure 2.10: CIR (left) and Vašiček (right) short rate paths for different values of α

The change in β by ϵ in the Vašiček model gives

$$r(t_{i+1}) = r(t_i) + \alpha(\beta + \epsilon - r(t_i))\Delta t + \sigma\sqrt{\Delta t}W_{i+1}$$

and for the CIR model

$$r(t_{i+1}) = r(t_i) + \alpha(\beta + \epsilon - r(t_i))\Delta t + \sigma\sqrt{r(t_i)}\sqrt{\Delta t}W_{i+1}$$

So for both models this results in a similar change in the short rate of $\epsilon\alpha\Delta t$ (figure 2.15).

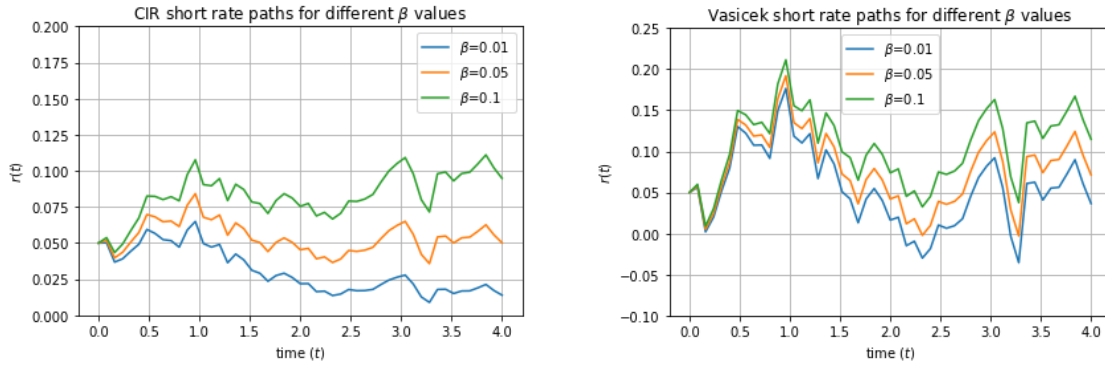


Figure 2.11: CIR (left) and Vašiček (right) short rate paths for different values of β

An other interesting short rate model is the Hull-White [17] model, where parameter β becomes time dependent, $\beta(t)$. In this thesis we will mainly focus on the CIR model but also make some comparisons with the Vašiček model.

2.3. Conventional Bond

In this section we will derive and analyse the pricing model of a conventional bond. It is important to recognize that a coupon-bearing bond can be decomposed as a portfolio of zero-coupon bonds [20]. Each coupon payment can be treated as a zero-coupon bond maturing at its respective payment date. So for a coupon bearing bond $B_c(t, r; T)$ maturing at T with cash flows CF_i at times t_i for $i = 1, 2, \dots, n$, where $t_1 \leq t_2 \leq \dots \leq t_n = T$ we can decompose it as

$$B_c(t, r; T) = \sum_{i=1}^n CF_i \times B(t, r; t_i)$$

2.3.1. Derivation of Pricing Model

In this section, we will derive the partial differential equation for a zero-coupon bond. We start by examining the dynamics of bond prices and their dependence on the short rate, which follows an Ito process. This approach allows us to express bond price changes in terms of drift and volatility components. Utilizing the no-arbitrage argument, we explore how bond prices are influenced by the market price of risk associated with the short rate, which is not a traded security. Our analysis further includes the transformation of the bond price under the real world probability measure \mathbb{P} to the risk-neutral probability measure \mathbb{Q} [3], assuming the bond price only depends on the short rate. Employing Itô's lemma (Lemma 1), we derive the dynamics of the bond price and align it with the initial bond price equation. This alignment helps us determine the drift rate and volatility of the bond price process. We also construct a portfolio consisting of bonds with different maturities and demonstrate how it can be hedged against interest rate risks. This leads to a conclusion about the market price of risk being consistent across different bond maturities, a key concept in a no-arbitrage market. We will follow the derivation as in [20]. So let us start with the following dynamics for a bond price:

$$dB = \mu_B(t, r)Bdt + \sigma_B(t, r)BdW_t \quad (2.5)$$

In the following equation we have a general SDE for the short rate r_t , which is an Itô process:

$$dr_t = m(t, r_t)dt + n(t, r_t)dW_t, \quad (2.6)$$

Here, dW_t represents the differential of the Wiener process, $m(t, r_t)$ the drift and $n(t, r_t)$ volatility of the short rate. We are going to derive the bond's PDE using the principle of no arbitrage. Given that the short rate is not a tradable asset, it is expected that the PDE equation will include the market price of risk in the short rate r_t . We will represent the bond price through the expected value under the real-world probability measure and subsequently derive the Radon–Nikodym derivative [3]. This derivative plays a important role in the shift from the real-world probability measure to the risk-neutral measure.

We assume that the bond value $B(t, r_t)$ is not influenced by other external factors such as default risk, liquidity, or other external variables. By the use of Itô's lemma 1 we obtain the following dynamics for $B(t, r)$

$$dB(t, r) = \frac{\partial B}{\partial t} dt + \frac{\partial B}{\partial r} dr_t + \frac{\partial^2 B}{\partial r^2} (dr_t)^2 \quad (2.7)$$

Now we fill in equation 2.6 and use Itô's table (2.1) to obtain:

$$dB(t, r) = \left(\frac{\partial B}{\partial t} + m(t, r_t) \frac{\partial B}{\partial r} + \frac{1}{2} n(t, r_t)^2 \frac{\partial^2 B}{\partial r^2} \right) dt + n(t, r_t) \frac{\partial B}{\partial r} dW_t. \quad (2.8)$$

The original equation 2.5 must match this SDE exactly:

$$dB = \mu_B(t, r) B dt + \sigma_B(t, r) B dW_t, \quad (2.9)$$

Setting the drift and diffusion coefficients equal we obtain the following drift rate $\mu_B(t, r)$ and volatility $\sigma_B(t, r)$ of the bond price:

$$\mu_B(t, r) B = \left(\frac{\partial B}{\partial t} + m \frac{\partial B}{\partial r} + \frac{1}{2} n^2 \frac{\partial^2 B}{\partial r^2} \right), \quad (2.10)$$

$$\sigma_B(t, r) B = n \frac{\partial B}{\partial r}. \quad (2.11)$$

Now we are going to construct a portfolio of two bonds. We buy one with value V_1 and maturity T_1 , and sell the second with value V_2 and maturity T_2 . We obtain the following portfolio denoted by Π :

$$\Pi = V_1 - V_2. \quad (2.12)$$

Denote now $\mu_B(t, r; T_i) := \mu_{B_i}$ and $\sigma_B(t, r; T_i) = \sigma_{B_i}$, for $i = 1, 2$. The variation in portfolio value over a time interval dt , by looking at the bond price dynamics in equation 2.8, is as follows:

$$d\Pi = (V_1 \mu_{B_1} - V_2 \mu_{B_2}) dt + (V_1 \sigma_{B_1} - V_2 \sigma_{B_2}) dW_t. \quad (2.13)$$

We choose V_1 and V_2 such that

$$V_1 = \frac{\sigma_{B_2}}{\sigma_{B_2} - \sigma_{B_1}} \cdot \Pi, \quad (2.14)$$

$$V_2 = \frac{\sigma_{B_1}}{\sigma_{B_2} - \sigma_{B_1}} \cdot \Pi, \quad (2.15)$$

Consequently, because the stochastic term in $d\Pi$ disappears, we arrive at

$$\frac{d\Pi}{\Pi} = \frac{\mu_{B_1} \sigma_{B_2} - \mu_{B_2} \sigma_{B_1}}{\sigma_{B_2} - \sigma_{B_1}} dt. \quad (2.16)$$

Given that the portfolio does not include risk, to preclude any arbitrage possibilities, it is required to earn the risk-free short rate such that

$$d\Pi = r \Pi dt. \quad (2.17)$$

Combining these two equations, we obtain:

$$\frac{\mu_{B_1} - r}{\sigma_{B_1}} = \frac{\mu_{B_2} - r}{\sigma_{B_1}}. \quad (2.18)$$

The stated equation is true for any maturity dates T_1 and T_2 , indicating that the expression $\frac{\mu_B(t, r) - r}{\sigma_B(t, r)}$ does not depend on maturity T . Let us define this common ratio as $\lambda(t, r)$, expressed as:

$$\frac{\mu_B(r, t) - r}{\sigma_B(r, t)} = \lambda(t, r). \quad (2.19)$$

This term, $\lambda(t, r)$, is the market price of risk for the short rate. It represents the additional expected return per extra unit of risk for a bond. In a no-arbitrage market, all hedgeable bonds, regardless of their maturities, should share this common market price of risk.

If we substitute $\mu_B(t, r)$ and $\sigma_B(t, r)$ into the equation above, we obtain the following governing differential equation for the price of a zero-coupon bond:

$$\frac{\partial B}{\partial t} + (m(t, r_t) - \lambda(t, r_t)n(t, r_t))\frac{\partial B}{\partial r} + \frac{1}{2}n(t, r_t)^2\frac{\partial^2 B}{\partial r^2} - rB(t, r) = 0, \quad t < T, \quad (2.20)$$

with final condition: $B(T, T) = 1$. If we have a known drift $m(t, r_t)$ and diffusion coefficient $n(t, r_t)$, we would still need an estimate for the λ_t to use this PDE. If the equation is not formulated this way, it becomes unusable. Moreover, it is important to observe that in this PDE, the coefficient of $\frac{\partial B}{\partial r}$ acts similar to the risk-adjusted drift in the dynamics of the short rate. Essentially, this is the same as using the drift component from the short-rate dynamics under the risk-neutral measure \mathbb{Q} . By applying Girsanov's theorem to equation 2.6, and transitioning from the Wiener process W_t under measure \mathbb{P} to the risk-neutral measure \mathbb{Q} , we derive a new SDE for r_t :

$$dr_t = (m(t, r_t) - \lambda(t, r)n(t, r_t))dt + n(t, r_t)d\tilde{W}_t \quad (2.21)$$

Here, the drift in the SDE is adjusted to account for short rate risk. When transitioning the bond price drift from $\mu(\cdot)$ to r_t , it becomes essential to shift the dynamics of the short rate from $m(t, r_t)$ to $(m(t, r_t) - \lambda(t, r)n(t, r_t))$. In this thesis, we will use the CIR model for the short rate:

$$dr_t = \alpha(\beta - r_t)dt + \sigma\sqrt{r_t}dW_t \quad (2.22)$$

We apply Girsanov's theorem and obtain the following short rate dynamics under the risk-neutral measure:

$$dr_t = (\alpha(\beta - r_t) - \lambda\sigma\sqrt{r_t})dt + \sigma\sqrt{r_t}d\tilde{W}_t \quad (2.23)$$

Consequently, we derive the PDE for the zero-coupon bond using the CIR model for the short rate:

$$\frac{\partial B}{\partial t} + (\alpha(\beta - r_t) - \lambda\sigma\sqrt{r_t})\frac{\partial B}{\partial r} + \frac{1}{2}\sigma^2r_t\frac{\partial^2 B}{\partial r^2} - rB(t, r) = 0, \quad t < T, \quad (2.24)$$

On the boundary $r_t = 0$ we solve the PDE

$$\frac{\partial B}{\partial t} + \alpha\beta\frac{\partial B}{\partial r} = 0, \quad t < T, \quad (2.25)$$

We know that when $r \rightarrow \infty$, the bond price $B \rightarrow 0$. But this is not practical if we retain r as the coordinate. In section 3 we will explain how to overcome this problem and how we can use $r_{\max} = 1.0$ as upper boundary.

A zero-coupon bond with Vařiřek as underlying short rate model would have the following PDE

$$\frac{\partial B}{\partial t} + (\alpha(\beta - r_t) - \lambda\sigma)\frac{\partial B}{\partial r} + \frac{1}{2}\sigma^2\frac{\partial^2 B}{\partial r^2} - rB(t, r) = 0, \quad t < T, \quad (2.26)$$

2.3.2. Parameter Analysis

In this section we will dive deeper into the bond's equation to better understand the effect of changes in its parameters from both an economical and mathematical point of view. We will only break down the bond's PDE with CIR as underlying short rate, because the PDE following from Vařiřek is very similar. We have the following PDE:

$$\frac{\partial B}{\partial t} + (\alpha(\beta - r_t) - \lambda\sigma\sqrt{r_t})\frac{\partial B}{\partial r} + \frac{1}{2}\sigma^2r_t\frac{\partial^2 B}{\partial r^2} - rB(t, r) = 0, \quad t < T, \quad (2.27)$$

- $\frac{\partial B}{\partial t}$: This is the time derivative of the bond price B. It captures the change in the bond's price as time progresses towards its maturity. In the context of bond pricing, this term often reflects the time decay or the reduction in the bond's price as it gets closer to its maturity, assuming other factors remain constant.
- $(\alpha(\beta - r_t) - \lambda\sigma\sqrt{r_t})\frac{\partial B}{\partial r}$: This term represents the combined effect of the mean reversion and the market price of risk on the rate of change of the bond price with respect to the interest rate (r). Here, $(\alpha(\beta - r_t))$ is the mean-reverting term, showing how the interest rate tends to revert to its long-term mean β at a speed determined by α . The term $\lambda\sigma\sqrt{r_t}$ adjusts this for the market price of risk, reflecting the additional return demanded by investors for bearing risk. This term can be seen as a "drift" term in the context of stochastic processes, indicating the systematic or directional movement of interest rates.

- $\frac{1}{2}\sigma^2 r_t^2 \frac{\partial^2 B}{\partial r^2}$: This term includes the variance of the interest rate (σ^2), which is a measure of its volatility, and its level (r_t). It measures the convexity of the bond's price in relation to the interest rate. In the context of bond pricing, this term is related to how the bond's sensitivity to interest rate changes (captured by the first derivative) as the interest rate itself changes. From a mathematical point of view, this is a diffusion term, capturing the random fluctuations and uncertainty in interest rates over time.
- $-rB(t, r)$: This term represents the cost of holding the bond. Regarding of bond pricing, this concept can be seen as the potential missed return from choosing to invest in the bond rather than investing the same amount in the risk-free interest rate.
- $= 0$: The equation equating to zero aligns with the no-arbitrage principle in financial mathematics, ensuring that the bond is priced in a way that prevents risk-free profit opportunities.

In figure 2.12 we can see the valuation of a coupon bond, with $FV = 1$, maturity $T = 4$ and 5% coupons paid every year under the two different short rate models. On the right we extended the short rate domain to include negative values for the bond valuation under the Vašiček short rate model. In section 2.2.4 we already learned about the inverse relationship between bond prices and short rates, which can be seen clearly in both graphs.

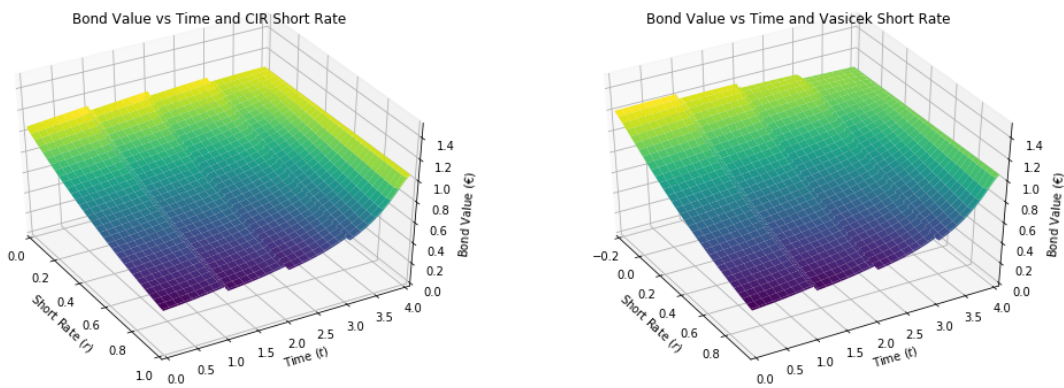


Figure 2.12: Value of a Coupon Bond, CIR model (left) and Vašiček model (right), $\alpha = 1.0$, $\beta = 0.05$, $\sigma_r = 0.15$, $\lambda_r = 0.01$, $T = 4$

For the following analyses, we decompose the coupon bond into zero-coupon bonds and analyse the Face Value of 1 that has to be paid back at $T = 4$. Let us start looking at the effect the volatility of the short rate, σ_r , has on the bond's price, for both models (figure 2.13). We can see that for both models, a higher σ_r consistently leads to an increase in bond price over the whole period. This effect is less pronounced when we look at the valuation under the CIR model, due to the extra $\sqrt{T_t}$ in the diffusion term. This increase in the value of the bond as the volatility rises, reflects the market's demand for higher returns to compensate for the increased risk.

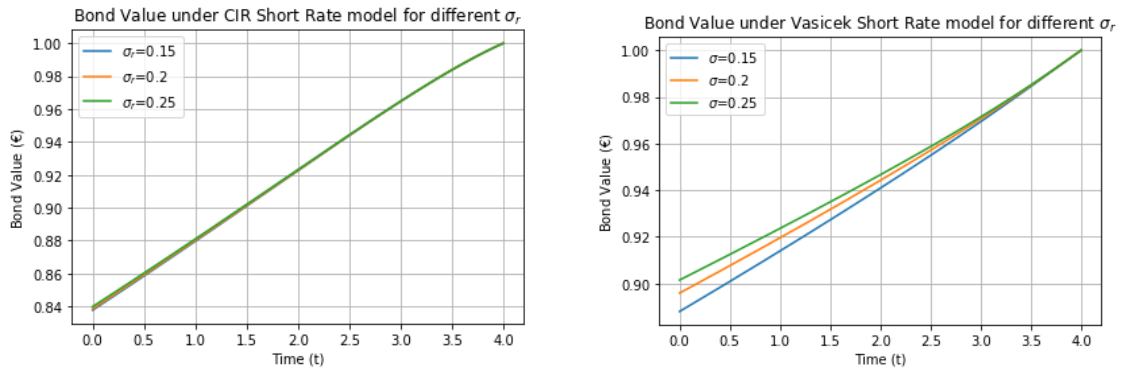


Figure 2.13: Value of a Coupon Bond, CIR model (left) and Vašiček model (right), $\alpha = 1.0$, $\beta = 0.05$, $\lambda_r = 0.01$, $T = 4$

Now, let us consider the speed of mean reversion parameter, α . For both models we obtain similar spreads for different values of α (figure 2.14). However, we can see that the value of the bond under the Vašíček model starts a bit higher, which comes from the possibility of having negative short rates. Furthermore, with a smaller α the probability of having smaller short rates becomes higher and drives up the value of the bond for both models.

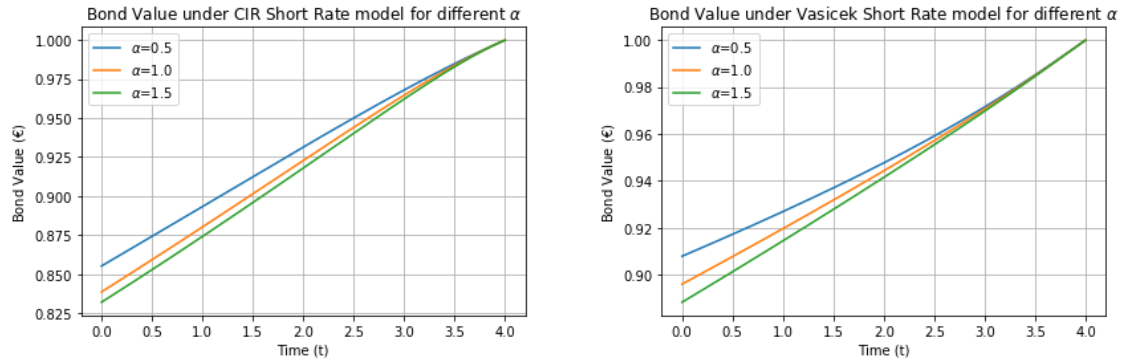


Figure 2.14: Value of a Coupon Bond, CIR model (left) and Vašíček model (right), $\beta = 0.05$, $\sigma_r = 0.15$, $\lambda_r = 0.01$, $T = 4$

In figure 2.15 we see that different values for the long-term mean, β , show similar results in both models. Important to notice is the big spread at $t = 0$, due to the anticipated future short rate increases/decreases.

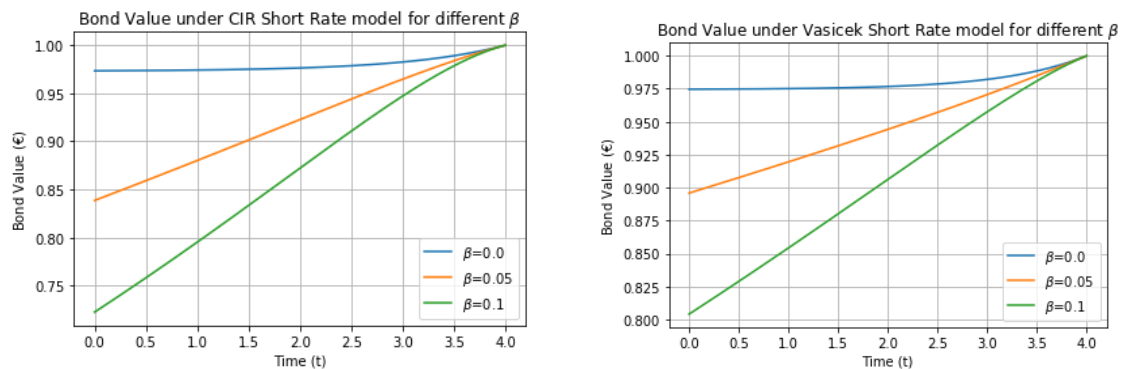


Figure 2.15: Value of a Coupon Bond, CIR model (left) and Vašíček model (right), $\alpha = 1.0$, $\sigma_r = 0.15$, $\lambda_r = 0.01$, $T = 4$

Now, let us look at how this market price of risk in the short rate parameter, λ_r , influences the bond's value. We can see that in both models, a more negative λ_r leads to a lower bond value (figure 2.16). This is in line with the fact the investors require more compensation for taking additional risk, which generally translates into a lower price for the bond.

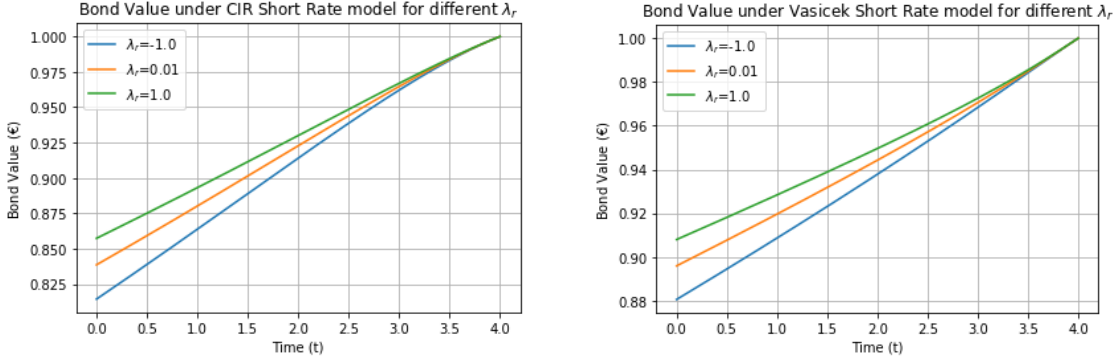


Figure 2.16: Bond Value over time, CIR model (left) and Vašiček model (right), $\alpha = 1.0$, $\beta = 0.05$, $\sigma_r = 0.15$, $T = 4$

2.4. Green Bond

In this section, we will develop a model for a green bond. As already stated, green bonds are specifically designed to finance projects that have a positive environmental effect, differentiating them from conventional bonds. A green bond does not only depend on the traditional financial metrics such as the short rate, but also on environmental factors. An important indicator of environmental impacts in the economy is the carbon price, primarily realized through the Emission Trading System (ETS). Our model for the green bond will be structured to incorporate the carbon price, such that it dynamically responds to environmental factors. By doing so, the model aligns the financial performance of the bond with its environmental impact, highlighting the green bond's significant role in promoting sustainable investment practices [22].

2.4.1. Carbon Pricing

Carbon pricing, also known as CO₂ pricing, is a strategy adopted by nations to combat climate change. It involves imposing a cost on greenhouse gas emissions, primarily from burning coal, oil, and gas, which are significant contributors to climate change. The idea is to motivate emitters to reduce their use of these fossil fuels [9]. This approach is broadly recognized and deemed efficient because it tackles the issue of emissions being a negative externality, meaning they cause harm without being directly priced in the market. There are typically two forms of carbon pricing: a carbon tax or a Cap-and-Trade system, often implemented through an Emissions Trading Scheme (ETS) [21]. This mechanism requires emitters to buy allowances for their emissions. Many economists consider carbon pricing the most cost-effective method for reducing emissions. It aims to minimize the costs associated with emission reduction, including both direct costs and the indirect inconvenience of using fewer fossil fuel-based goods and services. Economics suggests that command and control regulation, where the regulator decides who can emit and who cannot, is less efficient than market-based approaches like carbon pricing [29]. This inefficiency stems from the regulator's difficulty in accurately valuing each emitter's benefit from their emissions. In a Cap-and-Trade system, a market for permits helps set the carbon price to ensure compliance with an established emissions cap. The government sets this cap (e.g., 1000 tCO₂ per year) and then distributes allowances, either freely or through auction. These credits can then be traded privately and the price of these fluctuate in response to environmental changes: When fossil fuel use and emissions decrease, driven by efforts in environmental sustainability, this typically leads to lower demand for carbon credits in a Cap-and-Trade system, and consequently, a decrease in carbon prices. On the other hand, worsening environmental conditions and increased emissions push up the demand and price of carbon credits and [22] shows that higher levels of carbon price can stimulate the advancement of innovative green technologies and enhance the efficiency of emission reductions. This responsiveness makes carbon pricing a valuable indicator of environmental health, signaling the effectiveness of climate change mitigation efforts.

2.4.2. Pricing Model

In this section, we develop a model that represents the (floating) coupon rate of a green bond based on both the short rate and the carbon price. To develop this model we used the double barrier mechanism from [35] and combine this with the derivation of the PDE in [34]. The model dynamically adjusts the coupon rate in response to fluctuations in the carbon price by utilizing the mechanics of a European double knock-out option on this carbon price. By aligning the coupon rate with environmental performance, our model meets the increasing demand for sustainable investments, integrating financial returns with environmental sustainability.

In our model, we consider that the short rate, r_t , follows the CIR model with the specified stochastic differential equation, and the carbon price, c_t , is modeled using a geometric Brownian motion, as described by the following equations:

$$dr_t = \alpha(\beta - r_t)dt + \sigma_r\sqrt{r_t}dW_t^r, \quad (2.28)$$

$$dc_t = \mu c_t dt + \sigma_c c_t dW_t^c, \quad (2.29)$$

where W_t^r and W_t^c are Brownian motions, with $dW_t^c dW_t^r = \rho dt$. Here, α , β , σ_r , and σ_c are positive constants, and ρ and μ can either be positive or negative constants. As previously discussed, under CIR, the standard deviation factor $\sigma\sqrt{r_t}$ avoids the possibility of negative interest rates. In our model, after each year, a coupon payment is made, the amount of which is determined by the prevailing coupon

rate. The present value of these coupon payments in the i 'th year is represented by $V_i(t, r, c)$. In order to simplify notation while deriving our model just write V for $V_i(t, r, c)$. We follow [5] and apply Itô's lemma, to obtain

$$\frac{dV}{V} = k(t, r, c)dt + s_1(t, r, c)dW_t^c + s_2(t, r, c)dW_t^r,$$

where

$$k(t, r, c) = \frac{1}{V} \left(\frac{\partial V}{\partial t} + \mu c \frac{\partial V}{\partial c} + \alpha(\beta - r) \frac{\partial V}{\partial r} + c\rho\sigma_c\sigma_r\sqrt{r} \frac{\partial^2 V}{\partial r \partial c} + \frac{1}{2}\sigma_c^2 c^2 \frac{\partial^2 V}{\partial c^2} + \frac{1}{2}\sigma_r^2 r \frac{\partial^2 V}{\partial r^2} \right),$$

$$s_1(t, r, c) = \frac{1}{V} \sigma_c c \frac{\partial V}{\partial c}, \quad s_2(t, r, c) = \frac{1}{V} \sigma_r \sqrt{r} \frac{\partial V}{\partial r}.$$

Now, we consider forming a portfolio P by investing amounts x_1, x_2, x_3 in bonds of maturities t_1, t_2 , and t_3 , respectively. Then, the rate of return on the portfolio will be free-risk,

$$\frac{dP}{P} = rdt$$

such that we have

$$\begin{aligned} x_1 k(t_1) + x_2 k(t_2) + x_3 k(t_3) &= r, \\ x_1 s_1(t_1) + x_2 s_1(t_2) + x_3 s_1(t_3) &= 0, \\ x_1 s_2(t_1) + x_2 s_2(t_2) + x_3 s_2(t_3) &= 0. \end{aligned} \tag{2.30}$$

From 2.30 we can get

$$\begin{vmatrix} k(t_1) - r & k(t_2) - r & k(t_3) - r \\ s_1(t_1) & s_1(t_2) & s_1(t_3) \\ s_2(t_1) & s_2(t_2) & s_2(t_3) \end{vmatrix} = 0,$$

that is

$$k(t) - r = \lambda_c s_1 + \lambda_r s_2, \tag{2.31}$$

where $\lambda_r(t, r, c)$, $\lambda_c(t, r, c)$ are market prices of risk in the interest rate and the carbon price. We change from real world measure \mathbb{P} to risk-neutral measure \mathbb{Q} using Girsanov's theorem (2) on the SDE of the carbon price, and find

$$d\tilde{W}_t^c = \frac{\mu - \hat{r}_t}{\sigma_c} dt + dW_t^c.$$

This gives us

$$\lambda_c(t, r, c) = \frac{\mu - \hat{r}_t}{\sigma_c},$$

and

$$\begin{aligned} dc_t &= \mu c_t dt + \sigma_c c_t dW_t^c, && \text{under measure } \mathbb{P}, \\ dc_t &= \hat{r}_t c_t dt + \sigma_c c_t d\tilde{W}_t^c, && \text{under measure } \mathbb{Q}, \end{aligned}$$

Now we use Girsanov's theorem on the short rate r_t and obtain

$$\begin{aligned} dr_t &= \alpha(\beta - r_t)dt + \sigma_r \sqrt{r_t} dW_t^r, && \text{under measure } \mathbb{P}, \\ d\hat{r}_t &= [\alpha(\beta - \hat{r}_t) - \lambda_r \sigma_r \sqrt{\hat{r}_t}]dt + \sigma_r \sqrt{\hat{r}_t} d\tilde{W}_t^r, && \text{under measure } \mathbb{Q}, \end{aligned}$$

Substituting k, s_1, s_2, λ_1 and λ_2 into equation 2.31, we obtain the partial differential equation

$$\frac{\partial V}{\partial t} + (\mu c - \lambda_c \sigma_c c) \frac{\partial V}{\partial c} + (\alpha(\beta - r) - \lambda_r \sigma_r \sqrt{r}) \frac{\partial V}{\partial r} \tag{2.32}$$

$$+ \frac{1}{2} \left(\sigma_c^2 c^2 \frac{\partial^2 V}{\partial c^2} + \sigma_r^2 r \frac{\partial^2 V}{\partial r^2} + 2c\rho\sigma_c\sigma_r\sqrt{r} \frac{\partial^2 V}{\partial r \partial c} \right) - rV = 0, \tag{2.33}$$

This PDE shares similarities with the Black-Scholes PDE for pricing European call options on two assets [10]. Let us now consider the initial and boundary conditions for our PDE. The final condition at time $t = T_i$ for our model is defined by a European call option payoff. Our coupon rate is described

in percentages, so we will use percentage signs in the final and boundary conditions. Specifically, the coupon rate, at $t = T_i$ is given by $\max\{c_{T_i} - K, 0\}\% = (c_{T_i} - K)^+\%$ ($= 0.01 \cdot (c_{T_i} - K)^+$), where K represents the strike price associated with the carbon price, and c_{T_i} is the carbon price at maturity time T_i . We set the face value of the green bond equal to 1, such that the coupon rate directly translates to the coupon payment. For example, for a coupon rate of 5% ($= 0.05$), the coupon value is 0.05. Moreover, we introduce the following lower and upper barriers of the carbon price, c_{\min} and c_{\max} , where we define the coupon rate differently. At c_{\min} , the coupon rate is set to 0, reflecting the minimum incentive for emission reduction. Conversely, at c_{\max} , the coupon rate is set to $c_{\max} - K e^{-rt}$, aligning with extra incentive of emission reduction. For a bond, we know that when $r_t \rightarrow \infty$, that $B \rightarrow 0$. So we introduce a function $h_2(t, c)$ [28] such that we can handle this boundary condition with a much more realistic r_{\max} . For r_{\min} we introduce function $h_1(t, c)$ to have both boundaries aligned. These functions are only dependent on time t and carbon price c , allowing us to model the boundary conditions in a way that reflect the real-world dynamics of interest rates and carbon prices. Thus, on domain

$$D = \{(t, r, c) | 0 \leq t \leq T_i, \quad r_{\min} \leq r_t \leq r_{\max}, \quad c_{\min} \leq c_t \leq c_{\max}\},$$

the complete model for the coupon rate at time T_i becomes:

$$\frac{\partial V}{\partial t} + (\mu c - \lambda_c \sigma_c c) \frac{\partial V}{\partial c} + (\alpha(\beta - r) - \lambda_r \sigma_r \sqrt{r}) \frac{\partial V}{\partial r} + \frac{1}{2} \left(\sigma_c^2 c^2 \frac{\partial^2 V}{\partial c^2} + \sigma_r^2 r \frac{\partial^2 V}{\partial r^2} + 2c\rho\sigma_c\sigma_r\sqrt{r} \frac{\partial^2 V}{\partial r \partial c} \right) - rV = 0$$

$$\begin{cases} V_i(T_i, r, c) = (c_{T_i} - K_i, 0)^+\%, \\ V_i(t, r, c_{\min}) = 0, \\ V_i(t, r, c_{\max}) = (c_{\max} - K_i e^{-rt})\%, \\ V_i(t, r_{\min}, c) = h_1(t, c), \\ V_i(t, r_{\max}, c) = h_2(t, c), \end{cases}$$

where

1. $h_1(t, c)$ is obtained by solving the PDE:

$$\begin{cases} \frac{\partial V}{\partial t} + \frac{1}{2} \sigma_c^2 c^2 \frac{\partial^2 V}{\partial c^2} + (\mu c - \lambda_c \sigma_c c) \frac{\partial V}{\partial c} - r_{\min} V = 0, \\ V_i(t, r_{\min}, c_{\min}) = 0, \\ V_i(t, r_{\min}, c_{\max}) = (c_{\max} - K_i e^{-r_{\min} t})\%, \\ V_i(T_i, r_{\min}, c) = (c_{T_i} - K_i, 0)^+\% \end{cases}$$

2. Similarly, $h_2(t, c)$ is obtained by solving the PDE:

$$\begin{cases} \frac{\partial V}{\partial t} + \frac{1}{2} \sigma_c^2 c^2 \frac{\partial^2 V}{\partial c^2} + (\mu c - \lambda_c \sigma_c c) \frac{\partial V}{\partial c} - r_{\max} V = 0, \\ V_i(t, r_{\max}, c_{\min}) = 0, \\ V_i(t, r_{\max}, c_{\max}) = (c_{\max} - K_i e^{-r_{\max} t})\%, \\ V_i(T_i, r_{\max}, c) = (c_{T_i} - K_i, 0)^+\%. \end{cases}$$

Under the Vařiček model, to allow negative short rates, we would have obtained the following PDE:

$$\frac{\partial V}{\partial t} + (\mu c - \lambda_c \sigma_c c) \frac{\partial V}{\partial c} + (\alpha(\beta - r) - \lambda_r \sigma_r) \frac{\partial V}{\partial r} + \frac{1}{2} \left(\sigma_c^2 c^2 \frac{\partial^2 V}{\partial c^2} + \sigma_r^2 \frac{\partial^2 V}{\partial r^2} + 2c\rho\sigma_c\sigma_r \frac{\partial^2 V}{\partial r \partial c} \right) - rV = 0$$

2.4.3. Parameter Calibration

In this section we will calibrate the parameters using the maximum likelihood estimation technique [23]. Let c_n and r_n be the observations of c_t and r_t at time $t = t_n$, $t_n = ndt$ ($n = 0, 1, 2, \dots, N$). Discretizing the SDE's of the CIR short rate and carbon price gives us:

$$\begin{aligned} r_n &\approx r_{n-1} + \alpha(\beta - r_{n-1})dt + \sigma_r \sqrt{r_{n-1}} dW_t^r, \\ c_n &\approx c_{n-1} + \mu c_{n-1} dt + \sigma_c c_{n-1} dW_t^c \end{aligned}$$

Let us now look at the definition of the bivariate normal distribution:

Definition 16 (*Bivariate normal distribution*) Two random variables X and Y are said to have a bivariate normal distribution $\mathcal{N}(\mu_X, \mu_Y, \sigma_X^2, \sigma_Y^2, \rho)$ if their joint PDF is given by

$$f_{X,Y}(x,y) = \frac{1}{2\pi\sigma_X\sigma_Y\sqrt{1-\rho^2}} \exp \left\{ -\frac{1}{2(1-\rho^2)} \left[\left(\frac{x-\mu_X}{\sigma_X} \right)^2 + \left(\frac{y-\mu_Y}{\sigma_Y} \right)^2 - 2\rho \frac{(x-\mu_X)(y-\mu_Y)}{\sigma_X\sigma_Y} \right] \right\} \quad (2.34)$$

where $\mu_X, \mu_Y \in \mathbb{R}$, $\sigma_X, \sigma_Y > 0$ and $\rho \in (-1, 1)$ are all constants.

We know that (dW_t^c, dW_t^r) both follow a normal distribution with $(dW_t^c, dW_t^r) \sim \mathcal{N}(0, 0, dt, dt, \rho)$. So we can plug in our discretized SDE's and find:

$$(r_n, c_n) \sim \mathcal{N}(r_{n-1} + \alpha(\beta - r_{n-1})dt, c_{n-1} + \mu c_{n-1}dt, \sigma_r^2 r_{n-1}dt, \sigma_c^2 c_{n-1}^2 dt, \rho), \quad (2.35)$$

from which we can obtain an approximation of the conditional probability density function:

$$f(r_n, c_n | r_{n-1}, c_{n-1}) \approx \frac{1}{2\pi\sigma_r\sigma_c\sqrt{r_{n-1}c_{n-1}dt}\sqrt{1-\rho^2}} \times \exp \left\{ -\frac{1}{2(1-\rho^2)} \left[\frac{(r_n - (r_{n-1} + \alpha(\beta - r_{n-1})dt))^2}{\sigma_r^2 r_{n-1}dt} - 2\rho \frac{(r_n - (r_{n-1} + \alpha(\beta - r_{n-1})dt))(c_n - (c_{n-1} + \mu c_{n-1}dt))}{\sigma_c\sigma_r c_{n-1}\sqrt{r_{n-1}dt}} + \frac{(c_n - (c_{n-1} + \mu c_{n-1}dt))^2}{\sigma_c^2 c_{n-1}^2 dt} \right] \right\}$$

where $\exp\{x\} = e^x$.

To calibrate all the parameters, we need to have real historical data. We extract historical data on the yield curve spot rate of a 4-year-maturity government bond, represented as r_t , from data.ecb.europa.eu. We can use this spot rate for r_t because it provides a reliable benchmark for the risk-free interest rate (short rate). Additionally, we gather historical carbon price data, c_t , from icapcarbonaction.com. We import and plot our obtained data in RStudio and obtain figures 2.17 and 2.18. In our analysis we use the CIR model for the short rate and as you can see in figure 2.17, between 2015 and 2022 the yield curve spot rate was negative. As the CIR model does not allow for negative short rates, we have chosen to exclude all the data from before 2022 for our parameter estimation. After performing the maximum likelihood estimation in RStudio we obtain the following estimates for our parameters:

Parameter values	
α	0.91
β	0.0451
σ_c	0.832
σ_r	0.179
μ	0.058
ρ	0.2

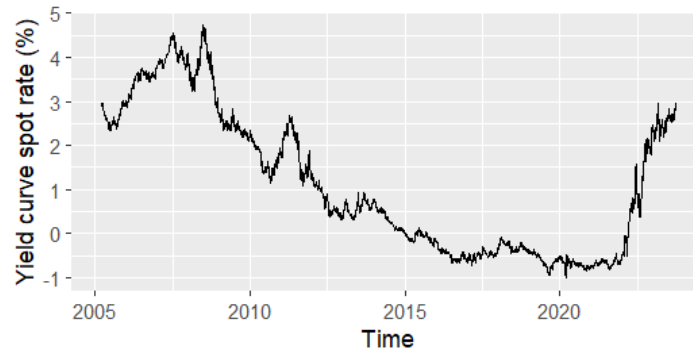


Figure 2.17: Yield curve spot rate, 4-year maturity - Government bond, rating triple A - Euro area

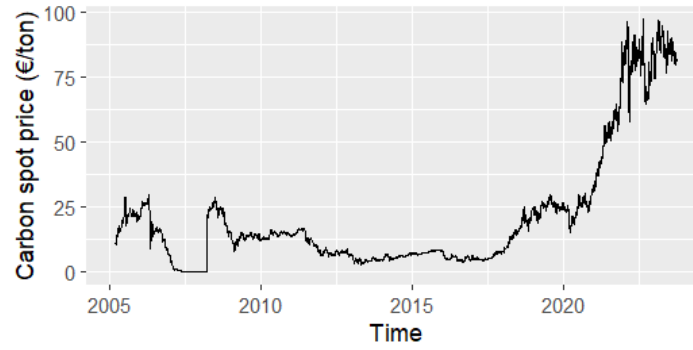


Figure 2.18: EU ETS

2.4.4. Parameter Analysis

In this section we will discuss the terms and parameters involved in our PDE for the green bond's coupon rate. The analysis aims to deepen our understanding of both the mathematical model and the interplay of economic and environmental factors. By doing so, we will learn about the dynamics that drive the valuation of green bonds. We break down the terms involved in the PDE:

- $\frac{\partial V}{\partial t}$: This term represents the time derivative of the coupon rate V . It indicates how the coupon rate changes over time, which could be influenced by market trends, nearing the green bond's maturity, or shifts in environmental regulations.
- $(\mu c - \lambda_c \sigma_c c) \frac{\partial V}{\partial c}$: This term reflects the effect of expected changes in the carbon price c on the coupon rate. With μc denoting the drift of the carbon price, $\lambda_c \sigma_c c$ adjusts this drift for the market price of carbon risk. In short, this term captures the coupon rate's sensitivity to fluctuations in the carbon market.
- $(\alpha(\beta - r) - \lambda_r \sigma_r \sqrt{r}) \frac{\partial V}{\partial r}$: Here, we see the impact of interest rate variations on the coupon rate. The term $\alpha(\beta - r)$ signifies the mean-reverting process of the short rate r , towards a long-term average β . The $\lambda_r \sigma_r \sqrt{r}$ part accounts for the risk associated with the short rate changes.
- $\frac{1}{2} \left(\sigma_c^2 c^2 \frac{\partial^2 V}{\partial c^2} + \sigma_r^2 r \frac{\partial^2 V}{\partial r^2} + 2c\rho\sigma_c\sigma_r\sqrt{r} \frac{\partial^2 V}{\partial r\partial c} \right)$: This complex term includes second-order derivatives, illustrating the coupon rate's convexity in response to shifts in both carbon price and interest rate. The components $\sigma_c^2 c^2 \frac{\partial^2 V}{\partial c^2}$ and $\sigma_r^2 r \frac{\partial^2 V}{\partial r^2}$ measure the coupon rate's sensitivity to changes in carbon price and interest rate, respectively. The cross-derivative term $2c\rho\sigma_c\sigma_r\sqrt{r} \frac{\partial^2 V}{\partial r\partial c}$ signifies the interaction between carbon price and interest rate variations.
- $-rV$: This term signifies the cost associated with the coupon rate. It represents the opportunity cost of the bond's coupon rate compared to the return rate of an investment at the risk-free interest rate r .
- $= 0$: Setting the equation to zero aligns with the no-arbitrage principle in financial mathematics. It suggests that the coupon rate is set in a manner that prevents risk-free profit opportunities, thus maintaining market balance.

Now that we have a gained better insight of the dynamics of the PDE governing the coupon rate of the green bond, we can analyse the parameters and assess which ones have the most significant influence on the coupon rate. We take a green bond with maturity of 4 years and choose our parameters as obtained in the previous section.

Parameter values	
α	0.91
β	0.0451
σ_c	0.832
σ_r	0.179
μ	0.058
ρ	0.2

We start with analysing the first coupon, scheduled for payment at $t = T_1 = 1$. The graphs in figure 2.19 demonstrate the valuation of the coupon payment for a fixed short rate r_t , and on the x - and y -axes the time t and carbon price c , respectively. As expected, we see the graph of a European call option, with at $t = 1$ the payoff $V_1(T_1, r, c) = (c_{T_1} - K_1, 0)^+$. When we look at the coupon value near c_{max} , we see that in the left graph (where $r_t = 0.08$), the coupon value is slightly larger compared to the right graph with $r_t = 0.05$. This can feel counter-intuitive to the typical bond price behavior, where an increase in the short rate results in a lower value for the bond. This can be understood by considering the coupon's structure, which has the mechanism of a double knockout call option. This offsets the decrease in the value of the underlying bond due to rising short rate.

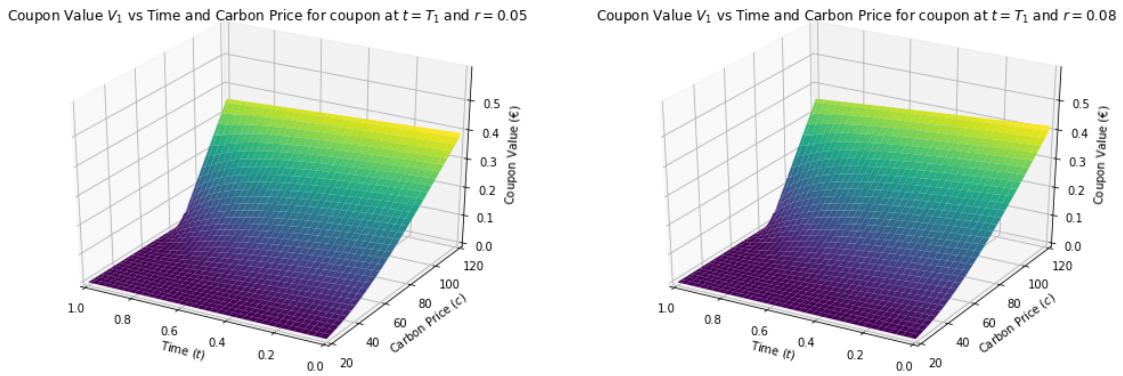


Figure 2.19: Difference in short rate r_t

In figure 2.20 we see the value of the first coupon V_1 valued at $t = 0$ (left) and $t = 0.5$ (right), with on the x - and y -axes the carbon price c_t and the short rate r_t , respectively. In both graphs we can see again that the higher the carbon price, the higher the value of the coupon. The graph on the left shows slightly higher values due to the extra time available for the carbon price to potentially increase.

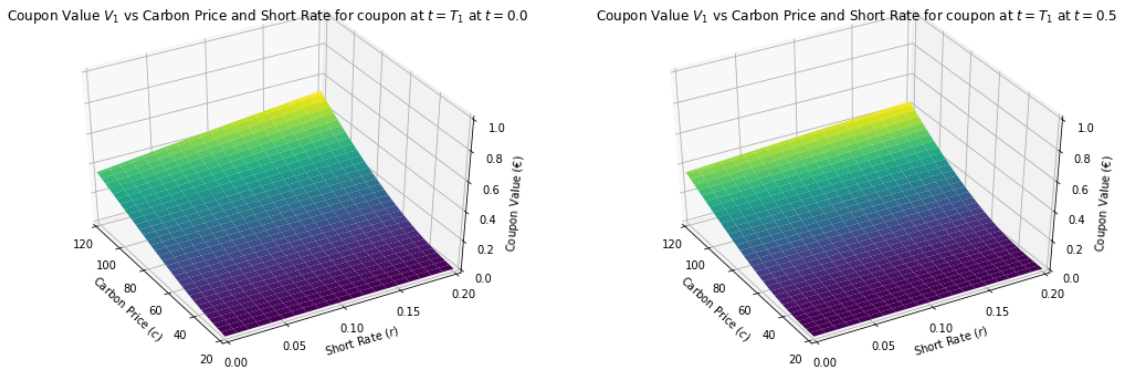


Figure 2.20: Valuation of coupon V_1 at different times t

Let us now look at the effect of changes in the parameter values on the coupon, V_1 (paid at $T = 1$) of the green bond. In figure 2.21 we see that a higher volatility (σ_c) in the carbon price suggests a larger range of potential future prices, which increases the coupon value at both $t = 0$ and $t = 0.5$. This is due to the risk premium demanded by investors for having this extra uncertainty. The model indicates that the possibility of upward movements in carbon price, and thus higher returns, weighs more heavily, leading to an overall increase in the present value of expected coupon payments. As the payment date is closer ($t = 0.5$), the effect of volatility subsides. This results in diverging coupon values across different levels of σ_c , showing reduced sensitivity to volatility as there is less time for price fluctuations to occur.

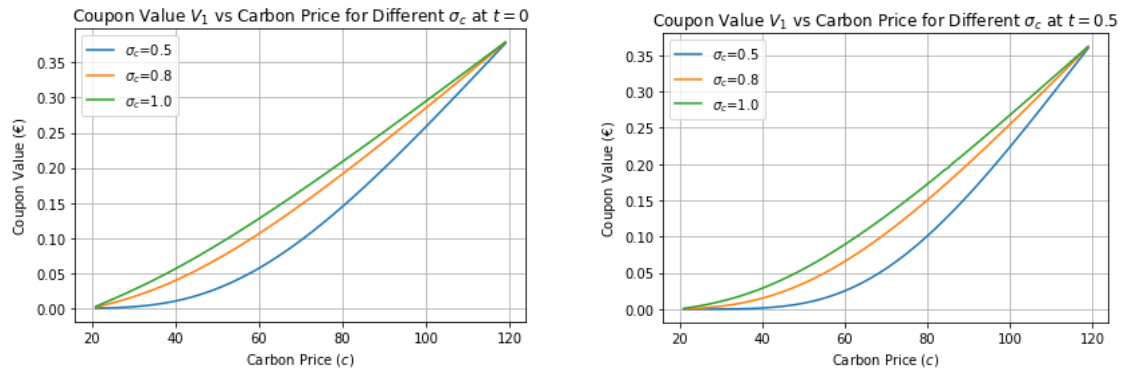


Figure 2.21: Sensitivity coupon V_1 for different values of σ_c

Figure 2.22 shows that the carbon price drift parameter μ significantly influences the coupon value, with its effects more pronounced as the coupon payment date approaches. A positive μ indicates expected upward trends in carbon prices, obviously leading to higher coupon values, while a negative μ suggests a downward trend, resulting in lower values. At $t = 0$, there is a wider spread in coupon values reflecting the market's long-term expectations. However, at $t = 0.5$, we can see that the spread narrows, showing less sensitivity to the drift, as there is less time for the drift to influence the carbon price.

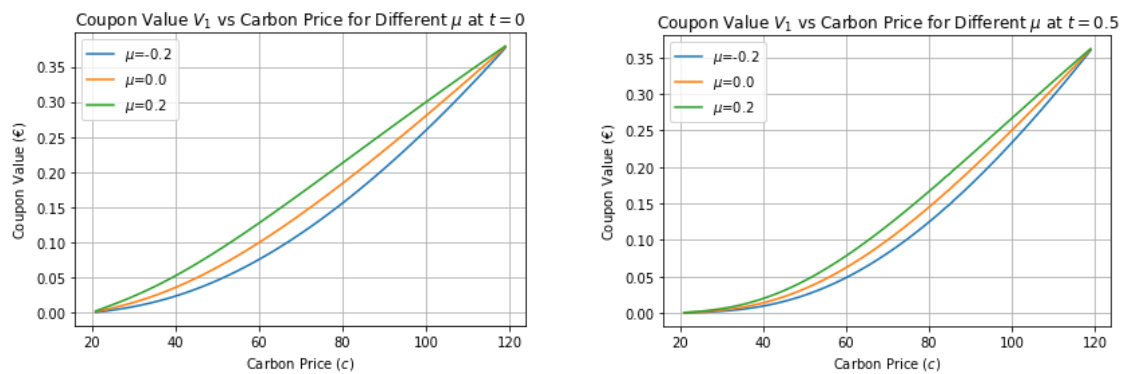


Figure 2.22: Sensitivity coupon V_1 for different values of μ

In figure 2.23 we see the effects of different λ_c values. This parameter reflects the market's attitude towards risk and its expectations about future carbon prices. We can see that negative values for λ_c suggest that the market is less concerned about the risk of changing carbon prices, leading to a higher coupon value. In contrast, a positive λ_c indicates larger concern over declining carbon prices, resulting in a lower coupon value. Moreover, we see that when the coupon payment date comes closer ($t = 0.5$), the market's immediate risk assessment has a more pronounced effect, narrowing the spread of coupon values.

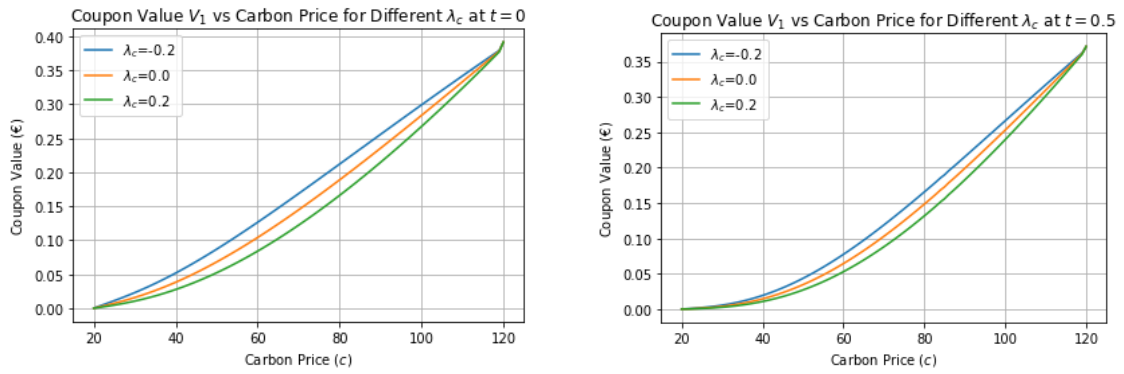


Figure 2.23: Sensitivity coupon V_1 for different values of λ_c

We can see in figure 2.24 that the correlation parameter ρ has a minimal impact on the coupon value V_1 when assessed at both $t = 0$ and $t = 0.5$. This is because the coupon value is more directly influenced by values of the other parameters rather than the interaction between carbon price and the short rate.

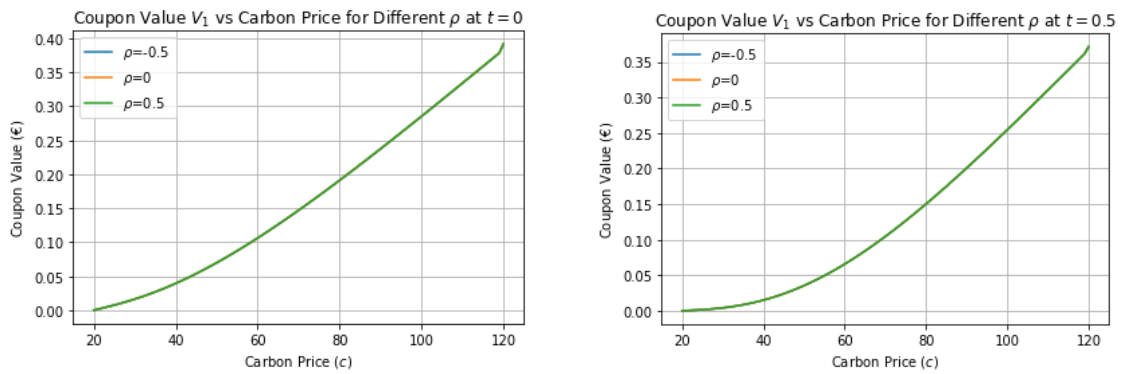


Figure 2.24: Sensitivity coupon V_1 for different values of ρ

Now we will consider the second coupon, V_2 , which is due to payment after 2 years ($t = T_2$). In figure 2.25 we observe the same, but stronger, effects in response to different short rate values as we have seen for coupon V_1 (figure 2.19). This is also the case when we look at figure 2.26 and compare the values with 2.20. This is in line with what we would expect because the carbon price has more time to increase, resulting in a higher payoff.

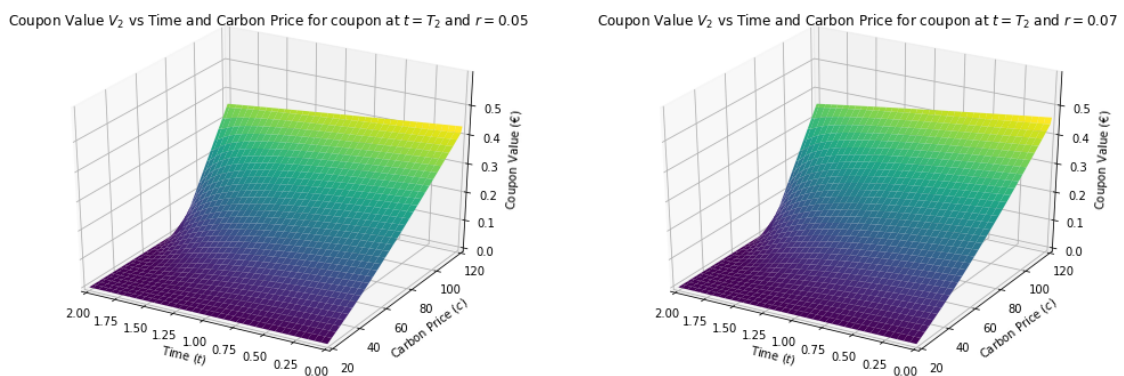


Figure 2.25: Difference in short rate r_t

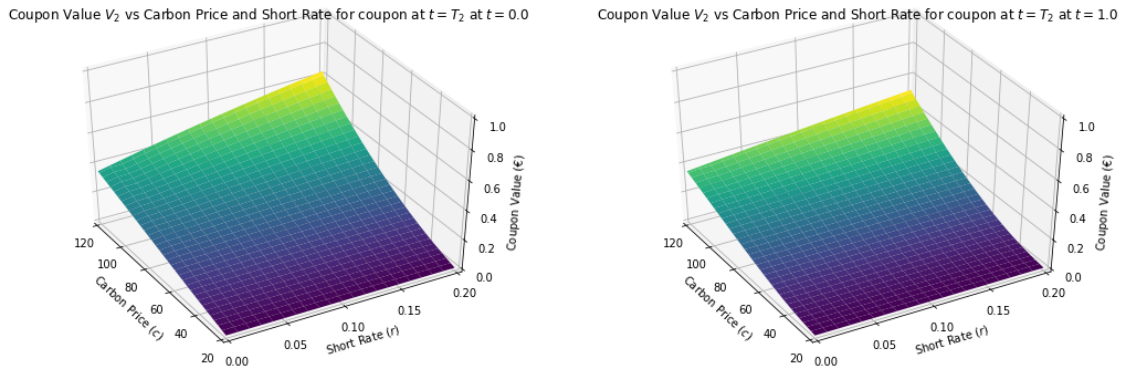


Figure 2.26: Valuation of coupon V_2 at different times t

We can see in figure 2.27 that for the same varied σ_c values, we obtain less dispersed coupon values. Actually, because the time to maturity became longer, the lower values σ_c can have more impact on the carbon price too, resulting in a higher coupon valuation.

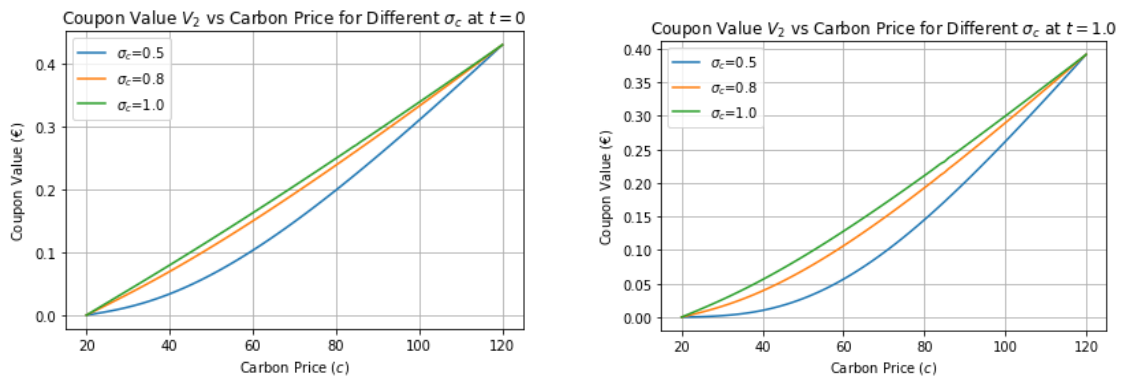


Figure 2.27: Sensitivity coupon V_2 for different values of σ_c

For coupon V_2 we can see something remarkable for a positive carbon price drift parameter μ (figure 2.28). We observe that V_2 exhibits a concave increase in response to higher carbon prices c_t . This is due to the compounding effects of the positive drift parameter μ as result of the longer time period.

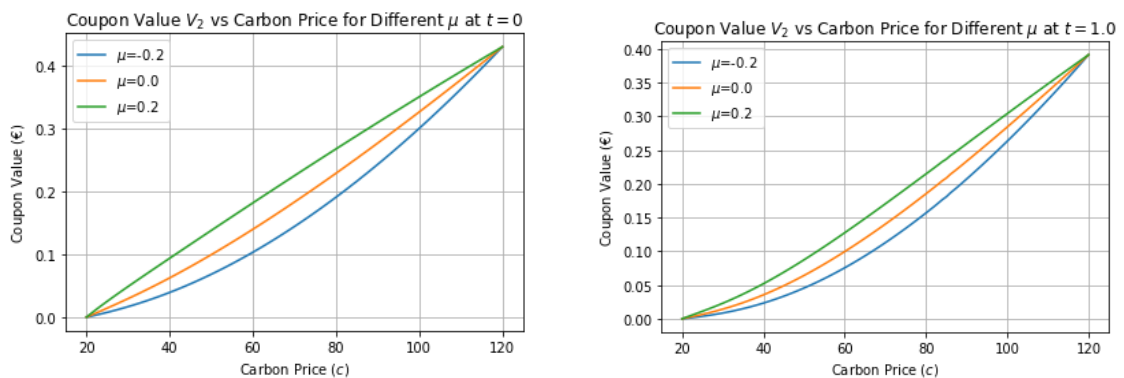


Figure 2.28: Sensitivity coupon V_2 for different values of μ

In figure 2.29, we observe a wider spread in values for the second coupon V_2 across different λ_c values, compared to the narrower range observed for the first coupon V_1 in figure 2.23. This is because the positive and negative λ_c values have a bigger impact on V_2 due to the longer period over which risk and carbon price expectations can evolve. This makes V_2 more sensitive to changes in λ_c , causing a wider spread in its values compared to the shorter-term V_1 .

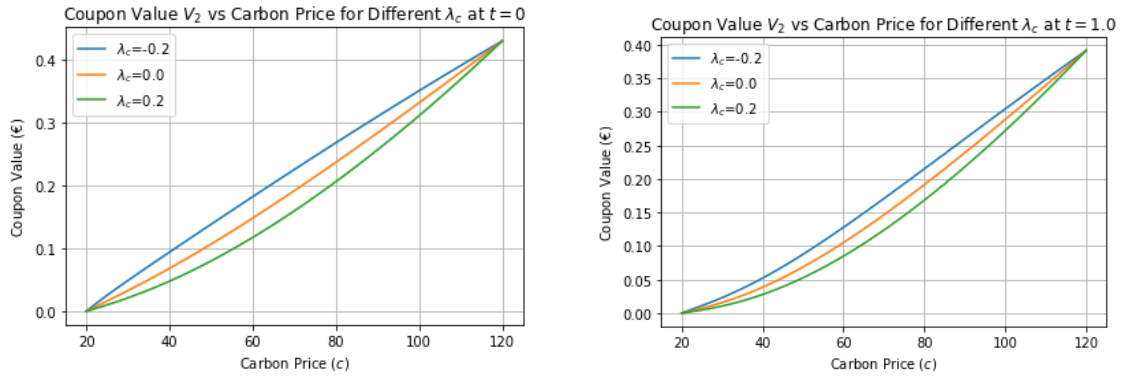


Figure 2.29: Sensitivity coupon V_2 for different values of λ_c

Looking at figure 2.30, we can see that the effect of ρ , the correlation between the short rate, r_t and carbon price c_t is negligible for coupon V_2 as well.

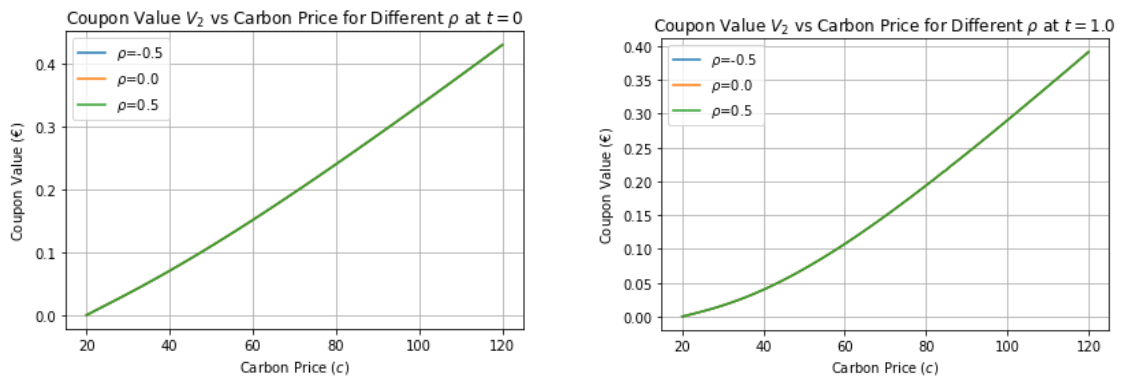


Figure 2.30: Sensitivity coupon V_2 for different values of ρ

3

Finite Difference Method

In this chapter, we will introduce the finite difference method, a pivotal numerical technique in approximating solutions to partial differential equations and ordinary differential equations. We will apply this method on both bond's PDE's.

3.1. Theory

The finite difference method is a numerical technique used to approximate the solution of partial differential equations and ordinary differential equations by discretizing the problem domain into a finite number of nodes. The finite difference method replaces the derivatives in the differential equations with their finite difference approximations. This is done in the time (t) and space (x) dimensions, resulting in a system of algebraic equations that can be solved numerically. Key to understanding the finite difference method is the distinction between explicit and implicit methods:

- Explicit methods directly compute the future state ($t + \Delta t$) from the current state (t). They are generally simple to implement, but stability is a major concern. The step size must be chosen with care; if it is not small enough, the solution may become unstable. The most basic explicit method is the forward/explicit Euler method. When
- Implicit methods compute the future state ($t + \Delta t$) by solving an equation that includes both the current (t) and future states ($t + \Delta t$). Although these methods are more stable than explicit methods, they often require solving a system of equations, which can be computationally intensive. The most basic form is called the backward/implicit Euler method.

A method that combines the forward and backward Euler methods is called the Crank-Nicolson method (figure 3.1, developed by John Crank and Phyllis Nicolson [12]). In the finite difference method we represent the partial derivatives in terms of solution values at discrete points within the domain of interest. These points are organized into a multi-dimensional grid. The formulation of a finite difference solution involves discretizing both the space and time derivatives, and the combination of these discretizations forms the basis of the finite difference algorithm. Each dimension can have a different number of mesh elements, reflecting the varying accuracy needs across different axes. For instance, let M represent the number of mesh elements in the time dimension, and N_1, N_2, \dots, N_d denote the number of mesh elements in each of the d space dimensions. The grid will have $(M+1) \times (N_1+1) \times (N_2+1) \times \dots \times (N_d+1)$ nodes, including those on the domain boundary Γ . The grid size in each dimension is determined accordingly depending on the size of the domain. For example, for time interval $[a, b]$, one often chooses $\Delta t = \frac{b-a}{M}$. This leads to the formation of a grid G_h with a multidimensional structure. A two-dimensional grid can be described with the following equation and figure 3.1

$$G_h = \{(x_i, y_j) | x_i = (i-1)h, y_j = (j-1)h; h = \frac{1}{N}, 1 \leq i, j \leq N+1; N \in \mathbb{N}\}.$$

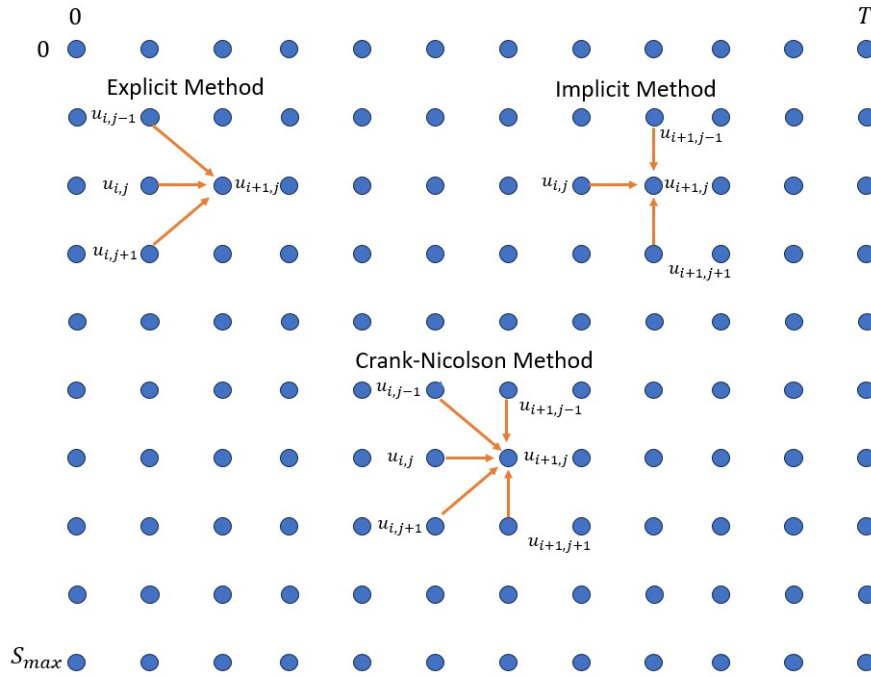


Figure 3.1: Representation of how the explicit method (upper left), implicit method (upper right) and Crank-Nicolson method (low middle) work on the nodes of a grid.

Consider the two-dimensional function $u(t, x)$ which depends on both time t and space x . We denote the step size in time as Δt and the step size in space as Δx . For simplicity, we denote $u(t, x)$ as $u_{i,j}$ where i refers to the temporal index and j refers to the spatial index. So $u(t + \Delta t, x)$ and $u(t - \Delta t, x)$ become $u_{i+1,j}$ and $u_{i-1,j}$, respectively. The same holds for space dimension x . When discretizing the partial derivatives, we can use forward, backward and central differences. The following approximations [32] provide discrete representations of the partial derivatives of $u(t, x)$ with respect to space and time. Forward Difference:

- Time: $\frac{\partial u}{\partial t} \approx \frac{u_{i+1,j} - u_{i,j}}{\Delta t} + \mathcal{O}(\Delta t)$
- Space: $\frac{\partial u}{\partial x} \approx \frac{u_{i,j+1} - u_{i,j}}{\Delta x} + \mathcal{O}(\Delta x)$

Backward Difference:

- Time: $\frac{\partial u}{\partial t} \approx \frac{u_{i,j} - u_{i-1,j}}{\Delta t} + \mathcal{O}(\Delta t)$
- Space: $\frac{\partial u}{\partial x} \approx \frac{u_{i,j} - u_{i,j-1}}{\Delta x} + \mathcal{O}(\Delta x)$

Central Difference:

- Time: $\frac{\partial u}{\partial t} \approx \frac{u_{i+1,j} - u_{i-1,j}}{2\Delta t} + \mathcal{O}(\Delta t^2)$ and $\frac{\partial^2 u}{\partial t^2} \approx \frac{u_{i+1,j} - 2u_{i,j} + u_{i-1,j}}{\Delta t^2} + \mathcal{O}(\Delta t^2)$
- Space: $\frac{\partial u}{\partial x} \approx \frac{u_{i,j+1} - u_{i,j-1}}{2\Delta x} + \mathcal{O}(\Delta x^2)$ and $\frac{\partial^2 u}{\partial x^2} \approx \frac{u_{i,j+1} - 2u_{i,j} + u_{i,j-1}}{\Delta x^2} + \mathcal{O}(\Delta x^2)$

As you can see, we denoted the second order derivative approximations under central differences as they are useful in most applications due to their higher accuracy and symmetry. When choosing a difference scheme for discretizing a PDE, stability and accuracy are key considerations. Stability requirements may necessitate a specific scheme, especially in time-sensitive problems. For example, explicit methods using forward differences need smaller time steps to maintain stability. Accuracy needs, on the other hand, often favor central differences for their higher precision, particularly in spatial derivatives. The choice between the schemes hinges on balancing these stability and accuracy demands according to the specific requirements of the problem. When solving PDE's, a crucial aspect are boundary conditions [32]. Boundary conditions ensure that the solution is well-defined and unique within the problem domain. The following three types of boundary conditions are most commonly encountered in PDE problems:

- Dirichlet: These conditions specify the value of the solution at the boundary of the domain. This translates to directly assigning known values to the boundary nodes.
- Neumann: These conditions involve specifying the value of the derivative of the solution at the boundary. These are a bit more complex to implement as they require approximating the derivative at the boundary using finite differences.
- Robin: Robin conditions are a combination of Dirichlet and Neumann conditions.

Incorporating these boundary conditions into the finite difference framework involves modifying the finite difference equations at the boundary points. This often involves creating special cases in the finite difference equations for nodes that are adjacent to the boundaries.

3.2. Conventional Bond

In this section we will apply the finite difference method to the PDE we obtained for a conventional bond. When pricing financial derivatives such as a bond, we treat the time variable a bit differently. We effectively go backward in time from the known final condition (maturity) to the present. We call this 'financial engineer's time' [28]. For a zero-coupon bond, the value at maturity is known: it is the amount to be paid back at maturity, the face value, FV . Given this backward induction, let us now discretize the PDE for the zero-coupon bond price by the Crank-Nicolson method. Under the CIR model for the short rate, our PDE is equal to:

$$\frac{\partial B}{\partial t} + (\alpha(\beta - r) - \lambda_r \sigma_r \sqrt{r}) \frac{\partial B}{\partial r} + \frac{1}{2} \sigma^2 r \frac{\partial^2 B}{\partial r^2} - rB = 0 \quad (3.1)$$

$$B(T, r) = FV \quad (3.2)$$

$$(3.3)$$

Let us consider the short rate, $r_t \in [0, \infty)$, boundary conditions. For the boundary conditions at $r_{\min} = 0$, we just solve

$$\frac{\partial B}{\partial t} + \alpha\beta \frac{\partial B}{\partial r} = 0 \quad (3.4)$$

The theoretical upper boundary condition $B = 0$ as $r_t \rightarrow \infty$ is not useful. This is because we want to retain r_t as a coordinate and this would make the grid of order of magnitude larger than necessary. So we want to use a much smaller r_{\max} and use the pricing equation itself on this boundary [28]. We will use central difference for the time derivative and central differences for the interest rate derivatives. Let M, N be the amount of time steps and short rate steps, and $\Delta t = T/M$ and $\Delta r = (r_{\max} - r_{\min})/N$ be the step sizes. Define $B_{i,j}$ to be the bond price at time $t_i = i \cdot \Delta t$ and interest rate $r_j = j \cdot \Delta r$. Central difference for $\frac{\partial B}{\partial t}$ gives us:

$$\frac{\partial B_{i-1/2,j}}{\partial t} \approx \frac{B_{i,j} - B_{i-1,j}}{\Delta t} + \mathcal{O}(\Delta t)$$

Central differences for $\frac{\partial B}{\partial r}$ and $\frac{\partial^2 B}{\partial r^2}$ give:

$$\frac{\partial B_{i-1/2,j}}{\partial r} \approx \frac{1}{2} \left(\frac{\partial B_{i-1,j}}{\partial r} + \frac{\partial B_{i,j}}{\partial r} \right) \approx \frac{1}{2} \left(\frac{B_{i-1,j+1} - B_{i-1,j-1}}{2\Delta r} + \frac{B_{i,j+1} - B_{i,j-1}}{2\Delta r} \right) + \mathcal{O}(\Delta r^2)$$

$$\frac{\partial^2 B_{i-1/2,j}}{\partial r^2} \approx \frac{1}{2} \left(\frac{\partial^2 B_{i-1,j}}{\partial r^2} + \frac{\partial^2 B_{i,j}}{\partial r^2} \right) \approx \frac{1}{2} \left(\frac{B_{i-1,j+1} - 2B_{i-1,j} + B_{i-1,j-1}}{\Delta r^2} + \frac{B_{i,j+1} - 2B_{i,j} + B_{i,j-1}}{\Delta r^2} \right) + \mathcal{O}(\Delta r^2)$$

We substitute these approximations into the PDE 3.1, combine the terms that affect the same node on the grid and obtain:

$$\frac{\Delta t}{4} \left(\frac{\alpha(\beta - r_j) - \lambda_r \sigma_r \sqrt{r_j}}{\Delta r} - \frac{\sigma^2 r_j}{\Delta r^2} \right) B_{i-1,j-1} + \left(1 + \frac{\Delta t}{2} \left(\frac{\sigma^2 r_j}{\Delta r^2} + r_j \right) \right) B_{i-1,j} + \frac{\Delta t}{4} \left(-\frac{\alpha(\beta - r_j) - \lambda_r \sigma_r \sqrt{r_j}}{\Delta r} - \frac{\sigma^2 r_j}{\Delta r^2} \right) B_{i-1,j+1} \quad (3.5)$$

$$= \frac{\Delta t}{4} \left(\frac{\sigma^2 r_j}{\Delta r^2} - \frac{\alpha(\beta - r_j) - \lambda_r \sigma_r \sqrt{r_j}}{\Delta r} \right) B_{i,j-1} + \left(1 - \frac{\Delta t}{2} \left(\frac{\sigma^2 r_j}{\Delta r^2} + r_j \right) \right) B_{i,j} - \frac{\Delta t}{4} \left(\frac{\sigma^2 r_j}{\Delta r^2} + \frac{\alpha(\beta - r_j) - \lambda_r \sigma_r \sqrt{r_j}}{\Delta r} \right) B_{i,j+1} \quad (3.6)$$

We rewrite this equation to a more concise and readable way

$$-\hat{a}B_{i-1,j-1} + (1 - \hat{b})B_{i-1,j} - \hat{c}B_{i-1,j+1} = \hat{a}B_{i,j-1} + (1 + \hat{b})B_{i,j} + \hat{c}B_{i,j+1}, \quad (3.7)$$

With

$$\begin{aligned} \hat{a} &= \frac{\Delta t}{4} \left(\frac{\sigma^2 r_j}{\Delta r^2} - \frac{\alpha(\beta - r_j) - \lambda_r \sigma_r \sqrt{r_j}}{\Delta r} \right) \\ \hat{b} &= -\frac{\Delta t}{2} \left(\frac{\sigma^2 r_j}{2\Delta r^2} + r_j \right) \\ \hat{c} &= \frac{\Delta t}{4} \left(\frac{\sigma^2 r_j}{\Delta r^2} + \frac{\alpha(\beta - r_j) - \lambda_r \sigma_r \sqrt{r_j}}{\Delta r} \right) \end{aligned}$$

We can put equation 3.7 into the following matrix equation:

$$CB_{i-1} = DB_i + K_{i-1} + K_i \quad (3.8)$$

where

$$B_i = \begin{pmatrix} B_{i,1} \\ B_{i,2} \\ \vdots \\ \vdots \\ B_{i,N-1} \end{pmatrix} \quad \text{and} \quad K_i = \begin{pmatrix} \hat{a}_1 B_{i,0} \\ 0 \\ \vdots \\ 0 \\ \hat{c}_{N-1} B_{i,N} \end{pmatrix} \quad (3.9)$$

$$C = \begin{pmatrix} 1 - \hat{b}_1 & -\hat{c}_1 & 0 & \dots & 0 \\ -\hat{a}_2 & 1 - \hat{b}_2 & -\hat{c}_2 & \dots & 0 \\ 0 & -\hat{a}_3 & 1 - \hat{b}_3 & \ddots & \dots \\ \vdots & \ddots & \ddots & \ddots & -\hat{c}_{N-2} \\ 0 & \dots & 0 & -\hat{a}_{N-1} & 1 - \hat{b}_{N-1} \end{pmatrix} \quad (3.10)$$

$$D = \begin{pmatrix} 1 + \hat{b}_1 & \hat{c}_1 & 0 & \dots & 0 \\ \hat{a}_2 & 1 + \hat{b}_2 & \hat{c}_2 & \dots & 0 \\ 0 & \hat{a}_3 & 1 + \hat{b}_3 & \ddots & \dots \\ \vdots & \ddots & \ddots & \ddots & \hat{c}_{N-2} \\ 0 & \dots & 0 & \hat{a}_{N-1} & 1 + \hat{b}_{N-1} \end{pmatrix} \quad (3.11)$$

To use the pricing equation itself on the boundary r_{\max} we perform a Crank-Nicolson scheme that couples three grid points at the boundary [28]: We use central difference for $\frac{\partial B}{\partial t}$ gives us:

$$\frac{\partial B_{i-1/2,j}}{\partial t} \approx \frac{B_{i,j} - B_{i-1,j}}{\Delta t} + \mathcal{O}(\Delta t)$$

Central differences for $\frac{\partial B}{\partial r}$ and $\frac{\partial^2 B}{\partial r^2}$ give:

$$\begin{aligned} \frac{\partial B_{i-1/2,j}}{\partial r} &\approx \frac{1}{2} \left(\frac{\partial B_{i-1,j}}{\partial r} + \frac{\partial B_{i,j}}{\partial r} \right) \approx \frac{1}{2} \left(\frac{3B_{i-1,j} - 4B_{i-1,j-1} + B_{i-1,j-2}}{2\Delta r} + \frac{3B_{i,j+1} - 4B_{i,j-1} + B_{i,j-2}}{2\Delta r} \right) + \mathcal{O}(\Delta r^2) \\ \frac{\partial^2 B_{i-1/2,j}}{\partial r^2} &\approx \frac{1}{2} \left(\frac{\partial^2 B_{i-1,j}}{\partial r^2} + \frac{\partial^2 B_{i,j}}{\partial r^2} \right) \approx \frac{1}{2} \left(\frac{B_{i-1,j} - 2B_{i-1,j-1} + B_{i-1,j-2}}{\Delta r^2} + \frac{B_{i,j} - 2B_{i,j-1} + B_{i,j-2}}{\Delta r^2} \right) + \mathcal{O}(\Delta r^2) \end{aligned}$$

3.3. Green Bond

In this section we will use the finite difference method on the PDE of the green bond coupon rate. The difference with the conventional bond is that this PDE is two dimensional in 'space': in the interest rate r and the carbon price c . As for the interest rate, we use central differences for the carbon price partial derivatives too. We can see that we also have the second order mixed partial derivative $\frac{\partial^2 V}{\partial r \partial c}$. Let $\Delta t = T/M$, $\Delta r = (r_{\max} - r_{\min})/N$, $\Delta c = (c_{\max} - c_{\min})/P$ be the step sizes in the time, short rate and carbon price, respectively. Define $B_{j,k}^i$ to be the bond price at time $t_i = i \cdot \Delta t$, interest rate $r_j = j \cdot \Delta r$ and carbon price $c_k = k \cdot \Delta c$, for $i = \{1, \dots, M\}$, $j = \{1, \dots, N\}$, $k = \{1, \dots, P\}$.

$$\frac{\partial V}{\partial t} + (\mu c - \lambda_1 \sigma_c c) \frac{\partial V}{\partial c} + (\alpha(\beta - r) - \lambda_2 \sigma_r \sqrt{r}) \frac{\partial V}{\partial r} \quad (3.12)$$

$$+ \frac{1}{2} \left(\sigma_c^2 c^2 \frac{\partial^2 V}{\partial c^2} + \sigma_r^2 r \frac{\partial^2 V}{\partial r^2} + 2c\rho\sigma_c\sigma_r\sqrt{r} \frac{\partial^2 V}{\partial r \partial c} \right) - rV = 0 \quad (3.13)$$

Central difference for $\frac{\partial V}{\partial t}$ gives us:

$$\frac{\partial V_{j,k}^{i-1/2}}{\partial t} \approx \frac{V_{j,k}^{i-1} - V_{j,k}^i}{\Delta t} + \mathcal{O}(\Delta t)$$

Central differences for $\frac{\partial V}{\partial r}$ and $\frac{\partial^2 V}{\partial r^2}$ give:

$$\frac{\partial V_{j,k}^{i-1/2}}{\partial r} \approx \frac{1}{2} \left(\frac{\partial V_{j,k}^{i-1}}{\partial r} + \frac{\partial V_{j,k}^i}{\partial r} \right) \approx \frac{1}{2} \left(\frac{V_{j+1,k}^{i-1} - V_{j-1,k}^{i-1}}{2\Delta r} + \frac{V_{j+1,k}^i - V_{j-1,k}^i}{2\Delta r} \right) + \mathcal{O}(\Delta r^2)$$

$$\frac{\partial^2 V_{j,k}^{i-1/2}}{\partial r^2} \approx \frac{1}{2} \left(\frac{\partial^2 V_{j,k}^{i-1}}{\partial r^2} + \frac{\partial^2 V_{j,k}^i}{\partial r^2} \right) \approx \frac{1}{2} \left(\frac{V_{j+1,k}^{i-1} - 2V_{j,k}^{i-1} + V_{j-1,k}^{i-1}}{\Delta r^2} + \frac{V_{j+1,k}^i - 2V_{j,k}^i + V_{j-1,k}^i}{\Delta r^2} \right) + \mathcal{O}(\Delta r^2)$$

Central differences for $\frac{\partial V}{\partial c}$ and $\frac{\partial^2 V}{\partial c^2}$ give:

$$\frac{\partial V_{j,k}^{i-1/2}}{\partial c} \approx \frac{1}{2} \left(\frac{\partial V_{j,k}^{i-1}}{\partial c} + \frac{\partial V_{j,k}^i}{\partial c} \right) \approx \frac{1}{2} \left(\frac{V_{j,k+1}^{i-1} - V_{j,k-1}^{i-1}}{2\Delta c} + \frac{V_{j,k+1}^i - V_{j,k-1}^i}{2\Delta c} \right) + \mathcal{O}(\Delta c^2)$$

$$\frac{\partial^2 V_{j,k}^{i-1/2}}{\partial c^2} \approx \frac{1}{2} \left(\frac{\partial^2 V_{j,k}^{i-1}}{\partial c^2} + \frac{\partial^2 V_{j,k}^i}{\partial c^2} \right) \approx \frac{1}{2} \left(\frac{V_{j,k+1}^{i-1} - 2V_{j,k}^{i-1} + V_{j,k-1}^{i-1}}{\Delta c^2} + \frac{V_{j,k+1}^i - 2V_{j,k}^i + V_{j,k-1}^i}{\Delta c^2} \right) + \mathcal{O}(\Delta c^2)$$

We approximate the mixed partial derivative $\frac{\partial^2 V}{\partial r \partial c}$ by central differences too:

$$\begin{aligned} \frac{\partial^2 V_{j,k}^{i-1/2}}{\partial r \partial c} &\approx \frac{1}{2} \left(\frac{\partial^2 V_{j,k}^{i-1}}{\partial r \partial c} + \frac{\partial^2 V_{j,k}^i}{\partial r \partial c} \right) \\ &\approx \frac{1}{2} \left(\frac{V_{j-1,k-1}^{i-1} - V_{j-1,k+1}^{i-1} - V_{j+1,k-1}^{i-1} + V_{j+1,k+1}^{i-1}}{4\Delta r \Delta c} + \frac{V_{j-1,k-1}^i - V_{j-1,k+1}^i - V_{j+1,k-1}^i + V_{j+1,k+1}^i}{4\Delta r \Delta c} \right) + \mathcal{O}(\Delta r \Delta c) \end{aligned}$$

We fill in the finite difference approximations and subsequently rearrange the equation and obtain:

$$-\hat{n}_1 V_{j-1,k-1}^{i-1} - \hat{n}_2 V_{j-1,k}^{i-1} - \hat{n}_3 V_{j-1,k+1}^{i-1} - \hat{n}_4 V_{j,k-1}^{i-1} + (1 - \hat{n}_5) V_{j,k}^{i-1} - \hat{n}_6 V_{j,k+1}^{i-1} - \hat{n}_7 V_{j+1,k-1}^{i-1} - \hat{n}_8 V_{j+1,k}^{i-1} - \hat{n}_9 V_{j+1,k+1}^{i-1} \quad (3.14)$$

$$= \hat{n}_1 V_{j-1,k-1}^i + \hat{n}_2 V_{j-1,k}^i + \hat{n}_3 V_{j-1,k+1}^i + \hat{n}_4 V_{j,k-1}^i + (1 + \hat{n}_5) V_{j,k}^i + \hat{n}_6 V_{j,k+1}^i + \hat{n}_7 V_{j+1,k-1}^i + \hat{n}_8 V_{j+1,k}^i + \hat{n}_9 V_{j+1,k+1}^i \quad (3.15)$$

with

$$\begin{aligned}\hat{n}_1 &= \frac{\Delta t}{2} \frac{c_k \sigma_c \sigma_r \rho \sqrt{r_j}}{4\Delta r \Delta c} & \hat{n}_2 &= \frac{\Delta t}{2} \left(\frac{\sigma_r^2 r_j}{2\Delta r^2} - \frac{\alpha(\beta - r_j) - \lambda_2 \sigma_r \sqrt{r_j}}{2\Delta r} \right) & \hat{n}_3 &= \frac{\Delta t}{2} \frac{-c_k \sigma_c \sigma_r \rho \sqrt{r_j}}{4\Delta r \Delta c} \\ \hat{n}_4 &= \frac{\Delta t}{2} \left(\frac{\sigma_c^2 c_k^2}{2\Delta c^2} - \frac{\mu c_k - \lambda_1 \sigma_c c_k}{2\Delta c} \right) & \hat{n}_5 &= -\frac{\Delta t}{2} \left(\frac{\sigma_r^2 r_j}{\Delta r^2} + \frac{\sigma_c^2 c_k}{\Delta c^2} + r_j \right) & \hat{n}_6 &= \frac{\Delta t}{2} \left(\frac{\sigma_c^2 c_k^2}{2\Delta c^2} + \frac{\mu c_k - \lambda_1 \sigma_c c_k}{2\Delta c} \right) \\ \hat{n}_7 &= \frac{\Delta t}{2} \frac{-c_k \sigma_c \sigma_r \rho \sqrt{r_j}}{4\Delta r \Delta c} & \hat{n}_8 &= \frac{\Delta t}{2} \left(\frac{\sigma_r^2 r_j}{2\Delta r^2} - \frac{\alpha(\beta - r_j) + \lambda_2 \sigma_r \sqrt{r_j}}{2\Delta r} \right) & \hat{n}_9 &= \frac{\Delta t}{2} \frac{c_k \sigma_c \sigma_r \rho \sqrt{r_j}}{4\Delta r \Delta c}\end{aligned}$$

We see that we have a nine-point stencil. For every timestep we obtain the following matrix equation:

$$CV^{i-1} = DV^i + K^{i-1} + K^i \quad (3.16)$$

With

$$V^i = \begin{pmatrix} V_{1,1}^i \\ V_{1,2}^i \\ \vdots \\ V_{1,P-1}^i \\ V_{2,1}^i \\ V_{2,P-1}^i \\ \vdots \\ V_{N-1,1}^i \\ \vdots \\ V_{N-1,P-1}^i \end{pmatrix} \quad \text{and} \quad K^i = \begin{pmatrix} \hat{n}_1 V_{0,0}^i + \hat{n}_2 V_{0,1}^i + \hat{n}_3 V_{0,2}^i + \hat{n}_4 V_{1,0}^i + \hat{n}_7 V_{2,0}^i \\ \hat{n}_1 V_{0,1}^i + \hat{n}_2 V_{0,2}^i + \hat{n}_3 V_{0,3}^i \\ \vdots \\ \hat{n}_1 V_{0,P-2}^i + \hat{n}_2 V_{0,P-1}^i + \hat{n}_3 V_{0,P}^i + \hat{n}_6 V_{1,P}^i + \hat{n}_9 V_{2,P}^i \\ \vdots \\ \hat{n}_1 V_{N-2,0}^i + \hat{n}_4 V_{N-1,0}^i + \hat{n}_7 V_{N,0}^i + \hat{n}_8 V_{N,1}^i + \hat{n}_9 V_{N,2}^i \\ \vdots \\ \hat{n}_7 V_{N,P-3}^i + \hat{n}_8 V_{N,P-2}^i + \hat{n}_9 V_{N,P-1}^i \\ \hat{n}_3 V_{N-2,P}^i + \hat{n}_6 V_{N-1,P+1}^i + \hat{n}_7 V_{N,P-2}^i + \hat{n}_8 V_{N,P-1}^i + \hat{n}_9 V_{N,P}^i \end{pmatrix} \quad (3.17)$$

$$C = \begin{pmatrix} 1 - \hat{n}_5 & -\hat{n}_6 & 0 & \dots & 0 & 0 & -\hat{n}_8 & -\hat{n}_9 & \dots & 0 \\ -\hat{n}_4 & 1 - \hat{n}_5 & -\hat{n}_6 & 0 & \dots & 0 & -\hat{n}_7 & -\hat{n}_8 & -\hat{n}_9 & 0 \\ 0 & -\hat{n}_4 & 1 - \hat{n}_5 & -\hat{n}_6 & 0 & \dots & \ddots & \ddots & \ddots & \ddots \\ 0 & 0 & -\hat{n}_4 & 1 - \hat{n}_5 & -\hat{n}_6 & 0 & \dots & \ddots & \ddots & \ddots \\ \vdots & \ddots & \vdots \\ \vdots & \ddots & 0 \\ -\hat{n}_1 & -\hat{n}_2 & -\hat{n}_3 & 0 & \dots & 0 & -\hat{n}_4 & 1 - \hat{n}_5 & -\hat{n}_6 & \ddots \\ \dots & -\hat{n}_1 & -\hat{n}_2 & -\hat{n}_3 & 0 & \dots & 0 & -\hat{n}_4 & 1 - \hat{n}_5 & -\hat{n}_6 \\ 0 & \dots & -\hat{n}_1 & -\hat{n}_2 & 0 & 0 & \dots & 0 & -\hat{n}_4 & 1 - \hat{n}_5 \end{pmatrix} \quad (3.18)$$

$$D = \begin{pmatrix} 1 + \hat{n}_5 & \hat{n}_6 & 0 & \dots & 0 & \hat{n}_7 & \hat{n}_8 & \hat{n}_9 & \dots & 0 \\ \hat{n}_4 & 1 + \hat{n}_5 & \hat{n}_6 & 0 & \dots & 0 & \hat{n}_7 & \hat{n}_8 & \hat{n}_9 & 0 \\ 0 & \hat{n}_4 & 1 + \hat{n}_5 & \hat{n}_6 & 0 & \dots & \ddots & \ddots & \ddots & \ddots \\ 0 & 0 & \hat{n}_4 & 1 + \hat{n}_5 & \hat{n}_6 & 0 & \dots & \ddots & \ddots & \ddots \\ \vdots & \ddots & \vdots \\ \vdots & \ddots & 0 \\ \hat{n}_1 & \hat{n}_2 & \hat{n}_3 & 0 & \dots & 0 & \hat{n}_4 & 1 + \hat{n}_5 & \hat{n}_6 & \ddots \\ \dots & \hat{n}_1 & \hat{n}_2 & \hat{n}_3 & 0 & \dots & 0 & \hat{n}_4 & 1 + \hat{n}_5 & \hat{n}_6 \\ 0 & \dots & \hat{n}_1 & \hat{n}_2 & \hat{n}_3 & 0 & \dots & 0 & \hat{n}_4 & 1 + \hat{n}_5 \end{pmatrix} \quad (3.19)$$

Now we will discretize the PDE's $h_1(t, c)$, $h_2(t, c)$ for the boundary conditions at r_{\min} , r_{\max} , respectively. In the previous section we applied the Crank-Nicolson discretization scheme to the conventional bond equation (3.1). The boundary condition h_1 (and h_2 with r_{\max}), described by

$$\frac{\partial V}{\partial t} + \frac{1}{2}\sigma_c^2 c^2 \frac{\partial^2 V}{\partial c^2} + (\mu c - \lambda_1 \sigma_c c) \frac{\partial V}{\partial c} - r_{\min} V = 0, \quad (3.20)$$

exhibits a similar convection-diffusion equation. Therefore, we only present the final discretized form for h_1 , avoiding the repetition of analogous discretization steps. For $h_1(t, c)$ we obtain

$$-\hat{x}V_{i-1,k-1} + (1 - \hat{y})V_{i-1,k} - \hat{z}V_{i-1,k+1} = \hat{x}V_{i,k-1} + (1 + \hat{y})V_{i,k} + \hat{z}V_{i,k+1}, \quad (3.21)$$

With

$$\begin{aligned} \hat{x} &= \frac{\Delta t}{4} \left(\frac{c_k^2 \sigma^2}{\Delta c^2} - \frac{\mu c_k - \lambda_1 \sigma_c c_k}{\Delta c} \right) \\ \hat{y} &= -\frac{\Delta t}{2} \left(\frac{c_k^2 \sigma^2}{2\Delta c^2} + r_{\min} \right) \\ \hat{z} &= \frac{\Delta t}{4} \left(\frac{c_k^2 \sigma^2}{\Delta c^2} + \frac{\mu c_k - \lambda_1 \sigma_c c_k}{\Delta c} \right) \end{aligned}$$

We can put equation 3.21 into the following matrix equation form:

$$CV_{i-1} = DV_i + K_{i-1} + K_i \quad (3.22)$$

where

$$V_i = \begin{pmatrix} V_{i,1} \\ V_{i,2} \\ \vdots \\ \vdots \\ V_{i,P-1} \end{pmatrix} \quad \text{and} \quad K_i = \begin{pmatrix} \hat{x}_1 V_{i,0} \\ 0 \\ \vdots \\ 0 \\ \hat{z}_{P-1} V_{i,P} \end{pmatrix} \quad (3.23)$$

$$C = \begin{pmatrix} 1 - \hat{y}_1 & -\hat{z}_1 & 0 & \dots & 0 \\ -\hat{x}_2 & 1 - \hat{y}_2 & -\hat{z}_2 & \dots & 0 \\ 0 & -\hat{x}_3 & 1 - \hat{y}_3 & \ddots & \dots \\ \vdots & \ddots & \ddots & \ddots & -\hat{z}_{P-2} \\ 0 & \dots & 0 & -\hat{x}_{P-1} & 1 - \hat{y}_{P-1} \end{pmatrix} \quad (3.24)$$

$$D = \begin{pmatrix} 1 + \hat{y}_1 & \hat{z}_1 & 0 & \dots & 0 \\ \hat{x}_2 & 1 + \hat{y}_2 & \hat{z}_2 & \dots & 0 \\ 0 & \hat{x}_3 & 1 + \hat{y}_3 & \ddots & \dots \\ \vdots & \ddots & \ddots & \ddots & \hat{z}_{P-2} \\ 0 & \dots & 0 & \hat{x}_{P-1} & 1 + \hat{y}_{P-1} \end{pmatrix} \quad (3.25)$$

To obtain the discretization and matrix equation for $h_2(t, c)$ we just replace r_{\min} by r_{\max} everywhere.

4

Numerical Results

In this chapter, we will perform comprehensive analysis of iterative methods in mathematics, with a specific focus on the Generalized Minimal Residual (GMRES) method and the Biconjugate Gradient Stabilized (Bi-CGSTAB) method. We will apply these methods to the two distinct models we obtained in the previous chapters: the conventional bond model and the green bond model. First we will introduce and explain the GMRES and Bi-CGSTAB algorithms to get knowledge about how these methods perform under different circumstances, particularly when enhanced with preconditioners. This first three sections primarily draw upon "Scientific Computing" by C. Vuik and D.J.P. Lahaye [32].

4.1. Direct methods

In the previous chapter we found systems of linear equations for the two different bond models. A standard approach for solving systems like

$$A\mathbf{u} = \mathbf{f} \tag{4.1}$$

is through direct solution methods. These methods serve as subdomain solvers in domain-decomposition techniques and as solvers for coarse grids in multigrid approaches. Consequently, they continue to be a crucial element in modern solvers. However, because they are computationally expensive, direct methods alone are not suitable for the large-scale problems often encountered in scientific computing. We show that the Gaussian Elimination method, utilizing an LU -decomposition, can be employed in our conventional bond model: If we look at equation 4.1, this method involves two phases. First, the coefficient matrix A is decomposed into two matrices, L and U such that their product is equal to $A \in \mathbb{R}^{n \times n}$. Here, L and U are, respectively, lower and upper triangular matrices with L 's diagonal elements all being equal to one. We obtain

$$LU\mathbf{u} = \mathbf{f}$$

Solving this linear system is straightforward, The process is executed as follows: $LU\mathbf{u} = \mathbf{f}$ leads to $L\mathbf{y} = \mathbf{f}$, and then $U\mathbf{u} = \mathbf{y}$ is solved to find solution \mathbf{u} . This results in a total computational cost equal to

$$\sum_{k=1}^{n-1} (n-k)(n-k+1) = \sum_{\ell=1}^{n-1} \ell(\ell-1) = \frac{2}{3}n^3 + O(n^2) \text{ flops.}$$

Therefore, the efficiency of this method is greatly influenced by the problem size, which is why iterative methods are favored for larger systems of linear equations.

4.2. Krylov subspace methods

In this section we look at the application of Krylov subspace method for iteratively solving large linear systems of equations. The preference for employing Krylov subspace methods over direct methods in large-scale systems is primarily due to their faster computational speed. Krylov subspace methods are specifically engineered to eliminate the need for matrix-matrix operations, which are computationally

intensive. Instead, these methods focus on matrix-vector multiplications. The iterative process in Krylov subspace methods is represented by the sequence

$$\{\mathbf{u}_k\}_{k \geq 0}, \quad \text{where } \mathbf{u}_k \rightarrow u \quad \text{as } k \rightarrow \infty$$

The Krylov subspace of dimension k , denoted as $K_k(A, r_0)$, is defined by the span of $\{r_0, Ar_0, \dots, A^{k-1}r_0\}$. This subspace corresponds to the matrix A and the initial residual r_0 . The two Krylov subspace iterative methods that we are going to use during this thesis are GMRES (Generalized Minimum Residual), and Bi-CG (Biconjugate Gradient). These methods vary in their specific requirements and optimal use scenarios:

- GMRES type methods: These methods say solution u_k is an element of $K_k(A; r_0)$ and are characterized by long recurrences, but come with particular properties of optimality. Due to these extended recurrences, there is a proportional increase in both the computational and memory effort per iteration as the iteration count rises.
- Bi-CG type methods: In these method, we also have that $u_k \in K_k(A; r_0)$. However, these feature short recurrences, but do not have an optimality property.

Another popular iterative method is CG (Congugate Gradient). This method is highly efficient but requires the coefficient matrix A to be SPD (def. 9.). Given that the matrices in our bond models are not SPD the CG method is unfortunately not applicable and hence will not be further discussed.

4.3. The GMRES and Bi-CGSTAB methods

The Generalized Minimal Residual (GMRES) method is an iterative algorithm used for solving a system of linear equations, particularly useful for large, sparse systems. It is especially effective when combined with preconditioning techniques, which we will describe in subsection 4.3.1. The method is described in [32] as follows: GMRES solves a linear system $Au = f$, where A is a non-singular matrix. The method iteratively builds a solution in a Krylov subspace, $K_n = K_n(A, r_0) = \text{span}\{r_0, Ar_0, A^2r_0, \dots, A^{n-1}r_0\}$. The key idea is to find an approximate solution within this subspace that minimizes the residual in the least-squares sense. Within the GMRES method, Arnoldi's method is employed to calculate an orthonormal basis, denoted as $\{v_1, \dots, v_k\}$, for the Krylov subspace $K^k(A; r_0)$. The process follows the modified Gram-Schmidt version of Arnoldi's method, which is as follows:

Algorithm 1: Gram-Schmidt version of Arnoldi to form an orthonormal basis [32]

- 1 Start: Choose initial vector v_1 with $\|v_1\| = 1$.
 - 2 **for** $j = 1, 2, \dots$ **do**
 - 3 a. Set $h_{i,j} = \langle Av_j, v_i \rangle, i = 1, 2, \dots, j$
 - 4 b. Set $\hat{v}_{j+1} = Av_j - \sum_{i=1}^j h_{i,j}v_i$
 - 5 c. Set $h_{j+1,j} = \|\hat{v}_{j+1}\|_2$
 - 6 d. Set $v_{j+1} = \frac{\hat{v}_{j+1}}{h_{j+1,j}}$
 - 7 The entries of the upper $k+1 \times k$ Hessenberg matrix \overline{H}_k are the scalars h_{ij} .
-

In GMRES, the approximate solution $u_k = u_0 + z_k$ with $z_k \in K_k(A; r_0)$ is such that

$$\|r_k\|_2 = \|f - Au_k\|_2 = \min_{z \in K^k(A; r_0)} \|r_0 - Az\|_2$$

As a consequence, r_k is orthogonal to $AK^k(A; r_0)$, so $r_k \perp K^k(A; r_0)$. For the matrix \overline{H}_k , it follows that $AV_k = V_{k+1}\overline{H}_k$ where the $N \times k$ matrix V_k is defined by $V_k = [v_1, \dots, v_k]$. With this equation, it is shown that $u_k = u_0 + V_k y_k$ where y_k is the solution of the following least squares problem:

$$\|\beta e_1 - \overline{H}_k y_k\|_2 = \min_{y \in \mathbb{R}^k} \|\beta e_1 - \overline{H}_k y\|_2,$$

with $\beta = \|r_0\|_2$ and e_1 is the first unit vector in \mathbb{R}^{k+1} . In the context of our bond pricing models, GMRES is utilized to refine solutions iteratively, proving especially suitable for large systems where direct methods are not feasible. Moreover, GMRES does not necessitate the matrix A to be symmetric or positive definite, aligning well with the properties of our bond pricing matrices.

The Bi-CGSTAB algorithm, with preconditioner M (see subsection 4.3.1), for solving linear system $A\mathbf{u} = \mathbf{b}$ has the following scheme:

Algorithm 2: Bi-CGSTAB Method

```

1  $u^0$  is initial guess;  $r^0 = b - Au^0$ 
2  $\bar{r}^0$  is arbitrary vector, such that  $(\bar{r}^0, r^0) \neq 0$ , e.g.,  $\bar{r}^0 = r^0$ 
3  $\rho_{-1} = \alpha_{-1} = \omega_{-1} = 1$ 
4  $v^{-1} = p^{-1} = 0$ 
5 for  $j = 1, 2, \dots$  do
6    $\rho_i = (\bar{r}^0, r^i); \beta_{i-1} \rho_i / \rho_{i-1} (\alpha_{i-1} / \omega_{i-1})$ 
7    $p^i = r^i + \beta_{i-1} (p^{i-1} - \omega_{i-1} v^{i-1})$ 
8    $\hat{p} = M^{-1} p^i$ 
9    $v_i = A\hat{p}$ 
10   $\alpha_i = \rho_i / (\bar{r}^0, v^i)$ 
11   $s = r^i - \alpha_i v^i$ 
12  if  $\|s\|$  is small enough then
13     $u_{i+1} = u_i + \alpha_i \hat{p}$ 
14    quit
15   $z = M^{-1} s$ 
16   $t = Az$ 
17   $\omega_i = (t, s) / (t, t)$ 
18   $u^{i+1} = u^i + \alpha_i \hat{p} + \omega_i z$ 
19  if  $u^{i+1}$  is accurate enough then
20    quit
21   $r^{i+1} = s - \omega_i t$ 

```

In fact, the algorithm follows Bi-CGSTAB for the explicitly postconditioned linear system

$$AM^{-1}\mathbf{y} = \mathbf{b},$$

but the residual vector and vector \mathbf{y}_i are transformed back to \mathbf{u}^i and \mathbf{r}^i corresponding to the original system $A\mathbf{u} = \mathbf{b}$. The benefit of these methods lies in their utilization of short recurrences. However, a drawback is their semi-optimality property. Consequently, this approach requires the use of additional matrix-vector products, and it is not possible to prove any convergence properties. Lastly, it is important to compare the norm of the updated residual with the exact residual $\|\mathbf{f} - A\mathbf{u}_k\|_2$. If a "near" breakdown has happened in the algorithm, these values might vary significantly, sometimes by multiple orders of magnitude.

4.3.1. Preconditioning

Iterative methods like GMRES and Bi-CGSTAB are often used with preconditioning to accelerate convergence [8]. A preconditioner M of a matrix A is a matrix such that $M^{-1}A$ has a smaller condition number than A . This results in the following equation

$$M^{-1}A\mathbf{u} = M^{-1}\mathbf{f}$$

As a result, this will improve the performance of iterative methods. We will use the following preconditioners:

- The Jacobi or diagonal preconditioner: Here matrix M is chosen to be the diagonal of matrix A , so $M = \text{diag}(A)$. This preconditioner is efficient for diagonally dominant matrices.
- Incomplete LU factorization: Here the factorization $A = LU$ is computed, with L a lower triangular matrix and U an upper triangular matrix. Then our preconditioner is $M = LU$ and the equation becomes

$$U^{-1}L^{-1}A\mathbf{u} = U^{-1}L^{-1}\mathbf{f}$$

The Jacobi preconditioner is less computationally expensive compared to ILU. This is because the Jacobi method simplifies calculations by focusing only on the diagonal elements of matrix A , whereas ILU involves a more extensive decomposition process.

4.3.2. Convergence of Iterative Methods

In the subsequent sections, the convergence of the iterative methods GMRES and Bi-CGSTAB on our bond models is examined. In this subsection we outline how certain matrix properties influence the number of iterations needed for convergence. The analysis specifically focuses on the eigenvalue ratio, diagonal dominance, symmetry of the matrix, and the effectiveness of ILU and Jacobi preconditioners. Suppose our system looks like:

$$A\mathbf{u} = \mathbf{f}$$

Key factors influencing the convergence of this system include:

1. **Eigenvalue Ratio:** The ratio of the largest to smallest eigenvalues of A , or the eigenvalue ratio, is a critical factor. A smaller ratio typically correlates with faster convergence for iterative methods.
2. **Diagonal Dominance:** The extent to which A is diagonally dominant affects convergence speed. Strong diagonal dominance, where diagonal elements considerably outweigh off-diagonal elements in magnitude, often results in quicker convergence.
3. **Symmetry:** The analysis particularly considers the impact of symmetry in A . In general, a more symmetric matrix usually enhances convergence properties of iterative methods than less symmetric matrices.
4. **Preconditioners:** The application of ILU and Jacobi preconditioners is explored. A well-chosen preconditioner can greatly reduce the number of iterations required by improving the condition number or influencing the eigenvalue distribution of A .

Other factors, such as sparsity pattern, bandwidth, magnitude of non-zero elements, and perturbations due to rounding errors, also influence convergence but are not the primary focus of this analysis. The numerical study in this thesis is particularly geared towards understanding how the eigenvalue ratio, diagonal dominance, and symmetry, along with the selected preconditioners, impact the efficiency of iterative methods in solving large systems of linear equations.

4.4. Conventional Bond Numerical Analysis

In this section, we delve into the numerical analysis of conventional bond pricing. Our focus is on understanding how changes in market parameters, influence the numerical behavior of our conventional bond pricing model. By observing the eigenvalue ratios and the symmetry of the obtained tridiagonal matrix, we aim to estimate the condition number and understand its implications on the matrix's numerical stability and complexity. Then we will look at the impact of these matrix properties on the efficiency of the iterative solvers discussed in the previous section.

It is important to note that the matrix obtained after applying the Crank-Nicolson finite difference scheme **to the conventional bond PDE is tridiagonal** (4.4). This specific structure means that the ILU preconditioner effectively becomes a complete LU decomposition, leading to a scenario where iterative methods like GMRES and Bi-CGSTAB converge in just one iteration. Due to this significant difference in the matrix structure and the efficiency of the iterative methods, we have decided not to include a direct comparison of the conventional bond model with the green bond model in our results tables. We obtained the following system for the conventional bond:

$$CB_{i-1} = DB_i + K_{i-1} + K_i \quad (4.2)$$

where

$$B_i = \begin{pmatrix} B_{i,1} \\ B_{i,2} \\ \vdots \\ \vdots \\ B_{i,N-1} \end{pmatrix} \quad \text{and} \quad K_i = \begin{pmatrix} \hat{a}_1 B_{i,0} \\ 0 \\ \vdots \\ 0 \\ \hat{c}_{N-1} B_{i,N} \end{pmatrix} \quad (4.3)$$

$$C = \begin{pmatrix} 1 - \hat{b}_1 & -\hat{c}_1 & 0 & \dots & 0 \\ -\hat{a}_2 & 1 - \hat{b}_2 & -\hat{c}_2 & \dots & 0 \\ 0 & -\hat{a}_3 & 1 - \hat{b}_3 & \ddots & \dots \\ \vdots & \ddots & \ddots & \ddots & -\hat{c}_{N-2} \\ 0 & \dots & 0 & -\hat{a}_{N-1} & 1 - \hat{b}_{N-1} \end{pmatrix} \quad (4.4)$$

$$D = \begin{pmatrix} 1 + \hat{b}_1 & \hat{c}_1 & 0 & \dots & 0 \\ \hat{a}_2 & 1 + \hat{b}_2 & \hat{c}_2 & \dots & 0 \\ 0 & \hat{a}_3 & 1 + \hat{b}_3 & \ddots & \dots \\ \vdots & \ddots & \ddots & \ddots & \hat{c}_{N-2} \\ 0 & \dots & 0 & \hat{a}_{N-1} & 1 + \hat{b}_{N-1} \end{pmatrix} \quad (4.5)$$

$$\hat{a} = \frac{\Delta t}{4} \left(\frac{\sigma_r^2 r_j}{\Delta r^2} - \frac{\alpha(\beta - r_j) - \lambda_r \sigma_r \sqrt{r_j}}{\Delta r} \right)$$

$$\hat{b} = -\frac{\Delta t}{2} \left(\frac{\sigma_r^2 r_j}{2\Delta r^2} + r_j \right)$$

$$\hat{c} = \frac{\Delta t}{4} \left(\frac{\sigma_r^2 r_j}{\Delta r^2} + \frac{\alpha(\beta - r_j) - \lambda_r \sigma_r \sqrt{r_j}}{\Delta r} \right)$$

Before analyzing the effects of parameter variations, let us consider some characteristics of our numerical scheme, particularly in terms of stability and eigenvalues. As we observe the coefficients of our discretized system, specifically \hat{a} , \hat{b} , and \hat{c} , we notice an interesting behavior as Δr approaches zero. The symmetric part (second derivative terms), becomes increasingly dominant over the non-symmetric part (first derivative terms). This is attributed to the coefficients of the second derivative terms incorporating a $(1/\Delta r)^2$ factor, becoming more prominent with decreasing Δr . This shift towards a relatively more symmetric matrix typically results in real and non-negative eigenvalues, indicating a stable numerical scheme vital for avoiding oscillations or exponential growth due to small perturbations like rounding

errors. However, this increasing relative symmetry contrasts with the absolute symmetry of the matrix which we will assess by taking the Frobenius norm (Def. 11), $\|C - C^T\|_F$. An increase in this norm reflects the absolute difference in symmetry, illustrating that even minor asymmetries in each element can accumulate to a significant overall asymmetry in a larger matrix. Hence, while finer discretizations improve relative symmetry and stability, they can simultaneously increase the matrix's absolute asymmetry, highlighting the nuanced balance in numerical methods between accuracy, stability, and matrix characteristics. Note that through this section λ_{\max} , λ_{\min} refer to the maximum and minimum eigenvalues of matrix C and that λ_r is a model parameter.

Now, let us start looking at the effect of changes in σ_r , the volatility of the short rate. We can see in table 4.1 and figures 4.1 and 4.2, that if the volatility of the short rate increases, the system becomes more numerically challenging, evidenced by a higher eigenvalue ratio and reduced matrix symmetry. Moreover, the table shows that when the grid size grows, the model becomes more sensitive to volatility changes, intensifying these matrix properties.

σ_r	N	$\lambda_{\max}/\lambda_{\min}$	$\ C - C^T\ _F$
0.15	10	1.6	3.7
	100	73.9	137.5
	200	308.4	392.0
	300	703.7	722.1
0.20	10	1.8	3.8
	100	133.8	139.3
	200	552.4	397.2
	300	1256.4	731.6
0.25	10	1.9	3.9
	100	205.4	141.7
	200	851.2	403.9
	300	1941.7	744.1

Table 4.1: Matrix properties different values of σ_r , $M = 11$, $\alpha = 1.0$, $\beta = 0.05$, $\lambda_r = 0.01$

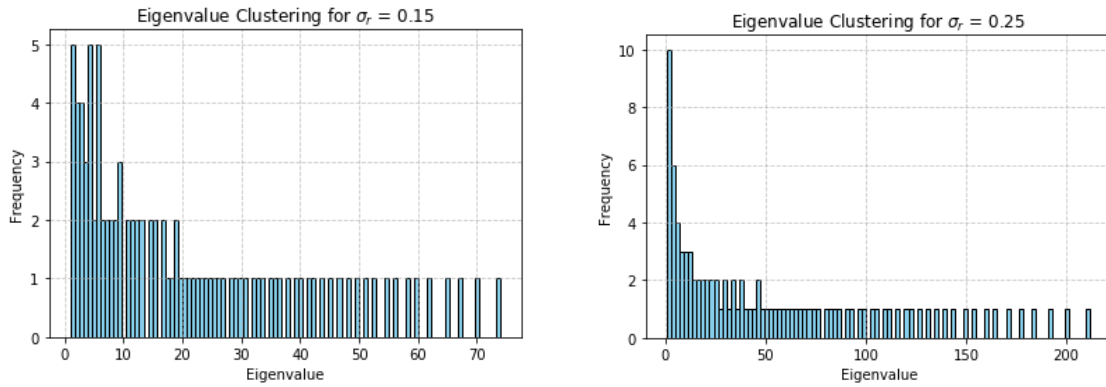


Figure 4.1: Eigenvalue distribution for different values of σ_r and $N = 100$

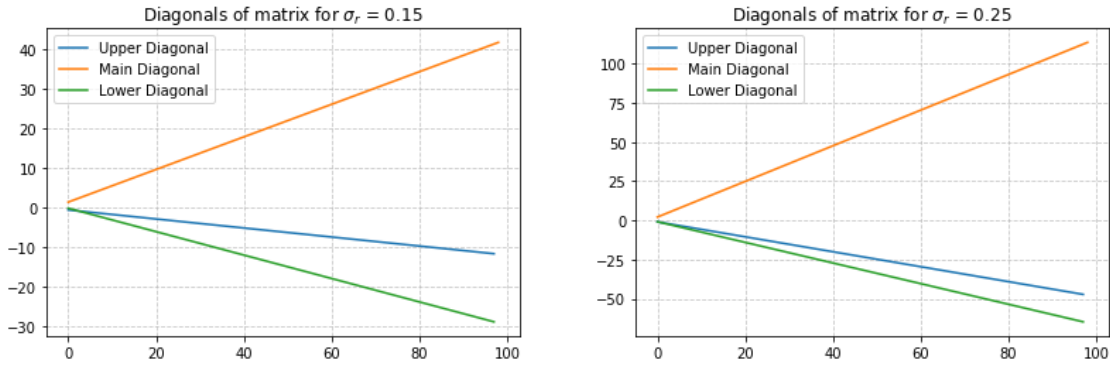


Figure 4.2: Diagonals of the matrix for different values of σ_r , and $N = 100$. (For a higher σ_r , the upper and lower diagonals are further apart from each other)

In tables (4.2), (4.3) we can see what the effect is of the increase in complexity of the matrix on the efficiency of the iterative solvers GMRES and Bi-CGSTAB. We notice that, in general, an increase in volatility increases the amount of iterations the methods need to reach the tolerance value $1e - 08$. If we look at gridsize N , we see that despite a bigger N providing a finer discretization and potentially more accurate solutions, both GMRES and Bi-CGSTAB demand effective preconditioners to ensure faster convergence. We can see that the Jacobi preconditioner has great impact on the convergence speed of both methods. The higher the volatility and gridsize the larger the effect is.

σ_r	N	Jacobi	None
0.15	10	8	9
	100	24	37
	200	50	71
	300	49	102
0.20	10	9	9
	100	26	46
	200	30	92
	300	38	133
0.25	10	9	7
	100	36	64
	200	43	115
	300	69	164

Table 4.2: Performance of GMRES for various σ_r values

σ_r	N	Jacobi	None
0.15	10	12	10
	100	47	72
	200	91	111
	300	150	153
0.20	10	11	9
	100	65	76
	200	120	127
	300	171	203
0.25	10	14	10
	100	75	89
	200	115	166
	300	199	223

Table 4.3: Performance of Bi-CGSTAB for various σ_r values

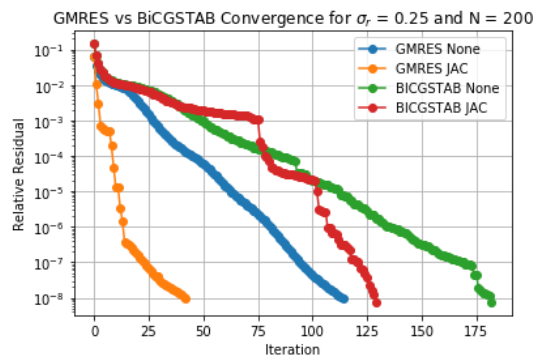
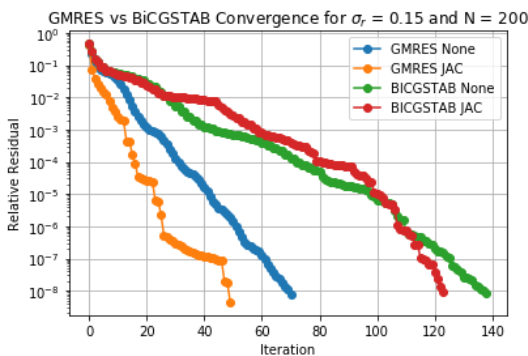


Figure 4.3: GMRES vs Bi-CGSTAB, for different values of σ_r , $tol = 10^{-8}$

Now we will look what happens to our system by changes in parameter α , the mean reversion speed of the short rate. If we look at table 4.4 and figure 4.4, we see that increasing/decreasing α has almost

no effect on the eigenvalue ratio of the matrix. However, when we look at the table 4.4 and figure 4.5, we see that differences in α have big impact on the symmetry of the matrix in our system. We can see that this asymmetry becomes even bigger when N , and thus the grid size, increases.

α	N	$\lambda_{\max}/\lambda_{\min}$	$\ C - C^T\ _F$
0.5	10	1.6	1.9
	100	132.3	71.7
	200	543.9	204.4
	300	1238.8	376.5
1.0	10	1.8	3.8
	100	133.8	139.3
	200	552.5	397.2
	300	1256.5	731.6
1.5	10	1.9	5.6
	100	132.7	206.9
	200	550.3	590.1
	300	1252.9	1086.9

Table 4.4: Matrix properties different values of α , $M = 11$, $\sigma_r = 0.2$, $\beta = 0.05$, $\lambda_r = 0.01$

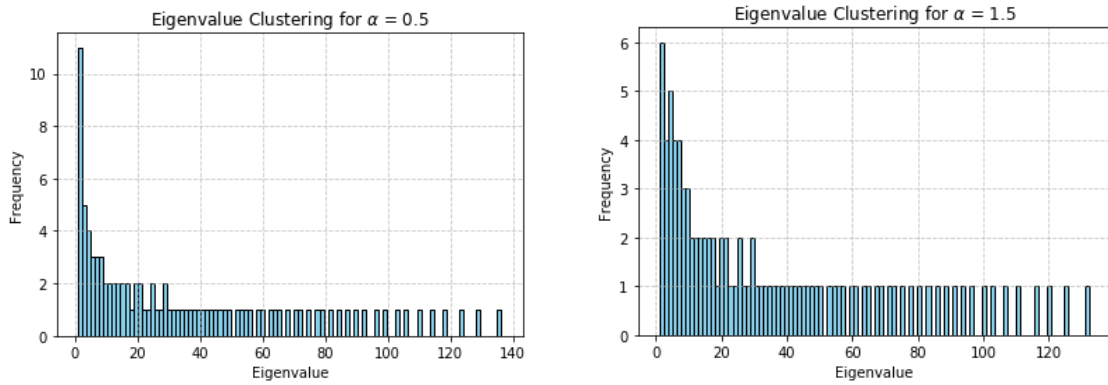


Figure 4.4: Eigenvalue distribution for different values of α and $N = 100$

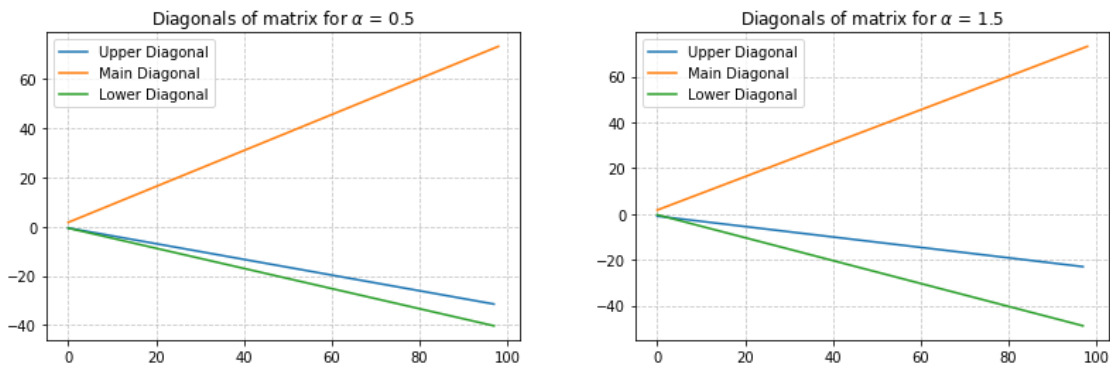


Figure 4.5: Diagonals of the matrix for different values of α and $N = 100$

Now, knowing that higher values of α lead to a more ill-conditioned matrix and reduced symmetry, let us look at the convergence behavior of GMRES and Bi-CGSTAB. Although both GMRES and Bi-CGSTAB show a general trend of increasing iterations with increasing grid size N , we see that they show different effects in response to changes in the parameter α . If we look at figure 4.6, we can see that for $N = 200$, an increase in α has a positive effect on the convergence speed of Bi-CGSTAB, but a

negative effect on GMRES. Moreover, we see that the use of preconditioners has great positive impact on the convergence speed, especially for GMRES.

α	N	Jacobi	None
0.5	10	6	6
	100	18	55
	200	17	104
	300	25	150
1.0	10	9	9
	100	26	46
	200	29	92
	300	34	133
1.5	10	7	9
	100	43	56
	200	30	95
	300	42	127

Table 4.5: Performance of GMRES for various α values

α	N	Jacobi	None
0.5	10	10	10
	100	80	81
	200	136	136
	300	201	207
1.0	10	11	9
	100	65	76
	200	120	127
	300	171	203
1.5	10	12	11
	100	36	76
	200	85	113
	300	137	182

Table 4.6: Performance of Bi-CGSTAB for various α values

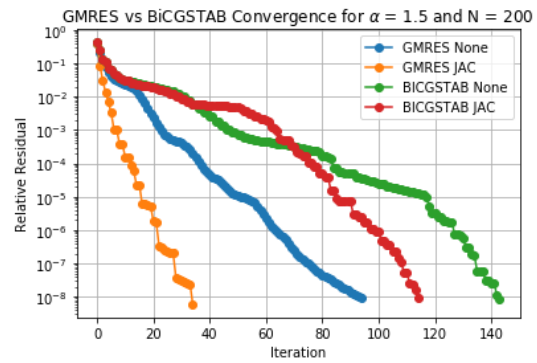
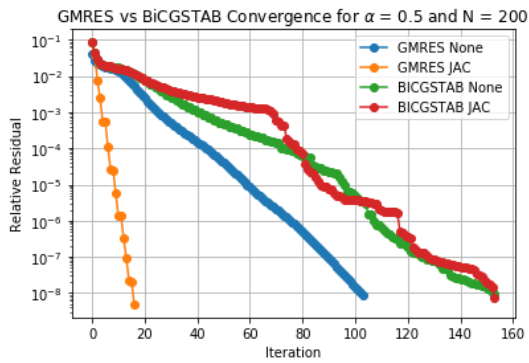


Figure 4.6: GMRES vs Bi-CGSTAB, for different values of α , $tol = 10^{-8}$

Let us now analyse the effects of the long-term mean parameter β on the system model. Table 4.7 shows that both the eigenvalue ratio and matrix symmetry are slightly influenced by changes in β . We see that increases in the grid size N have a more significant effect on the matrix properties. Looking at the Frobenius norm of $C - C^T$, we see that the matrix tends to become a little bit more symmetric with higher β values.

β	N	$\lambda_{\max}/\lambda_{\min}$	$\ C - C^T\ _F$
0.03	10	1.7	3.9
	100	129.4	143.7
	200	540.6	409.6
	300	1236.5	754.5
0.05	10	1.8	3.8
	100	133.8	139.3
	200	552.5	397.2
	300	1256.5	731.6
0.07	10	1.8	3.7
	100	134.0	135.0
	200	550.1	384.9
	300	1250.5	709.0

Table 4.7: Matrix properties different values of β , $M = 11$, $\sigma_r = 0.2$, $\alpha = 1.0$, $\lambda_r = 0.01$

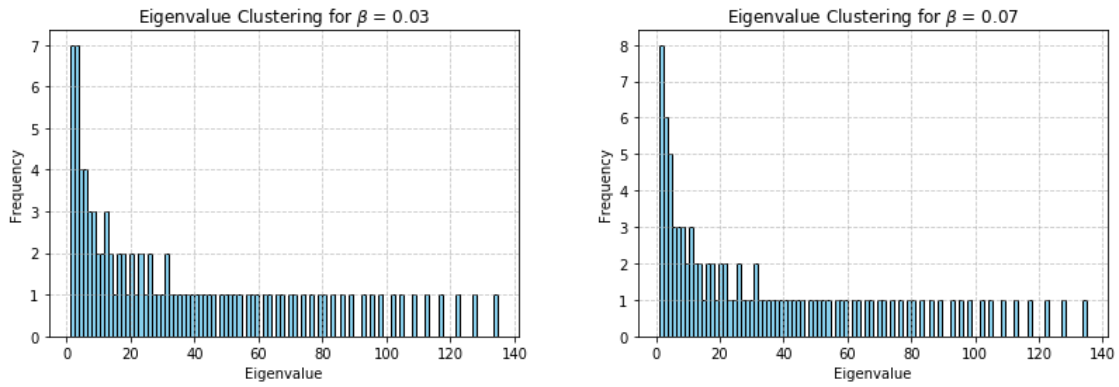


Figure 4.7: Eigenvalue distribution for different values of β and $N = 100$

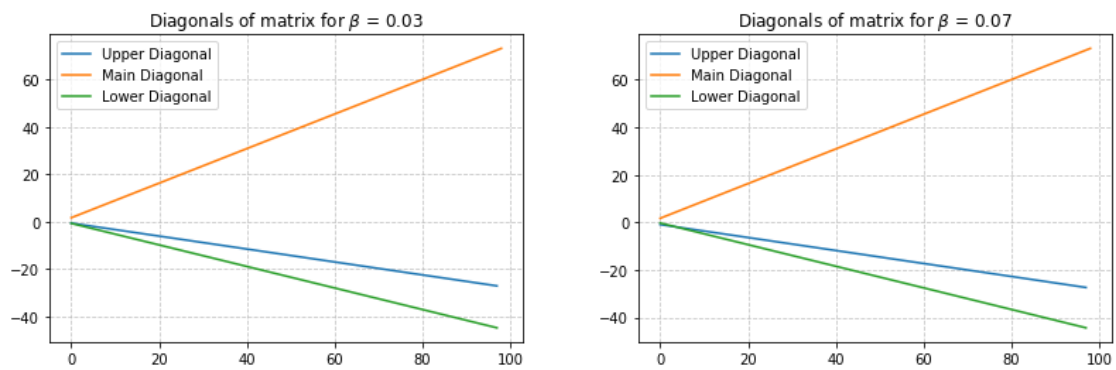


Figure 4.8: Diagonals of the matrix for different values of β and $N = 100$

If we look at the convergence of GMRES and Bi-CGSTAB, we see that they are not as sensitive to changes in β as to the other parameters, suggesting a relatively stable behavior across different long-term mean values.

β	N	Jacobi	None
0.03	10	11	9
	100	38	55
	200	24	99
	300	31	136
0.05	10	9	9
	100	26	46
	200	29	92
	300	34	133
0.07	10	9	9
	100	27	51
	200	29	95
	300	57	136

Table 4.8: Performance of GMRES for various β values

β	N	Jacobi	None
0.03	10	11	11
	100	63	81
	200	123	139
	300	190	205
	300	190	205
0.05	10	11	9
	100	65	76
	200	120	127
	300	171	203
	300	171	203
0.07	10	11	11
	100	65	84
	200	120	130
	300	168	195
	300	168	195

Table 4.9: Performance of Bi-CGSTAB for various β values

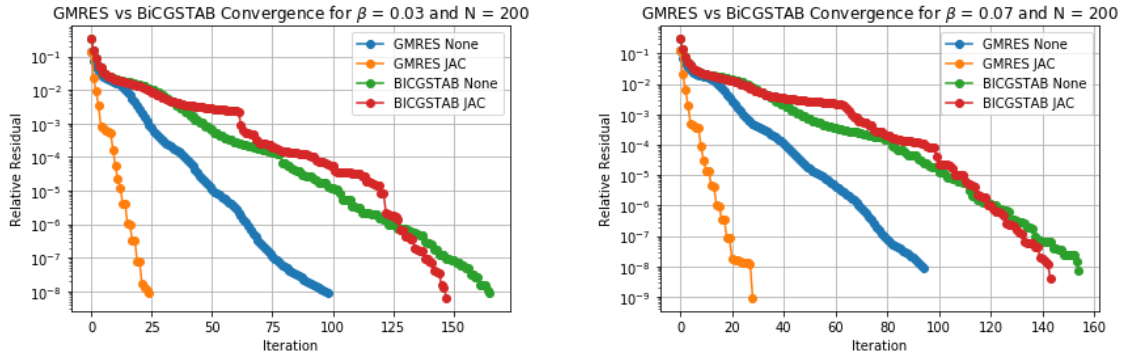


Figure 4.9: GMRES vs Bi-CGSTAB, for different values of β , $tol = 10^{-8}$

Let us now look at changes in the matrix properties (table 4.10) in response to different values of parameter λ_r , the market price of risk. Like the other parameters, we see a consistent increase in the eigenvalue ratio and asymmetry for larger grid sizes. A positive λ_r shows the most substantial decrease in symmetry (figure 4.11), particularly in larger grids, while positive values, both large and small, also impact the absolute symmetry but to varying degrees. Moreover, the different values of λ_r have almost no effect on the eigenvalue ratio of the matrix our system (see figure 4.10).

λ_r	N	$\lambda_{\max}/\lambda_{\min}$	$\ C - C^T\ _F$
-1.0	10	1.7	3.0
	100	134.3	110.4
	200	551.8	314.7
	300	1253.9	579.7
0.01	10	1.8	3.8
	100	133.8	139.3
	200	552.5	397.2
	300	1256.5	731.6
1.0	10	1.8	4.6
	100	132.7	168.9
	200	552.5	481.4
	300	1258.1	886.6

Table 4.10: Matrix properties for different values of λ_r , $M = 11$, $\sigma_r = 0.2$, $\alpha = 1.0$, $\beta = 0.05$

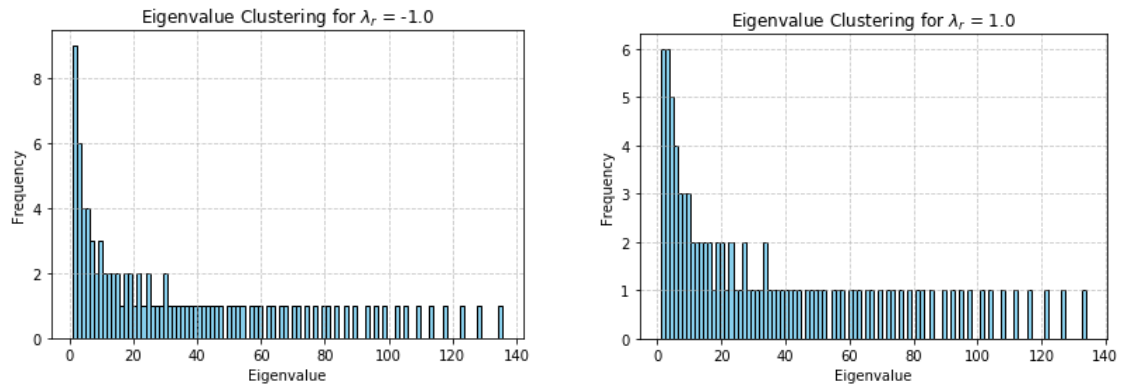


Figure 4.10: Eigenvalue distribution for different values of λ_r , and $N = 100$

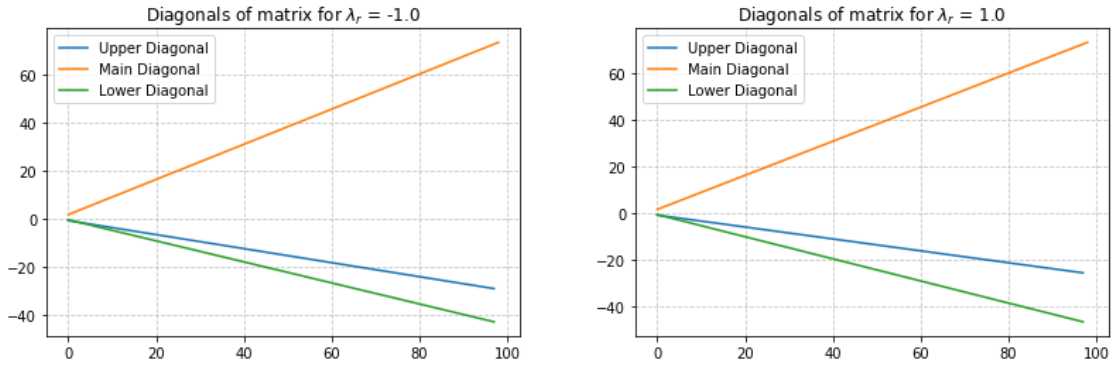


Figure 4.11: Diagonals of the matrix for different values of λ_r and $N = 100$

Let us now look at tables 4.11, 4.12 and figure 4.12 to see the influence of λ_r on the efficiency of GMRES and Bi-CGSTAB. We find that with both GMRES and Bi-CGSTAB, the iteration amount varies subtly across different λ_r values, showing no clear trend of increase or decrease. This suggests that the sensitivity to changes in λ_r is nuanced.

λ_r	N	Jacobi	None
-1.0	10	10	8
	100	24	50
	200	18	95
	300	27	137
0.01	10	10	9
	100	26	46
	200	30	92
	300	38	133
1.0	10	9	9
	100	34	46
	200	28	89
	300	38	129

Table 4.11: Performance of GMRES for various λ_r values

λ_r	N	Jacobi	None
-1.0	10	11	11
	100	70	82
	200	142	137
	300	218	183
0.01	10	11	9
	100	65	76
	200	120	127
	300	171	203
1.0	10	13	11
	100	50	76
	200	112	135
	300	166	198

Table 4.12: Performance of Bi-CGSTAB for various λ_r values

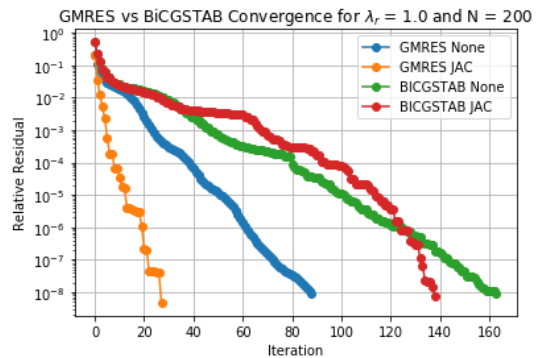
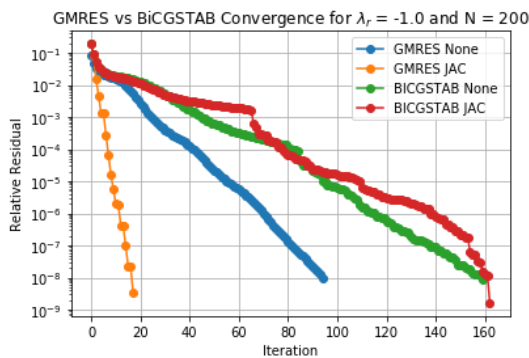


Figure 4.12: GMRES vs Bi-CGSTAB, for different values of λ_r , $tol = 10^{-8}$

4.5. Green Bond GMRES analysis

In this section we will delve into the effect of various parameters on the behavior of the matrix equation used to determine the coupon rate of a green bond. A critical aspect of this analysis is to understand how different parts of the discretized PDE contribute to the matrix structure and its resulting characteristics. Unlike the observed tridiagonal matrix in the conventional bond model, we can see that matrix C (4.7)

in this model is much more difficult due to the inclusion of the carbon price variable c_t . In this matrix C , decreasing Δr and Δc significantly influences both the diagonal dominance and the relative symmetry of the matrix. The main diagonal element \hat{n}_5 increases more rapidly due to its dependence on both $(1/\Delta r)^2$ and $(1/\Delta c)^2$, enhancing diagonal dominance. This is contrasted with the other \hat{n} coefficients in the matrix, which grow slower as they depend on single quadratic terms. This differential scaling not only leads to a matrix that is more diagonally dominant and relatively symmetric but also impacts the eigenvalues and stability of the system. The eigenvalues become real and positive, which are indicative for a more stable numerical scheme. The enhanced diagonal dominance and symmetry typically result in real, positive eigenvalues, which are indicative of a stable numerical scheme. This stability is crucial in ensuring that the numerical solutions are reliable and not prone to oscillations or numerical instabilities. Note that through this section λ_{\max} , λ_{\min} refer to the maximum and minimum eigenvalues of matrix C and that λ_r and λ_c are model parameters. Because C is not tridiagonal, the ILU-decomposition is not the same as LU-decomposition, so we can use it as a preconditioner. We obtained the following system of equations for the green bond:

$$CB^{i-1} = DB^i + K^{i-1} + K^i \quad (4.6)$$

where

$$C = \begin{pmatrix} 1 - \hat{n}_5 & -\hat{n}_6 & 0 & \dots & 0 & 0 & -\hat{n}_8 & -\hat{n}_9 & \dots & 0 \\ -\hat{n}_4 & 1 - \hat{n}_5 & -\hat{n}_6 & 0 & \dots & 0 & -\hat{n}_7 & -\hat{n}_8 & -\hat{n}_9 & 0 \\ 0 & -\hat{n}_4 & 1 - \hat{n}_5 & -\hat{n}_6 & 0 & \dots & \ddots & \ddots & \ddots & \ddots \\ 0 & 0 & -\hat{n}_4 & 1 - \hat{n}_5 & -\hat{n}_6 & 0 & \dots & \ddots & \ddots & \ddots \\ 0 & 0 & 0 & -\hat{n}_4 & 1 - \hat{n}_5 & -\hat{n}_6 & 0 & \dots & \ddots & \ddots \\ \vdots & \ddots & \vdots \\ \vdots & \ddots & 0 \\ -\hat{n}_1 & -\hat{n}_2 & -\hat{n}_3 & 0 & \dots & 0 & -\hat{n}_4 & 1 - \hat{n}_5 & -\hat{n}_6 & \ddots \\ \dots & -\hat{n}_1 & -\hat{n}_2 & -\hat{n}_3 & 0 & \dots & 0 & -\hat{n}_4 & 1 - \hat{n}_5 & -\hat{n}_6 \\ 0 & \dots & -\hat{n}_1 & -\hat{n}_2 & 0 & 0 & \dots & 0 & -\hat{n}_4 & 1 - \hat{n}_5 \end{pmatrix} \quad (4.7)$$

with

$$\begin{aligned} \hat{n}_1 &= \frac{\Delta t}{2} \frac{c_k \sigma_c \sigma_r \rho \sqrt{r_j}}{4 \Delta r \Delta c} & \hat{n}_2 &= \frac{\Delta t}{2} \left(\frac{\sigma_r^2 r_j}{2 \Delta r^2} - \frac{\alpha(\beta - r_j) - \lambda_2 \sigma_r \sqrt{r_j}}{2 \Delta r} \right) & \hat{n}_3 &= \frac{\Delta t}{2} \frac{-c_k \sigma_c \sigma_r \rho \sqrt{r_j}}{4 \Delta r \Delta c} \\ \hat{n}_4 &= \frac{\Delta t}{2} \left(\frac{\sigma_c^2 c_k^2}{2 \Delta c^2} - \frac{\mu c_k - \lambda_1 \sigma_c c_k}{2 \Delta c} \right) & \hat{n}_5 &= -\frac{\Delta t}{2} \left(\frac{\sigma_r^2 r_j}{\Delta r^2} + \frac{\sigma_c^2 c_k^2}{\Delta c^2} + r_j \right) & \hat{n}_6 &= \frac{\Delta t}{2} \left(\frac{\sigma_c^2 c_k^2}{2 \Delta c^2} + \frac{\mu c_k - \lambda_1 \sigma_c c_k}{2 \Delta c} \right) \\ \hat{n}_7 &= \frac{\Delta t}{2} \frac{-c_k \sigma_c \sigma_r \rho \sqrt{r_j}}{4 \Delta r \Delta c} & \hat{n}_8 &= \frac{\Delta t}{2} \left(\frac{\sigma_r^2 r_j}{2 \Delta r^2} - \frac{\alpha(\beta - r_j) + \lambda_2 \sigma_r \sqrt{r_j}}{2 \Delta r} \right) & \hat{n}_9 &= \frac{\Delta t}{2} \frac{c_k \sigma_c \sigma_r \rho \sqrt{r_j}}{4 \Delta r \Delta c} \end{aligned}$$

Now, we will consider the effect changing the volatility of the carbon price parameter, σ_c , has on the matrix. We can see that when we increase σ_c , the term $(0.5\sigma_c^2 c_k^2)$ in \hat{n}_4 , \hat{n}_5 and \hat{n}_6 becomes larger. Consequently, this increases the values on the main-, super- and sub-diagonal of the central band, impacting the matrix's diagonal dominance and eigenvalue distribution. Moreover, an increase in σ_c in our PDE, enhances $(c \sigma_c \sigma_r \rho \sqrt{r})$ and will contribute to the terms \hat{n}_1 , \hat{n}_3 , \hat{n}_7 and \hat{n}_9 . This has effect on the off-diagonal elements on the upper and lower band of the matrix. If we look at table 4.13, we see that increasing σ_c enhances both the diagonal and certain off-diagonal elements, which leads to a larger eigenvalue spread. This is because the matrix becomes less diagonally dominant and more difficult. The increase in far off-diagonal elements contributes to the matrix's absolute asymmetry, increasing the Frobenius norm of $C - C^T$.

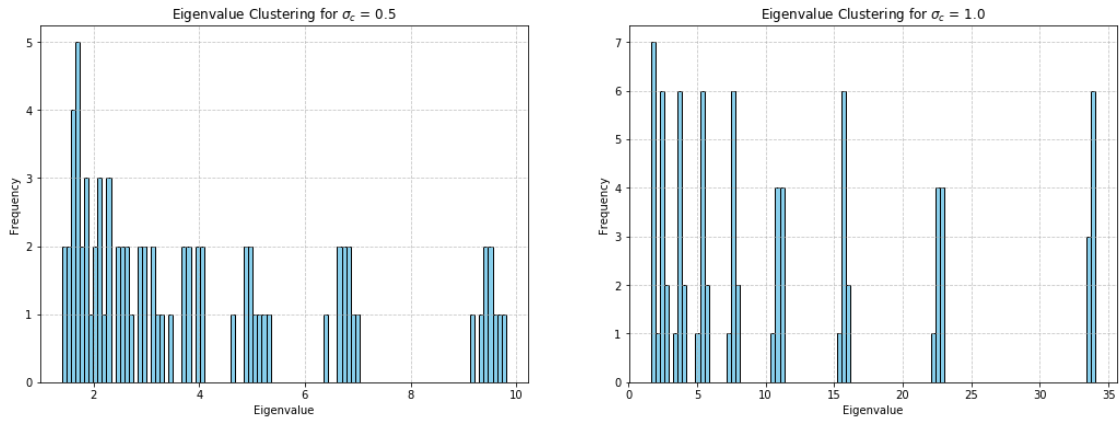


Figure 4.13: Eigenvalue distribution for different values of σ_c and $N = 10$

σ_c	$N = P$	$\lambda_{\max}/\lambda_{\min}$	$\ C - C^T\ _F$
0.5	10	8.4	11.7
	100	1223.9	1422.8
	200	5081.6	5749.8
	300	11592.6	12981.3
0.8	10	17.5	14.6
	100	2652.0	1760.0
	200	11013.7	7109.0
	300	25131.8	16047.5
1.0	10	24.6	18.7
	100	3741.9	2248.3
	200	15539.9	9079.2
	300	35462.8	20493.0

Table 4.13: Matrix properties for different values of σ_c

We can see in table 4.14 that the number of iterations required for convergence in GMRES (with and without preconditioners) increases with higher σ_c and larger grid sizes. This is the direct consequence of the increasing eigenvalue spread and decreasing symmetry, as both these factors can make the numerical solution more difficult. We see that the ILU and JAC preconditioners significantly improve convergence compared to GMRES without preconditioners, particularly at higher volatilities. The effectiveness of ILU in reducing iterations more than JAC can be attributed to its ability to better approximate the inverse of the matrix.

σ_c	$N = P$	ILU	Jacobi	None
0.5	10	2	27	30
	100	6	185	220
	200	8	338	420
	300	9	478	613
0.8	10	2	33	39
	100	6	213	314
	200	9	390	587
	300	9	557	833
1.0	10	2	35	41
	100	6	217	363
	200	9	417	696
	300	9	595	996

Table 4.14: Performance of GMRES for various σ_c values

σ_c	$N = P$	ILU	Jacobi	None
0.5	10	3	15	17
	100	5	108	159
	200	6	201	331
	300	7	297	425
0.8	10	3	18	25
	100	5	142	244
	200	6	255	457
	300	7	347	689
1.0	10	3	20	27
	100	5	134	276
	200	6	286	507
	300	8	361	792

Table 4.15: Performance of Bi-CGSTAB for various σ_c values

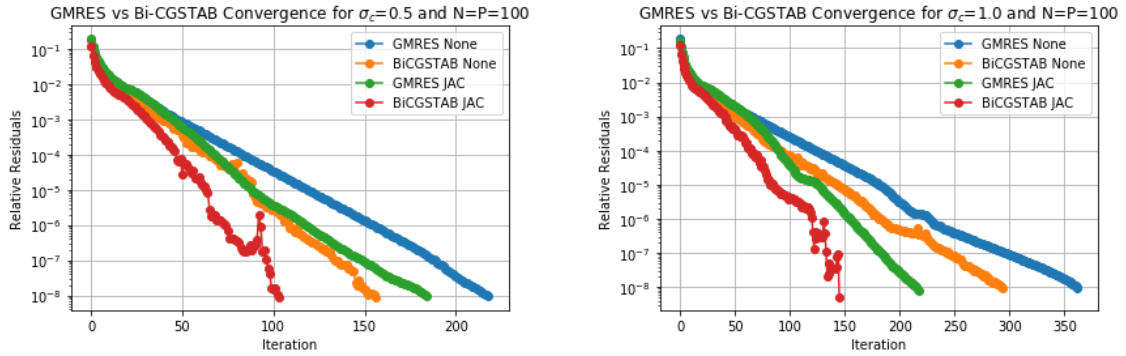


Figure 4.14: GMRES vs Bi-CGSTAB for different values of σ_c

In tables 4.16 and 4.17 we show the effect of the short rate volatility parameter σ_r on our model. We see that when σ_r increases, the amount of iterations GMRES and Bi-CGSTAB also grows. But let us now compare the effects of σ_r and σ_c on the efficiency of the iterative solvers. We notice the volatility of the carbon price, σ_c has a more pronounced effect on the efficiency of the iterative solvers than the volatility of the short rate. In the next section (4.6) we will discuss this in more detail.

σ_r	$N = P$	ILU	Jacobi	None
0.15	100	6	210	311
	200	8	385	582
	300	8	548	825
0.2	100	6	213	314
	200	8	390	587
	300	9	557	833
0.25	100	6	229	317
	200	8	425	590
	300	9	604	838

Table 4.16: Performance of GMRES for various σ_r values

σ_r	$N = P$	ILU	Jacobi	None
0.15	100	5	126	230
	200	6	258	453
	300	7	363	584
0.2	100	5	142	244
	200	6	255	480
	300	7	347	689
0.25	100	5	159	236
	200	6	265	483
	300	8	357	698

Table 4.17: Performance of Bi-CGSTAB for various σ_r values

Now we will look at the correlation coefficient ρ . We observe in table 4.18 that for larger grid sizes ($N = P \geq 100$), both the eigenvalue ratios and the Frobenius norms are the same for the different values of ρ . This means that the impact of the correlation coefficient ρ on the matrix characteristics becomes less pronounced as the grid size increases. But, we can see in figure 4.15 that even if the eigenvalue ratios are the same, the actual distribution of the eigenvalues in the complex plane can be different. This is why we still see some differences in the amount of iterations GMRES performs for different values of ρ .

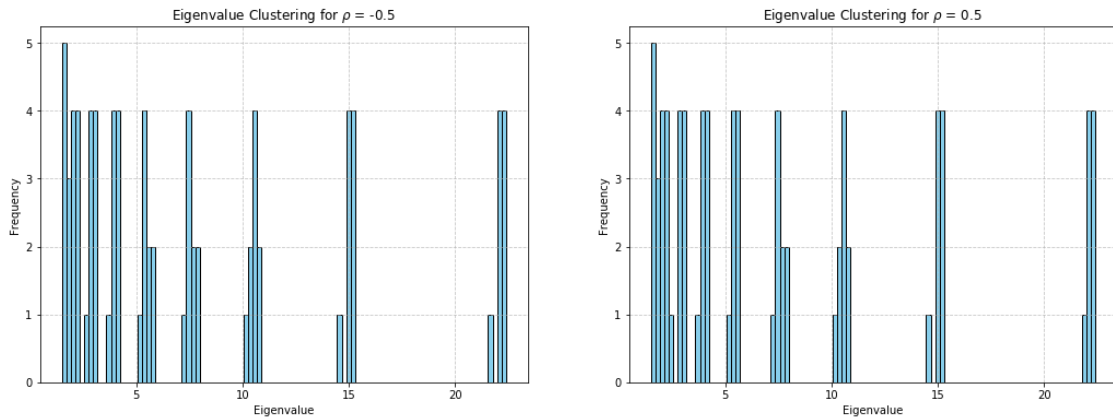


Figure 4.15: Eigenvalue distribution for different values of ρ and $N = 10$

ρ	$N = P$	$\lambda_{\max}/\lambda_{\min}$	$\ C - C^T\ _F$
-0.5	10	17.2	14.6
	100	2652.0	1760.0
	200	11013.7	7109.0
	300	25131.8	16047.5
0.0	10	17.4	14.6
	100	2652.0	1760.0
	200	11013.7	7109.0
	300	25131.8	16047.5
0.5	10	17.5	14.6
	100	2652.0	1760.0
	200	11013.7	7109.0
	300	25131.8	16047.5

Table 4.18: Matrix properties for different values of ρ

ρ	$N = P$	ILU	Jacobi	None
-0.5	10	2	32	38
	100	6	213	314
	200	9	390	587
	300	8	557	833
0.0	10	2	32	38
	100	6	213	314
	200	9	390	587
	300	8	557	833
0.05	10	2	33	39
	100	6	213	314
	200	9	390	587
	300	8	557	833

Table 4.19: Performance of GMRES for various ρ values

ρ	$N = P$	ILU	Jacobi	None
-0.5	10	3	18	25
	100	5	141	233
	200	6	257	455
	300	7	350	688
0.0	10	3	18	25
	100	5	140	212
	200	6	255	457
	300	7	428	700
0.05	10	3	18	25
	100	5	142	244
	200	6	255	480
	300	7	347	689

Table 4.20: Performance of Bi-CGSTAB for various ρ values

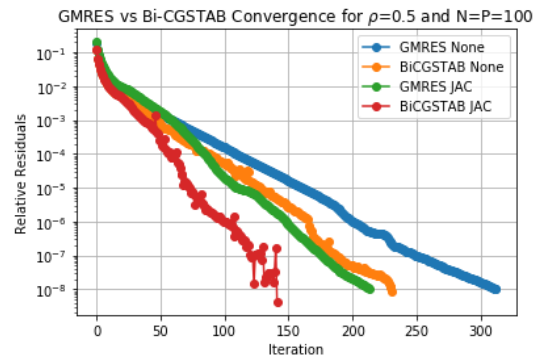
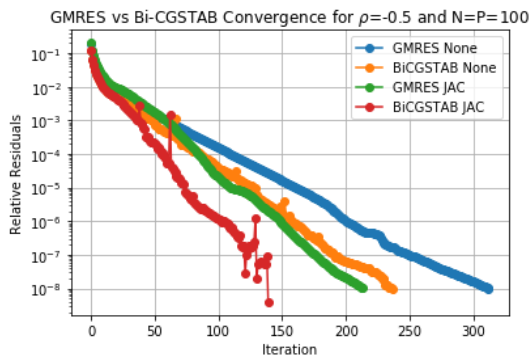


Figure 4.16: GMRES vs Bi-CGSTAB for different values of ρ

The carbon price drift parameter μ directly affects terms \hat{n}_4 and \hat{n}_6 in the matrix. These terms influence the rate of change of the coupon rate with respect to the carbon price. If we look at figure 4.17 and table 4.21, we can see that changes in μ do not show great impact on the eigenvalue ratio. Because μ only impacts \hat{n}_4 and \hat{n}_6 , we see that the influence on the absolute asymmetry is significant but not the sole factor. The variation in the number of iterations across different μ values show that μ has some role in the convergence behavior for GMRES.

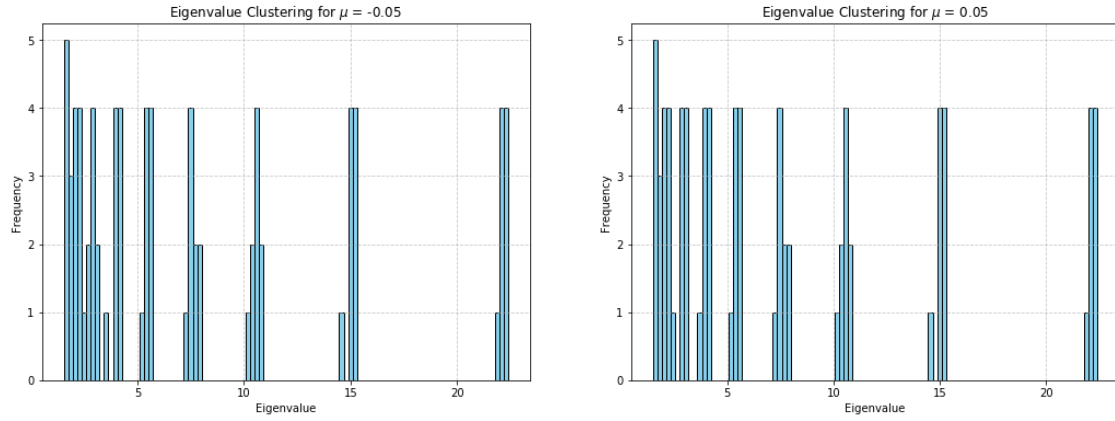


Figure 4.17: Eigenvalue distribution for different values of μ and $N = 10$

μ	$N = P$	$\lambda_{\max}/\lambda_{\min}$	$\ C - C^T\ _F$
-0.05	10	17.5	15.7
	100	2633.0	1885.0
	200	10934.7	7613.9
	300	24951.6	17186.8
0.0	10	17.5	15.1
	100	2643.2	1821.0
	200	10977.3	7355.6
	300	25048.8	16604.0
0.05	10	17.5	14.6
	100	2652.0	1759.8
	200	11013.7	7108.9
	300	25131.8	16047.5

Table 4.21: Matrix properties for different values of μ

μ	$N = P$	ILU	Jacobi	None
-0.05	10	2	32	38
	100	6	213	311
	200	9	387	577
	300	8	553	819
0.0	10	2	32	39
	100	6	213	312
	200	9	388	582
	300	8	555	826
0.05	10	2	33	39
	100	6	213	314
	200	9	390	587
	300	8	557	833

Table 4.22: Performance of GMRES for various μ values

μ	$N = P$	ILU	Jacobi	None
-0.05	10	3	17	25
	100	5	141	233
	200	6	255	398
	300	7	350	667
0.0	10	3	18	25
	100	5	128	230
	200	6	274	466
	300	7	385	691
0.05	10	3	18	25
	100	5	142	244
	200	6	255	480
	300	7	347	689

Table 4.23: Performance of Bi-CGSTAB for various μ values

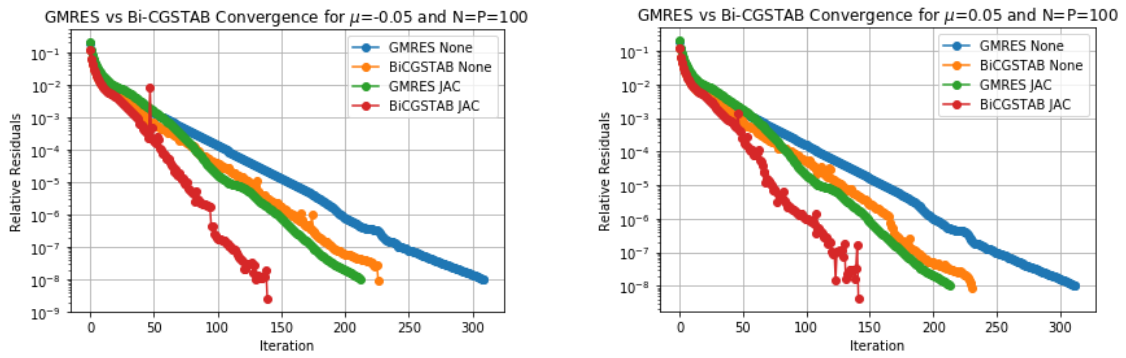


Figure 4.18: GMRES vs Bi-CGSTAB for different values of μ

In table 4.24 we show the effects of λ_c , the market price of risk for the carbon price. When we look at the eigenvalue ratio and $\|C - C^T\|$ columns, we can see that when $\lambda_c = 1.0$, matrix C has the smallest eigenvalue ratio, but is the least symmetric. Moreover, GMRES performs the best when $\lambda_c = 1.0$. So we can conclude that the lower eigenvalue ratio has more impact on the condition number of the matrix C , than the symmetry.

λ_c	$N = P$	$\lambda_{\max}/\lambda_{\min}$	$\ C - C^T\ _F$
-1.0	10	16.7	11.8
	100	2585.6	1433.0
	200	10737.7	5791.1
	300	24502.1	13074.4
-0.01	10	17.5	14.7
	100	2650.7	1769.4
	200	11008.3	7147.6
	300	25119.5	16134.7
1.0	10	16.1	25.0
	100	2350.7	2992.8
	200	9760.8	12083.3
	300	22273.6	27271.6

Table 4.24: Matrix properties for different values of λ_c

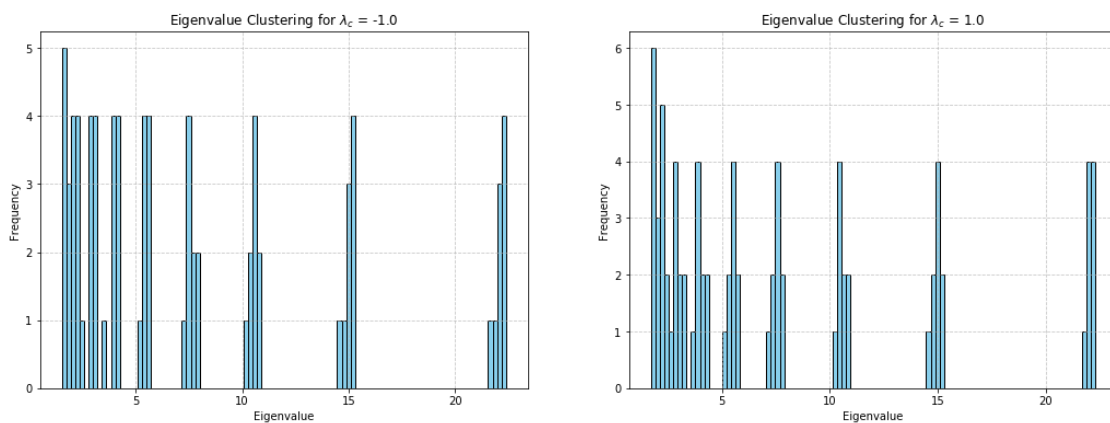


Figure 4.19: Eigenvalue distribution for different values of λ_c and $N = 10$

λ_c	$N = P$	ILU	Jacobi	None
-1.0	10	2	34	40
	100	6	214	328
	200	9	401	627
	300	9	573	906
-0.01	10	2	33	39
	100	6	213	314
	200	9	390	586
	300	8	557	832
1.0	10	2	28	34
	100	5	202	262
	200	6	364	477
	300	7	521	681

Table 4.25: Performance of GMRES for various λ_c values

λ_c	$N = P$	ILU	Jacobi	None
-1.0	10	3	22	27
	100	5	144	245
	200	6	254	501
	300	7	383	678
-0.01	10	3	18	25
	100	5	142	244
	200	6	255	480
	300	7	347	689
1.0	10	3	17	19
	100	5	138	225
	200	6	273	385
	300	7	403	528

Table 4.26: Performance of Bi-CGSTAB for various λ_c values

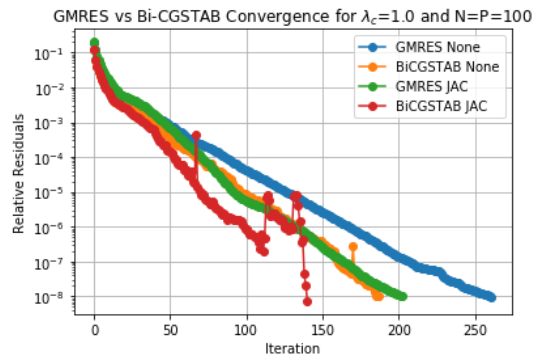
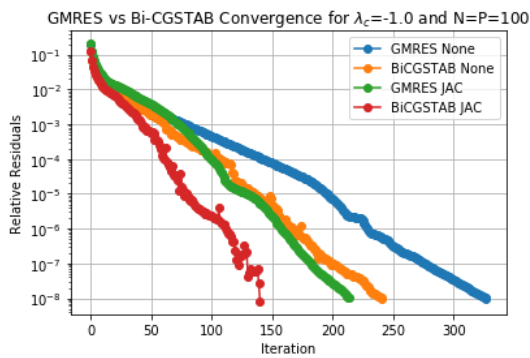


Figure 4.20: GMRES vs Bi-CGSTAB for different values of λ_c

λ_r	$N = P$	ILU	JAC	None
-1.0	10	2	29	35
	100	6	212	318
	200	8	392	592
	300	8	548	839
0.01	10	2	33	39
	100	6	214	313
	200	9	390	586
	300	8	557	831
1.0	10	2	35	40
	100	5	237	333
	200	9	419	580
	300	7	590	823

Table 4.27: Performance of GMRES for various λ_r values

λ_r	$N = P$	ILU	JAC	None
-1.0	10	3	16	22
	100	5	135	245
	200	6	264	426
	300	7	354	686
0.01	10	3	19	25
	100	5	142	232
	200	6	256	466
	300	7	380	650
1.0	10	3	22	29
	100	5	156	231
	200	9	284	441
	300	7	404	579

Table 4.28: Performance of Bi-CGSTAB for various λ_r values

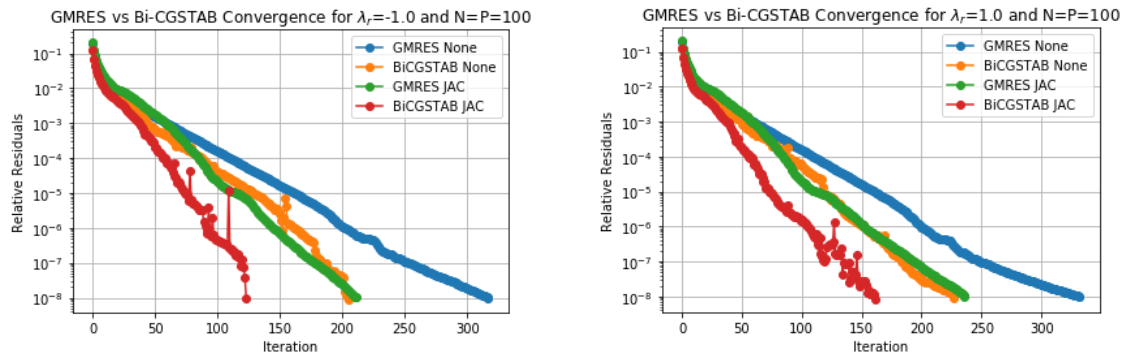


Figure 4.21: GMRES vs Bi-CGSTAB for different values of λ_r .

Let us now compare the GMRES and Bi-CGSTAB methods between the different coupons at the same time step i . We use the parameter setting as described in the table below and obtain table 4.29. We observe that for V_1 the most iterations are needed and fewer for subsequent coupons. This is because, as the model progresses back in time, the solutions for each time step are closer to the previous solutions. In iterative solvers, the convergence rate is often influenced by how "close" the initial guess is to the true solution.

Parameter values			
α	1.0	β	0.05
σ_c	0.8	σ_r	0.2
μ	0.05	ρ	0.2

$N = P = 300$	GMRES			Bi-CGSTAB			
	$M = 11$	ILU	Jacobi	None	ILU	Jacobi	None
V_1		6	214	313	5	141	247
V_2		6	209	249	5	132	195
V_3		5	199	241	5	115	190
V_4		5	195	238	4	114	187

Table 4.29: Performance of GMRES and Bi-CGSTAB for different coupons

4.6. Comparative Analysis of the Conventional and Green Bond models

Having thoroughly analyzed the numerical properties and behaviors of the models, we will conduct a comparative analysis of the results from the previous sections. This analysis aims to enhance our understanding of how environmental factors impact the convergence efficiency of the iterative methods. Let us begin by looking at the green bond model, focusing on the volatility parameters σ_r and σ_c . The iteration counts for convergence, as observed in the tables in the previous section, reveal that carbon price volatility σ_c significantly impacts the model more than short rate volatility σ_r (tables 4.30, 4.31). This effect indicates that variations in carbon price introduce a higher degree of variability into the model than changes in the short rate do. This heightened sensitivity to σ_c stems from the particular way the carbon price interacts with the model and its variables. The inclusion of the double knock-out call option on the carbon price further accentuates this effect. This feature means that high σ_c can lead to more frequent triggering of the knockout barriers, resulting in abrupt and significant changes in the coupon rate's valuation. This does not hold for σ_r because this parameter does not directly interact with this part of the model. We can conclude that the double knockout option on the carbon price, while making the model more dynamic and market-responsive, also increases computational complexity, especially in high volatility scenarios.

$N = P = 300$	GMRES			Bi-CGSTAB		
σ_r	ILU	Jacobi	None	ILU	Jacobi	None
0.15	8	548	825	7	363	584
0.25	9	604	838	8	357	698

Table 4.30: Performance of GMRES and Bi-CGSTAB for various σ_r values in the Green Bond model

$N = P = 300$	GMRES			Bi-CGSTAB		
σ_c	ILU	Jacobi	None	ILU	Jacobi	None
0.5	9	478	613	7	297	425
1.0	9	595	996	8	361	792

Table 4.31: Performance of GMRES and Bi-CGSTAB for various σ_c values in the Green Bond model

Let us now examine how the short rate volatility affects both the GMRES and Bi-CGSTAB solvers for both bond models. We choose the same values for the short rate σ_r in both models and look at table (4.30, Green bond), and table (4.32, Conventional Bond). The first thing we notice is the vast difference in iteration counts between the two models. So the extra complexity in the green bond model, due to the carbon price influence compounded by the double knockout mechanism, requires substantially more iterations for convergence. This is present in scenarios with and without preconditioners. Furthermore, the GMRES solver shows a substantial increase in iterations from 548 to 604 as σ_r rises from 0.15 to 0.25. This increase, being more significant in absolute terms, has a lower increase in percentages compared to the conventional bond model. This suggests that while the green bond model's difficulty leads to higher absolute numbers, its sensitivity to short rate volatility is less dominant.

$N = 300$	GMRES		Bi-CGSTAB	
σ_r	Jacobi	None	Jacobi	None
0.15	49	102	170	167
0.25	68	164	236	236

Table 4.32: Performance of GMRES and Bi-CGSTAB for various σ_r values in the Conventional Bond model

Let us now look at the amount of iterations for lower values of the carbon price volatility, σ_c . As evident from table 4.33, the iteration counts required for convergence in the green bond model with lower σ_c values are not much higher than those for the conventional bond model. However, it is important to note that these lower volatility scenarios are not entirely representative of the typical market conditions for the carbon price due to the great amount of factors influencing the price [19]. This higher volatility is

also consistent with our parameter calibration earlier. Thus, while lower volatility scenarios show more similar convergence rates, they probably do not typically represent the real-world conditions under which green bonds operate [13][14].

$N = P = 300$	GMRES			Bi-CGSTAB		
σ_c	ILU	Jacobi	None	ILU	Jacobi	None
0.15	7	329	338	5	197	244
0.25	7	371	409	6	246	315

Table 4.33: Performance of GMRES and Bi-CGSTAB for lower σ_c values in the Green Bond model

Another factor we have to consider is the increasing trend in the introduction of new environmental regulations by governments all around the world. These regulations typically drive the carbon price upwards, reflected in a larger or positive μ in our model. In table 4.34, we can see how a positive μ affects the performance of GMRES and Bi-CGSTAB. We observe that as μ becomes more positive, the number of iterations required for convergence slightly increases for both GMRES and Bi-CGSTAB. This effect is less pronounced when using one of the preconditioners. In addition to influencing the drift parameter μ of the carbon price, regulatory shifts and policy changes often introduce uncertainties and rapid adjustments in the market, which can significantly increase its volatility σ_c in our model. As previously shown in table 4.31 this has a notable impact on the convergence efficiency of the iterative solvers.

$N = P = 300$	GMRES			Bi-CGSTAB		
μ	ILU	Jacobi	None	ILU	Jacobi	None
-0.05	8	553	819	7	350	667
0.05	8	557	833	7	347	689
0.10	8	559	838	7	350	713

Table 4.34: Performance of GMRES and Bi-CGSTAB for various μ values in the Green Bond model

Furthermore, abnormal changes in traditional energy prices, particularly oil, can significantly impact the carbon market [33]. For example, as we have seen last year, a sudden increase in oil prices might make alternative energy sources, including renewable energy, more economically attractive. Such fluctuations can cause uncertainty in the demand for and supply of carbon credit allowances, leading to increased price volatility σ_c , thereby, as we comprehensively established thus far, resulting in an increase in required iterations.

Now we will analyse the 'Greenium' effect on the performance of GMRES and Bi-CGSTAB in both bond models. As a brief reminder, the 'Greenium' effect, is the phenomenon where investors exhibit a higher willingness to accept risks and lower returns for green bonds due to their sustainable nature[4]. In the context of financial engineering, this would mean the market price of risk parameter λ tends to be more negative. Let us start considering the effect of both market price of risk parameters, λ_r and λ_c in the green bond model. We can see in tables 4.35 and 4.36 that more negative values of λ_r and λ_c lead to iterations required for both GMRES and Bi-CGSTAB solvers.

$N = P = 300$	GMRES			Bi-CGSTAB		
λ_c	ILU	Jacobi	None	ILU	Jacobi	None
-1.0	9	573	906	7	383	678
-0.01	8	557	832	7	347	689

Table 4.35: Performance of GMRES and Bi-CGSTAB for various λ_c values in the Green Bond model

$N = P = 300$	GMRES			Bi-CGSTAB		
λ_r	ILU	Jacobi	None	ILU	Jacobi	None
-1.0	8	548	839	7	354	686
-0.01	8	557	831	8	380	629

Table 4.36: Performance of GMRES and Bi-CGSTAB for various λ_r values in the Green Bond model

The conventional bond model only includes the market price of risk in the short rate, λ_r . Here, λ_r is likely to be positive, reflecting investors' preference for higher returns, as sustainability factors are not considered. We can see in table 4.37 that more positive values of λ_r result in fewer iterations required for both solvers.

$N = 300$	GMRES		Bi-CGSTAB	
λ_r	Jacobi	None	Jacobi	None
0.01	38	301	193	227
1.0	38	273	193	220

Table 4.37: Performance of GMRES and Bi-CGSTAB for various λ_r values in the Conventional Bond model

Thus, this Greenium effect has significant impact on the performance of GMRES and Bi-CGSTAB and can be seen as another environmental factor that increases the difficulty for iterative solvers in the context of green bonds, differentiating them from conventional bonds.

In conclusion, this comparative analysis between the conventional and green bond models highlights the substantial influence of environmental factors on the convergence of the iterative methods GMRES and Bi-CGSTAB. We observe that the green bond model's sensitivity to carbon price volatility, σ_c , notably increases the computational complexity. The 'Greenium' effect further differentiates the green bond model by affecting the market price of risk parameters, thereby increasing solver iterations. These findings underscore the significant impact environmental variables have in the performance and robustness of established numerical methods.

Additionally, it is important to discuss the impact of grid size on our models, particularly in the context of the green bond model. In our analyses, the grid size was constrained to a maximum of 300×300 , which was the maximum for practicality. However, we observed the rapid increase in the number of iterations required for convergence as the grid size increases, especially for the carbon price volatility, σ_c .

5

Conclusion & Discussion

The primary objective of this thesis was to explore the impact environmental factors have on the pricing methods of green bonds. During the literature review, we discovered that environmental factors significantly influence the carbon price and its dynamics. Consequently, we developed a model for the coupon rate of a green bond that is not only dependent on traditional financial factors, such as the short rate (r_t), but also depends on the carbon price c_t . With this approach, we were able to integrate environmental aspects into the valuation of green bonds, thereby reflecting the evolving landscape of sustainable finance. The coupon rate had the payoff mechanism of a European call option on the carbon price. From a financial perspective, this is reasonable as green bonds are issued to fund projects with environmental benefits. When issuers perform well, they contribute positively to the environment, which in turn can lead to a reduced demand for carbon allowances. This reduction in demand can cause a decrease in the carbon price, consequently leading to lower coupon payouts. This mechanism not only incentivizes issuers to perform better environmentally but also aligns the interests of investors with sustainable environmental practices. We fitted the model to real market data to obtain estimations for all the parameters. We compared this model with the model for the coupon rate of a conventional bond, only dependent on the short rate r_t .

In chapter 4 we did a detailed analysis of both the model's numerical properties, focusing on matrix characteristics, eigenvalue distributions, and the influence of various parameters. This comparative analysis highlighted the unique challenges and complexities introduced by environmental factors. Then we investigated the performance of the GMRES and Bi-CGSTAB methods found that the green bond model consistently required more iterations for these methods to converge. This increased demand for iterations was primarily attributed to the high volatility of the carbon price σ_c . We showed that when the values of the carbon price volatility (σ_c) were low, the models exhibited similar requirements in terms of the number of iterations needed. However, considering the multitude of environmental factors and their inherent uncertainties, which in our model are collectively represented through the carbon price, a realistically high σ_c is more appropriate. This aligns with the calibration we conducted in Chapter 2. Additionally, we investigated the 'Greenium' effect, where investors are willing to accept higher risks and lower returns for green bonds. We observed that this also resulted in extra required iterations for the iterative methods.

The performance of GMRES and Bi-CGSTAB varied between the green and conventional bond models. Notably, for the green bond model, Bi-CGSTAB outperformed GMRES in terms of efficiency and required iterations. However, for the conventional bond model, GMRES demonstrated superior performance compared to Bi-CGSTAB. Furthermore, the use of ILU and Jacobi preconditioners was found to be effective in increasing the convergence rate of the GMRES and Bi-CGSTAB methods for both bond models.

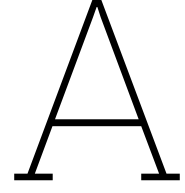
Having achieved significant findings, these also presents opportunities for further research. There are many other innovative ways of integrating environmental impacts into financial models. For instance, environmental impact could be modeled as a direct modifier of the green bond's face value, FV , or as a factor influencing its maturity time T . Moreover, future studies could expand this scope to include diverse environmental metrics such as carbon footprint and sustainability ratings. In Chapter 4 we only considered the CIR model, future research could incorporate the Vašíček model, which does allow for

negative rates. Exploring additional matrix properties could also provide a deeper understanding of the numerical behaviors and challenges in sustainable finance modeling. Our analyses were constrained to a grid size of 300×300 , which indicated a rapid increase in the number of iterations required for convergence, especially in the green bond model, as the grid size increases. This suggests that larger grids, potentially necessary for more detailed market modeling, could significantly escalate computational demands. The limitation to GMRES and Bi-CGSTAB methods with ILU and Jacobi preconditioners also suggest there are many more other iterative methods and preconditioning techniques to investigate. This exploration could potentially uncover more efficient strategies for handling complex financial models.

References

- [1] Dimitri P. Bertsekas and John N. Tsitsiklis. *Introduction to Probability*. 2nd ed. Library of Congress Control Number: 2002092167. Belmont, Massachusetts: Athena Scientific, 2008. ISBN: 978-1-886529-23-6.
- [2] Umair Saeed Bhutta et al. *Green bonds for sustainable development: Review of literature on development and impact of green bonds*. 2022.
- [3] Patrick Billingsley. *Probability and Measure*. 3rd ed. New York: John Wiley & Sons, 1995, pp. 419–427. ISBN: 0-471-00710-2.
- [4] Martijn Boermans. “Preferred Habitat Investors in the Green Bond Market”. In: *Working Paper No. 773* (2023). * Views expressed are those of the authors and do not necessarily reflect official positions of De Nederlandsche Bank.
- [5] Michael J. Brennan and Eduardo S. Schwartz. “A continuous time approach to the pricing of bonds”. In: *Journal of Banking & Finance* 3.2 (1979), pp. 133–155. DOI: 10.1016/0378-4266(79)90011-6.
- [6] Gerald W. Jr. Buetow, Bernd Hanke, and Frank J. Fabozzi. “Impact of Different Interest Rate Models on Bond Value Measures”. In: *Journal or Book Title* (2002). Copyright © 2002 Institutional Investor, Inc. All Rights Reserved.
- [7] Marek Capiński and Ekkehard Kopp. *The Black–Scholes Model*. Mastering Mathematical Finance. Library of Congress Cataloguing in Publication data: HG6024.A3C364 2013, 332.64, dc23 2012023180. Cambridge, UK: Cambridge University Press, 2012. ISBN: 978-1-107-00169-5.
- [8] R. Chandra. “Conjugate gradient methods for partial differential equations”. PhD thesis. New Haven, CT: Yale University, 1978.
- [9] Julien Chevallier. “Carbon Price Drivers: An Updated Literature Review”. In: (2011).
- [10] Mauricio Contreras, Alejandro Llanquihuén, and Marcelo Villena. “On the Solution of the Multi-Asset Black-Scholes Model: Correlations, Eigenvalues and Geometry”. In: *Journal of Mathematical Finance* 6.4 (2016). Facultad de Ingeniería y Ciencias, Universidad Adolfo Ibáñez, Santiago, Chile; Facultad de Ciencias Exactas, Universidad Andrés Bello, Santiago, Chile. DOI: 10.4236/jmf.2016.64043.
- [11] J.C. Cox, J.E. Ingersoll, and S.A. Ross. “A Theory of the Term Structure of Interest Rates”. In: *Econometrica* 53.2 (1985), pp. 385–407. DOI: 10.2307/1911242.
- [12] J. Crank and P. Nicolson. “A practical method for numerical evaluation of solutions of partial differential equations of the heat conduction type”. In: *Proceedings of the Cambridge Philosophical Society* 43.1 (1947), pp. 50–67. DOI: 10.1017/S0305004100023197.
- [13] Feng Dong et al. “Exploring volatility of carbon price in European Union due to COVID-19 pandemic”. In: *Environmental Science and Pollution Research International* 29.6 (2022), pp. 8269–8280. DOI: 10.1007/s11356-021-16052-1.
- [14] Zhen-Hua Feng, Le-Le Zou, and Yi-Ming Wei. “Carbon price volatility: Evidence from EU ETS”. In: *Applied Energy* 88.3 (2011), pp. 590–598. DOI: 10.1016/j.apenergy.2010.06.017.
- [15] I. V. Girsanov. “On Transforming a Certain Class of Stochastic Processes by Absolutely Continuous Substitution of Measures”. In: *Theory of Probability & Its Applications* 5.3 (1960), pp. 285–301.
- [16] Britta Hachenberg and Dirk Schiereck. *Are green bonds priced differently from conventional bonds?* 2018.
- [17] John C. Hull. “Interest Rate Derivatives: Models of the Short Rate”. In: *Options, Futures, and Other Derivatives*. 6th ed. Upper Saddle River, N.J: Prentice Hall, 2006, pp. 657–658. ISBN: 0-13-149908-4.

- [18] John C. Hull. *Options, Futures, and Other Derivatives*. 8th ed. Boston, MA: Pearson Education, Inc., publishing as Prentice Hall, 2012. ISBN: 978-0-13-216494-8.
- [19] C Ji, Y Hu, and B Tang. "Research on carbon market price mechanism and influencing factors: a literature review". In: *Natural Hazards* 92 (2018), pp. 761–782.
- [20] Yue-Kuen Kwok. *Mathematical Models of Financial Derivatives*. Revised and enlarged 2nd edition to the 1st edition originally published by Springer Singapore 1998 (ISBN 981-3083-25-5). Hong Kong, PR China: Springer Berlin Heidelberg, 2008. ISBN: 978-3-540-42288-4.
- [21] Timothy Laing et al. "The effects and side-effects of the EU emissions trading scheme". In: (2014).
- [22] Y Li et al. "Could carbon emission control firms achieve an effective financing in the carbon market? A case study of China's emission trading scheme". In: *Journal of Cleaner Production* 314 (2021), p. 128004.
- [23] In Jae Myung. "Tutorial on maximum likelihood estimation". In: *Journal of Mathematical Psychology* 47.1 (2003), pp. 90–100. DOI: 10.1016/S0022-2496(02)00028-7. URL: [https://doi.org/10.1016/S0022-2496\(02\)00028-7](https://doi.org/10.1016/S0022-2496(02)00028-7).
- [24] Cornelis Oosterlee and Lech Grzelak. *Mathematical Modeling and Computation in Finance*. 2020.
- [25] Allegra Pietsch and Dilyara Salakhova. *Pricing of green bonds: drivers and dynamics of the greenium*. 2022.
- [26] Miklós Rásonyi. "Arbitrage pricing theory and risk-neutral measures". In: (2004).
- [27] Yousef Saad. *Iterative Methods for Sparse Linear Systems*. Second. Society for Industrial and Applied Mathematics, 2003. DOI: 10.1137/1.9780898718003. eprint: <https://epubs.siam.org/doi/pdf/10.1137/1.9780898718003>. URL: <https://epubs.siam.org/doi/abs/10.1137/1.9780898718003>.
- [28] Domingo Tavella and Curt Randall. *Pricing Financial Instruments: The Finite Difference Method*. Wiley, Apr. 2000, p. 256. ISBN: 978-0-471-19760-7.
- [29] The London School of Economics and Political Science. "What is a carbon price and why do we need one?" In: *The London School of Economics and Political Science - Explainers* (2019). Accessed: 2023-11-14. URL: <https://www.lse.ac.uk/granthaminstitute/explainers/what-is-a-carbon-price-and-why-do-we-need-one/>.
- [30] H. G. Tucker. *A Graduate Course in Probability*. New York: Academic Press, 1967.
- [31] Oldřich A. Vasicek. "An equilibrium characterization of the term structure". In: *Journal of Financial Economics* 5 (1977), pp. 177–188.
- [32] Kees Vuik and Domenico Lahaye. *Scientific Computing*. 2019.
- [33] Haixu Yu et al. "Carbon market volatility analysis based on structural breaks: Evidence from EU-ETS and China". In: *Frontiers in Environmental Science* 10 (2022). This article is part of the Research Topic "Green Indicators to Inform Circular Economy under Climate Change". DOI: 10.3389/fenvs.2022.973855. URL: <https://www.frontiersin.org/articles/10.3389/fenvs.2022.973855/full>.
- [34] Shuhua Zhang and Zhuo Yang. "The Valuation of Carbon Bonds Linked with Carbon Price". In: *Computational Methods in Applied Mathematics* (2015). Received February 26, 2015; revised May 18, 2015; accepted August 20, 2015. DOI: 10.1515/cmam-2016-0001.
- [35] Shuhua Zhang, Zhuo Yang, and Song Wang. "Design of Green Bonds by Double-Barrier Options". In: *Discrete and Continuous Dynamical Systems - Series S* 13.6 (2020), pp. 1867–1882. DOI: 10.3934/dcdss.2020110.



Black-Scholes PDE Derivation

Let $V(t, S)$ denote the option value, dependent on time t and the stochastic process S . Using Itô's lemma, we derive its dynamics

$$\begin{aligned}dV(t, S) &= \frac{\partial V}{\partial t} dt + \frac{\partial V}{\partial S} dS + \frac{1}{2} \frac{\partial^2 V}{\partial S^2} (dS)^2 \\ &= \left(\frac{\partial V}{\partial t} + \mu S \frac{\partial V}{\partial S} + \frac{1}{2} \sigma^2 S^2 \frac{\partial^2 V}{\partial S^2} \right) dt + \sigma S \frac{\partial V}{\partial S} dW_{\mathbb{P}}.\end{aligned}$$

We then construct a portfolio $\Pi(t, S)$ containing one option $V(t, S)$ as well as some amount $-\Delta$ of the underlying asset $S(t)$. This yields

$$\Pi(t, S) = V(t, S) - \Delta S(t). \quad (\text{A.1})$$

We use the result of Itô's lemma to derive the dynamics of portfolio Π

$$d\Pi = dV - \Delta dS \quad (\text{A.2})$$

$$\begin{aligned}&= \left(\frac{\partial V}{\partial t} + \mu S \frac{\partial V}{\partial S} + \frac{1}{2} \sigma^2 S^2 \frac{\partial^2 V}{\partial S^2} \right) dt + \sigma S \frac{\partial V}{\partial S} dW_P - \Delta(\mu S dt + \sigma S dW_P) \\ &= \left[\frac{\partial V}{\partial t} + \mu S \left(\frac{\partial V}{\partial S} - \Delta \right) + \frac{1}{2} \sigma^2 S^2 \frac{\partial^2 V}{\partial S^2} \right] dt + \sigma S \left(\frac{\partial V}{\partial S} - \Delta \right) dW_P.\end{aligned} \quad (\text{A.3})$$

This portfolio contains randomness due to the $\sigma S \left(\frac{\partial V}{\partial S} - \Delta \right) dW_P$ term, which we want remove by choosing

$$\Delta = \frac{\partial V}{\partial S}. \quad (\text{A.4})$$

Then, equation A.2 becomes

$$d\Pi = \left(\frac{\partial V}{\partial t} + \frac{1}{2} \sigma^2 S^2 \frac{\partial^2 V}{\partial S^2} \right) dt.$$

To avoid arbitrage, the money invested in a risk free savings account must be exactly the same as the value this portfolio would generate. We model this for amount, $\Pi(t, S)$, as

$$\begin{aligned}d\Pi &= r\Pi dt \\ &= r \left(V - S \frac{\partial V}{\partial S} \right) dt\end{aligned} \quad (\text{A.5})$$

In the second equality, we used equations A.1 and A.4. Finally, by equating equations A.3 and A.5 and dividing by dt , we obtain the Black-Scholes PDE:

$$\frac{\partial V}{\partial t} + rS \frac{\partial V}{\partial S} + \frac{1}{2} \sigma^2 S^2 \frac{\partial^2 V}{\partial S^2} - rV = 0.$$